N73-21364
NASA CR-2223

SPECIFICATION OF MESOSPHERIC DENSITY, PRESSURE, AND TEMPERATURE BY EXTRAPOLATION

by M. E. Graves, Y. S. Lou, and A. H. Miller

Prepared by
NORTHROP SERVICES, INC.
Huntsville, Ala.
for George C. Marshall Space Flight Center

1. REPORT NO. NASA CR-2223	2. GOVERNMENT ACCESSION NO.	3. RECIPIENT'S CATALOG NO.
4. TITLE AND SUBTITLE SPECIFICATION OF MESOSPHERIC DENSITY, PRESSURE, AND TEMPERATURE BY EXTRAPOLATION		5. REPORT DATE March 1973
		6. PERFORMING ORGANIZATION CODE
7. AUTHOR(S) M. E. Graves, Y. S. Lou, A. H. Miller		8. PERFORMING ORGANIZATION REPORT # M113
9. PERFORMING ORGANIZATION NAME AND ADDRESS Northrop Services, Inc. 6025 Technology Dr. Huntsville, AL		10. WORK UNIT NO.
		11. CONTRACT OR GRANT NO. NAS 8-21810
		13. TYPE OF REPORT & PERIOD COVERED
12. SPONSORING AGENCY NAME AND ADDRESS National Aeronautics and Space Administration Washington, D. C. 20546		CONTRACTOR
		14. SPONSORING AGENCY CODE

15. SUPPLEMENTARY NOTES
Prepared under the technical monitorship of the Aerospace Environment Division, Aero-Astrodynamics Laboratory, NASA-Marshall Space Flight Center.

16. ABSTRACT

A procedure is presented which uses an extrapolation technique to obtain estimates of density, pressure, and temperature up to 90 km from 52 km data. The resulting errors are investigated. The procedure is combined with a special temperature interpolation method around the stratopause to produce such estimates at eight levels between 36 km and 90 km from North American sectional chart data at 5, 2, and 0.4 mb. Fifty charts were processed to obtain mean values and standard deviations at grid points for midseasonal months from 1964 to 1966. The mean values were compared with Groves' model, and internal consistency tests were performed upon the statistics. Through application of the extrapolation procedure, the atmospheric structure of a stratospheric warming event is studied.

17. KEY WORDS Mesospheric Density Pressure Temperature Statistical Values Stratospheric Warming	18. DISTRIBUTION STATEMENT

19. SECURITY CLASSIF. (of this report) Unclassified	20. SECURITY CLASSIF. (of this page) Unclassified	21. NO. OF PAGES 105	22. PRICE $3.00

PREFACE

A design goal of the Space Shuttle is that it have a minimum operational constraint due to natural environment conditions. One aspect of the design problem is the control of aerodynamic heating of the Space Shuttle vehicle entering the earth's atmosphere from space. The natural environment parameters of importance to this design problem are density, temperature, and pressure at mesospheric altitudes. While there are several atmospheric models available for re-entry studies none gives the variation of the parameters along the re-entry path.

Since a Space Shuttle orbiter re-entry trajectory from a polar orbit gives the highest aerodynamic heating an atmospheric model extending around the earth along the meridian which passes through the landing site with an altitude range from sea level to 185 km would find important applications for the Space Shuttle program in the areas of design and performance analysis. This model should account for variations in the vertical and horizontal structure of density and be consistent with the equation of state and hydrostatic equation to produce associated values for pressure and temperature. A natural extension of this model concept is to cover all meridians, thus producing a 4-D model. This 4-D model would give the pressure, temperature, and density variables with their structure as a function of latitude, longitude, altitude, time (seasonal), and possibly time of day over the altitude range from sea level to 185 km.

The objective of the study described in this report was to develop a procedure to obtain estimates of density, temperature, and pressure at mesospheric altitudes and to develop statistics of these parameters for as wide a range of latitude and longitude as possible. Hopefully, this will be of value in Space Shuttle atmospheric entry studies and will contribute to the evenutal development of the atmospheric model described above.

William W. Vaughan
Chief, Aerospace Environment Division
Aero-Astrodynamics Laboratory
NASA-Marshall Space Flight Center

FOREWORD

TABLE OF CONTENTS

Section	Title	Page

LIST OF ILLUSTRATIONS

LIST OF ILLUSTRATIONS (Continued)

LIST OF ILLUSTRATIONS (Continued)

LIST OF ILLUSTRATIONS (Continued)

LIST OF ILLUSTRATIONS (Concluded)

LIST OF TABLES

Section I

INTRODUCTION

The mesospheric and thermospheric layers of the atmosphere between 60 km and 150 km have been sparsely probed. Immediately below these layers, however, the Meteorological Rocket Network (ref. 1) has acquired a substantial number of soundings at a few sites during the past 12 years. Furthermore, a regression technique has been reported by Gelman, Miller, and Woolf (ref. 2) which presents the possibility of using satellite infrared spectrometer data to obtain temperature profiles at 30 to 55 km over much of the earth. Above 60 km, about 210 grenade and pitot-tube soundings have been taken since 1960 (refs. 3, 4), mainly at Pt. Barrow, Alaska; Ft. Churchill, Manitoba; Wallops Island, Va.; and Ascension Island. In addition, some data have been obtained up to 110 km in experiments with falling spheres by the ABRES Density Variations Project (ref. 5), and photographic meteor data have been analyzed by Verniani and Viani (ref. 6) to yield diurnal and seasonal variations of the 90-km temperature at one site. The gradual accumulation of data from these and other projects has permitted a recent discussion of a semiannual variation in temperature at the base of the thermosphere (80-105 km) by Kochanski (ref. 7).

When there is a relative abundance of data for the structure variables immediately below a layer with inadequate information, regression has been used to estimate the values within the deficient layer, as in the example cited above (ref. 2) and in a study by Quiroz and Thompson (ref. 8). Regression will again be the extrapolation tool in this work, and it will have the objective of building an improved data base for density, pressure, and temperature up to 90 km through the use of rocket grenade and pitot-tube soundings. Consequently, it will be somewhat more empirical than the recent effort by Bowman, Palmer, and Schuknecht (ref. 9) to supply such structure data on a hemispheric scale through a twelve-level model based upon 100 mb data and the potential absolute vorticity equation. A four-dimensional aspect will be secured by applying our extrapolation technique to 50 midseasonal North American charts of geopotential height and temperature for the 5-mb, 2-mb, and 0.4-mb levels.

1

Section II

EXTRAPOLATION TECHNIQUE

The selection of a technique to extrapolate the structure variables is aided by the height-lag correlations of density with pressure, temperature, and density at 24-56 km as related by Quiroz and Miller (ref. 10). Of special interest are the interlevel correlations of density with pressure, which are consistently above 0.95 when height lags of 4 to 8 km are taken between pressure, at the lower level, and density, at the higher level. Above 35 km, a lag interval of 8 km, or one scale height of pressure or density, produces maximum correlations in their study. Furthermore, when height lags are greater than 2 km, the interlevel correlation of pressure with density exceeds the interlevel correlation of density with density.

This striking correlation at an 8-kilometer interval of pressure at the base of a layer with density at the top encourages one to use the grenade and pitot-tube data to compute regression coefficients for a series of layers of one scale height in depth. The data are mostly from the period, 1964-1969, with a few soundings dating back to 1957. A major part of the 209 soundings come from the four sites named in Section I; Figure 1, giving the monthly distribution of the reports, indicates some unevenness in their distribution. In a few cases, two to four observations are taken on a particular day. However, in spite of these disparities, all available data are incorporated into the computation of one set of regression coefficients. Table 1 gives the results of such calculations for layers from 52-60 km, 60-68 km, 68-76 km, 76-84 km, 84-90 km. Columns headed a, b, and c in this table refer to regression coefficients of equations (1) and (2), wherein density at the top of a layer is predicted by pressure at the base, or by pressure and temperature at the base.

$$\rho_2 = a + b\ P_1 \tag{1}$$

$$\rho_2 = a + b\ P_1 + c\ T_1 \tag{2}$$

$$\rho = \text{density}$$
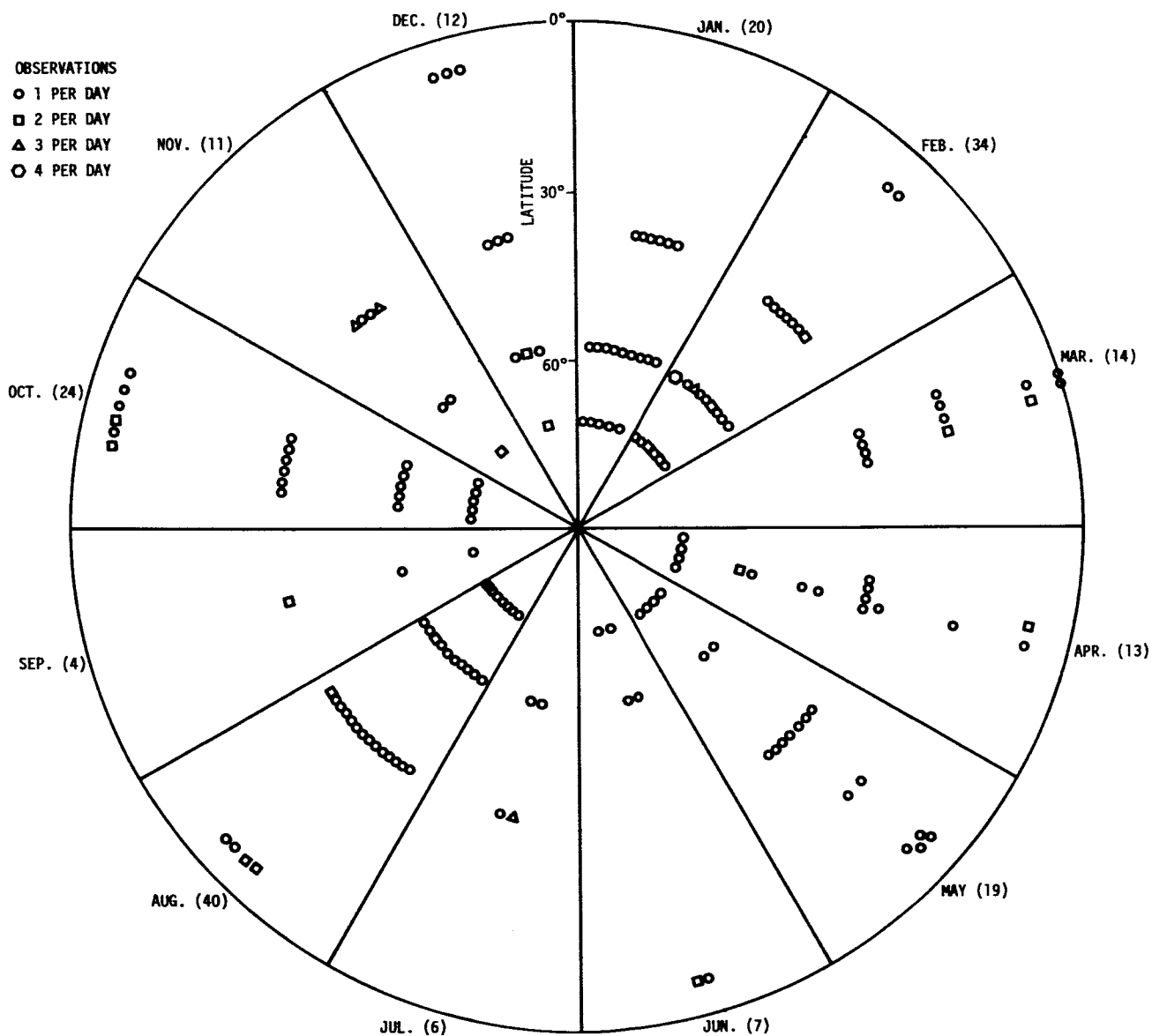
Figure 1. MONTHLY AND LATITUDINAL DISTRIBUTION OF ROCKET
GRENADE AND PITOT-TUBE SOUNDING REPORTS.
NUMBER OF OBSERVATIONS PER MONTH IS IN
PARENTHESES

3

Table 1. RESULTS OF LAYER BY LAYER REGRESSION, USING EQUATION 1, EQUATION 2, AND GRENADE DATA

Z_1	Z_2	N	a	b	c	$\varepsilon_2(\hat{\rho})$	$\varepsilon_1(\hat{\rho})$	$B(\hat{\rho})$	$r(\hat{\rho}, \rho)$
52 km	60 km	195	-1.650×10^{-5}	5.201×10^{-4}	3.137×10^{-7}	2.39%	1.70%	0.08%	0.990
		209	-8.163×10^{-5}	4.926×10^{-4}		2.70	1.79	0.11	0.981
60	68	209	-5.427×10^{-6}	5.238×10^{-4}	1.576×10^{-7}	3.22	2.37	0.22	0.988
			-4.283×10^{-5}	5.160×10^{-4}		3.14	2.18	0.10	
68	76	205	-1.694×10^{-6}	5.138×10^{-4}	1.021×10^{-7}	5.13	3.67	0.44	0.986
			-2.651×10^{-5}	5.391×10^{-4}		3.94	2.95	0.08	
76	84	188	1.643×10^{-7}	4.617×10^{-4}	5.623×10^{-9}	6.60	5.00	0.41	0.960
			-8.973×10^{-7}	4.569×10^{-4}		6.17	4.56	0.70	
84	90	138	4.848×10^{-8}	6.359×10^{-4}	2.442×10^{-9}	8.90	6.98	0.74	0.896
			-2.979×10^{-7}	6.087×10^{-4}		8.36	6.50	1.09	

LEGEND:

Z_1 = height of base level

Z_2 = height of top level

N = number of observations

a, b, c = regression coefficients

$\varepsilon_1(\hat{\rho})$ = mean error in $\hat{\rho}$ from Equation (3)

$\varepsilon_2(\hat{\rho})$ = rms error in $\hat{\rho}$ from Equation (4)

$B(\hat{\rho})$ = bias in $\hat{\rho}$ from Equation (5)

$r(\hat{\rho}, \rho)$ = correlation coefficient between estimated and observed density

P = pressure

T = temperature

The error computations in this table and succeeding tables and graphs are based upon relative differences. Thus, the mean absolute error in percent, ε_1, is given by

$$\varepsilon_1 = \frac{1}{N} \sum_{i=1}^{N} |\hat{X}_i - X_i|/X_i \cdot 100 \tag{3}$$

N = number of observations

$\hat{X}_i$ = estimated value

X_i = observed value

The root-mean square error in percent, ε_2, is given by

$$\varepsilon_2 = \left[\frac{1}{N} \sum_{i=1}^{N} \left(\frac{\hat{X}_i - X}{X_i} \right)^2 (100)^2 \right]^{1/2} \tag{4}$$

The biases are measured by removing the absolute value signs of equation (3). Bias in percent is

$$B = \frac{1}{N} \sum_{i=1}^{N} (\hat{X}_i - X)/X_i \cdot 100 \tag{5}$$

Referring again to Table 1, which has error quantities for ρ, one finds that ε_1 ranges from 1.70 percent at the lowest layer to 6.98 percent at the top layer, when P is used alone as a predictor. The rms error varies from 2.39 to 8.90 percent. When T is added as a second predictor, there is a small but worthwhile reduction in the error quantities, except in the layer from 52 to 60 km where a small increase of error occurs because of an enlargement of the data sample from 195 cases to 209 cases. Table 1 also indicates that a small bias is incurred in the regression. Finally, in the column at the right, the correlation coefficient $r(\hat{\rho}, \rho)$ is given to show the agreement of the predicted and observed densities at the top of each layer. Here, $\hat{\rho}$, is the predicted value by regression. The agreement is quite good throughout, giving

5

support to the idea of extrapolating upward by regression, using pressure and temperature to predict density at 8-km intervals.

Figure 2 illustrates an extrapolation technique in which the regression is followed by an integration process, using a numerical approximation to the hydrostatic law to get the pressure at the top of a layer from 1) the pressure at the base, and 2) the distribution of density and gravity through the layer at suitably spaced points. Application of the equation of state[*] then yields the temperature at the top, and predictors P and T are thus provided for regression through the next layer.

In an attempt to improve the estimates of P and T at the top of a layer, various iteration schemes were tried, employing both single and bivariate regression of the structure variables and the isothermal approximation for pressure,

$$P_2 = P_1 \exp(-g\Delta Z/R\bar{T}) \tag{6}$$

where

P_2 = pressure at top
P_1 = pressure at base
g = gravity
ΔZ = thickness
R = gas constant
$\bar{T}$ = mean temperature.

Common to these schemes was the calculation of a mean layer temperature based upon a known temperature at the base of a layer and an estimated temperature at the top. An iterative procedure was eventually found which converged to particular values of ρ, P, and T, but these values did not show significant improvement over initial guesses based upon regression. Therefore, all iteration schemes were abandoned, and the study proceeded with a layer-by-layer bootstrapping technique based upon bivariate regression.

[*]Valid only if the mean molecular weight remains constant - this may not remain true in upper layers.

1. REGRESSION

$$\hat{\rho}_2 = a + b\, P_1 + c\, T_1$$

2. INTEGRATION

$$\hat{P}_2 = P_1 - \sum_{i=1}^{N} \bar{\rho}_i(Z)\, \bar{g}_i(Z, \phi)\, \Delta Z$$

$$\Delta Z = 1\ \text{KM}$$

3. EQUATION OF STATE

$$\hat{T}_2 = \hat{P}_2\, (R\, \hat{\rho}_2)^{-1}$$

KM

90 — 90

— 84

80 —

— 76

70 —

— 68

60 — 60

— 52 (BASE LEVEL)

50 —
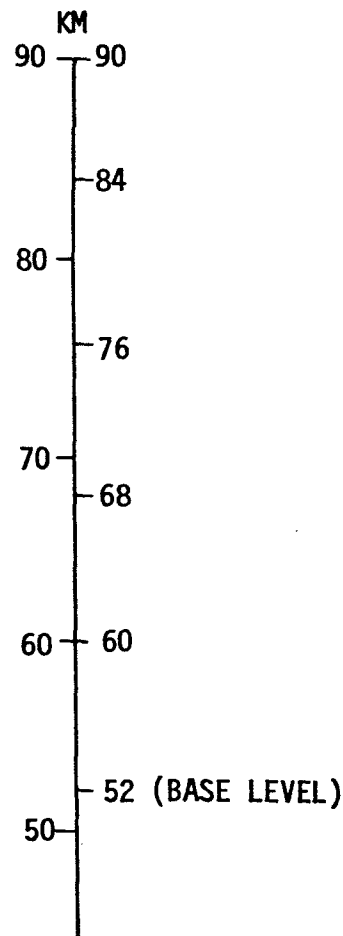
Figure 2. EXTRAPOLATION TECHNIQUE. THE 3 STEPS ARE LISTED AT THE LEFT WITH THE PERTINENT EQUATIONS. $\hat{\rho}_2$, $\hat{P}_2$, AND $\hat{T}_2$ ARE ESTIMATED QUANTITIES AT THE TOP OF A LAYER. AT THE RIGHT IS A SCALE GIVING THE EXTRAPOLATED LEVELS (60, 68, 76, 84, 90 km).
Z = GEOMETRIC ALTITUDE
ϕ = LATITUDE
N = 8 OR 6

Using 209 cases of rocket grenade and pitot-tube data (hereafter called the "grenade data"; there are but five pitot-tube soundings) at 52 km as the basic data for the extrapolation, the technique was applied. Error quantities were computed at 60, 68, 76, 84, and 90 km. It was immediately evident that a bias was being accrued as one progressed upward, with the bias at 90 km reaching about 10 percent for T, 20 percent for ρ, and 30 percent for P. This systematic error was found to be the cause of unacceptable departures from the observed check values at the higher levels. A second kind of bias present in the data is the nonuniform distribution of soundings in the seasons (Figure 1). This bias will have an effect upon independent data with a different seasonal distribution. Investigation of the integration step (Figure 2) was centered upon the exponential approximation of the density as a function of height within each layer. This approximation is perfectly valid for an isothermal atmosphere, but when the technique is tried on another atmosphere, such as US62 (ref. 11), a notable error is sustained amounting to almost 10 percent in the 76 to 84-km layer. This result is shown in Figure 3 along with the integration error associated with January .nd July 45 degrees N Supplementary Atmospheres (ref. 12). These curves denote great seasonal variation in this error, but as an initial step, an adjustment was computed for just the US62 Standard Atmosphere to be applied to the grenade data. The adjustment removed most of the bias in the density estimates, bringing the density rms error down to 16 percent at 90 km, but too much residual systematic error was present in the temperature and pressure estimates. Therefore, more of the US Supplementary Atmospheres were used to produce climatological adjustment, or correction curves for latitudes 15, 30, 45 and 60 degrees in January, July, and April/October, representing winte:, summer, and transition seasons, respectively. These curves are shown in Figures 4 through 6. The larger corrections indicated by these curves in the 10 to 15-percent range are associated with large lapse rates, cold temperatures, or a combination of the two, as are commonly found in the mesosphere.

Since the model atmospheres of Groves (ref. 13) are much more complete than the U. S. Supplementary Atmospheres, they constitute a preferable basis for climatological adjustment of pressure at any latitude in a specified month. Although data are sometimes sparse in upper levels, these model

8
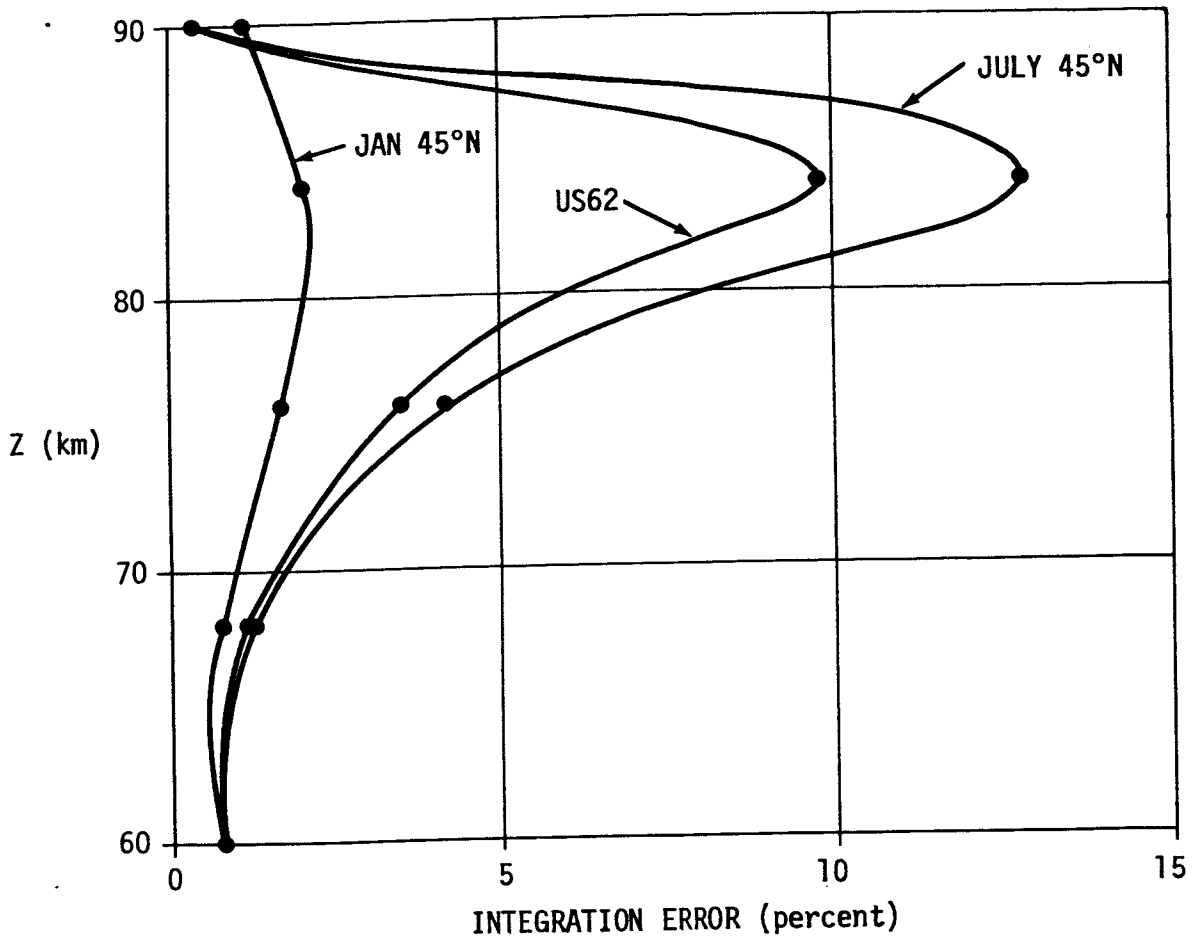
Figure 3. ACCURACY OF THE NUMERICAL INTEGRATION OF STEP 2, FIGURE 2, WHEN P_1, $\bar{\rho}_i$, AND $\bar{g}_i$ ARE SUPPLIED BY A SPECIFIED REFERENCE ATMOSPHERE
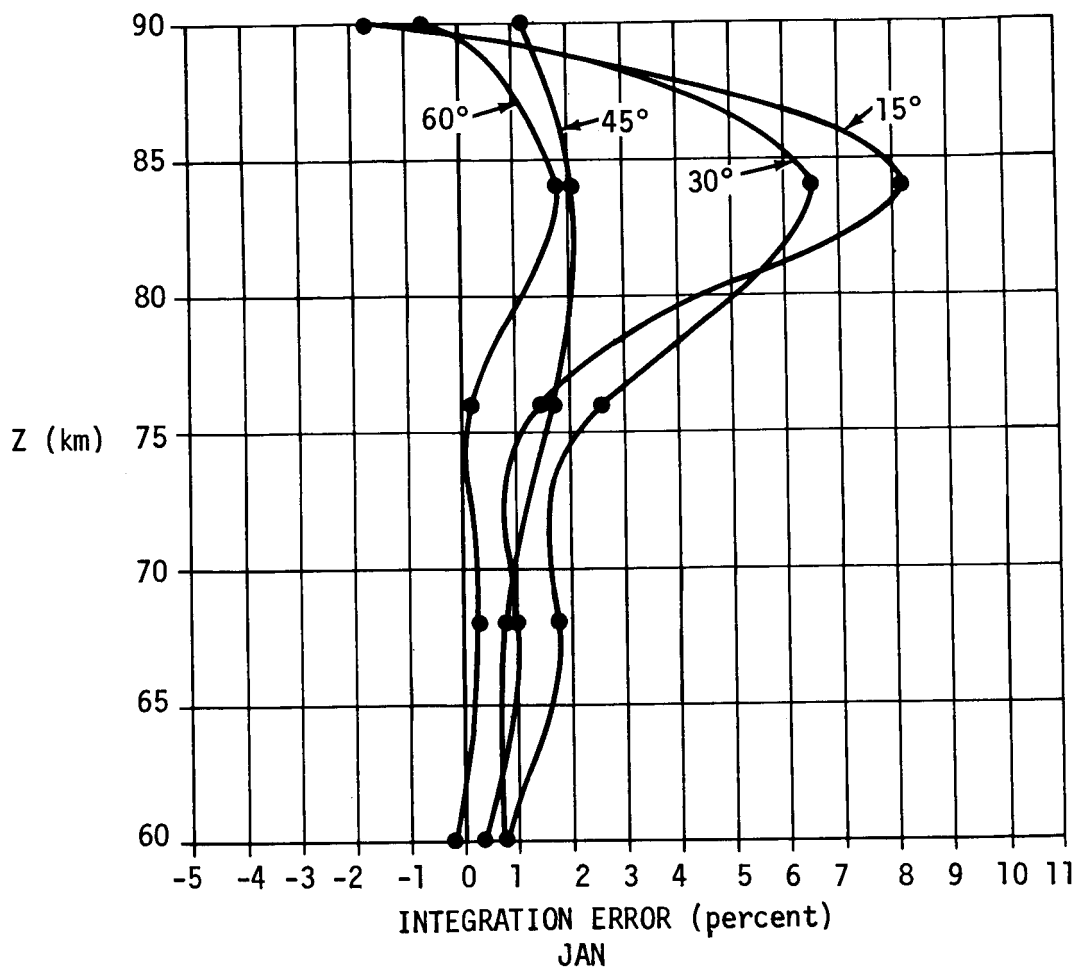
Figure 4.   ACCURACY OF THE NUMERICAL INTEGRATION OF STEP 2, FIGURE 2, WHEN P_1, $\bar{\rho}_i$, AND $\bar{g}_i$ ARE SUPPLIED BY A SET OF JANUARY REFERENCE ATMOSPHERES
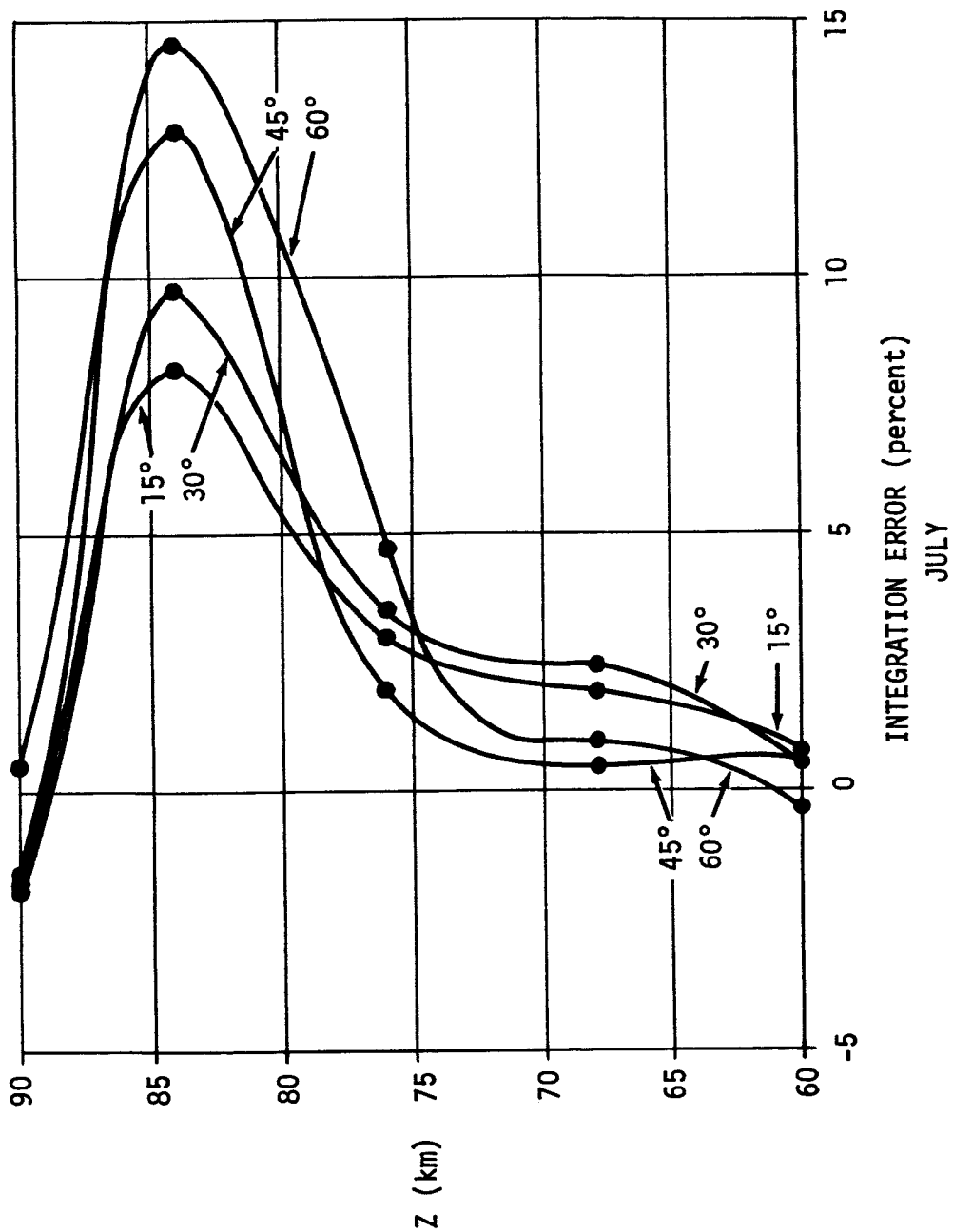
Figure 5.   ACCURACY OF THE NUMERICAL INTEGRATION OF STEP 2, FIGURE 2, WHEN $\bar{P}_1$, ρ_1, AND $\bar{g}_1$ ARE SUPPLIED BY A SET OF JULY REFERENCE ATMOSPHERES
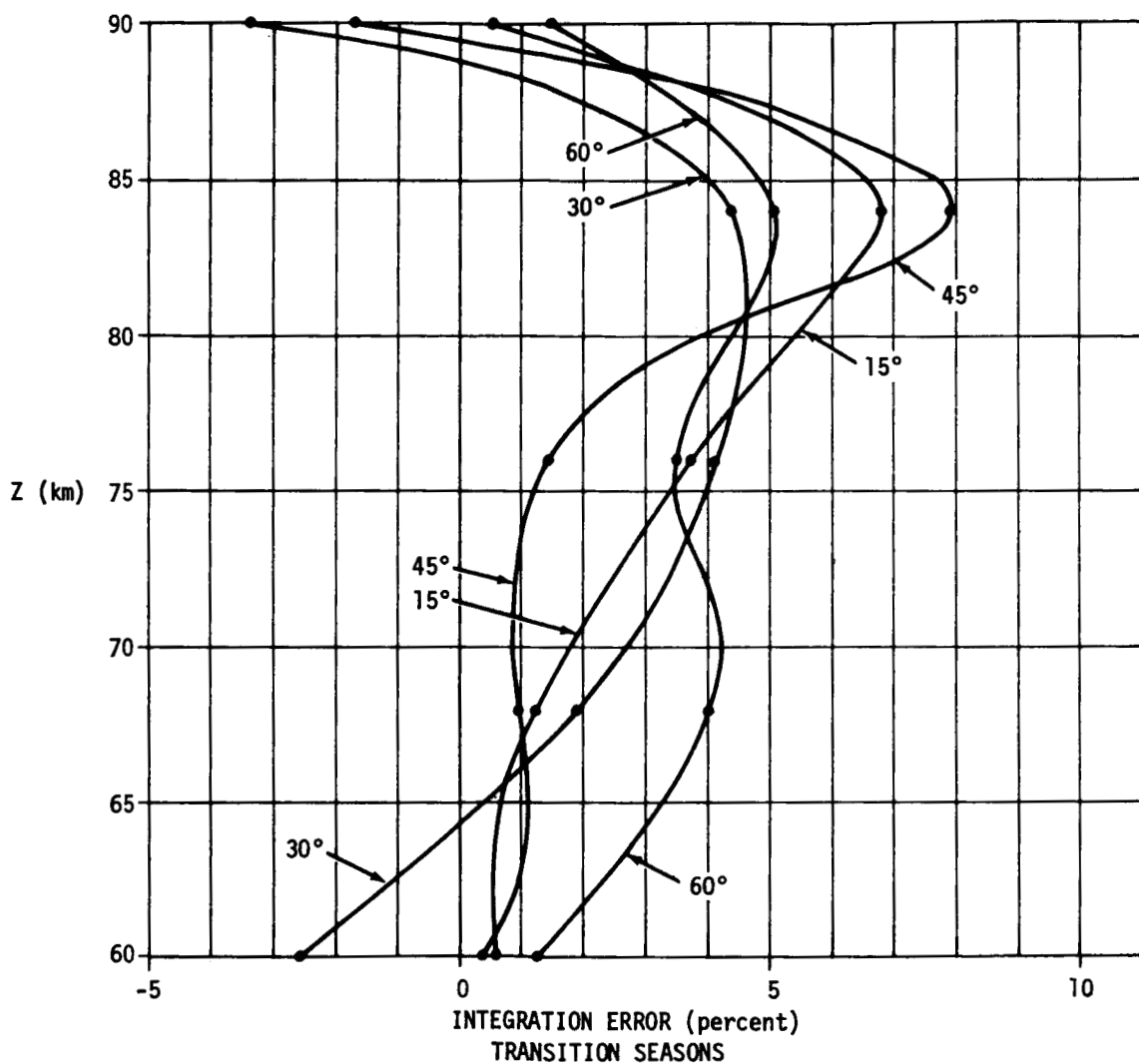
Figure 6. ACCURACY OF THE NUMERICAL INTEGRATION OF STEP 2, FIGURE 2, WHEN P_1, $\bar{\rho}_i$, AND $\bar{g}_i$ ARE SUPPLIED BY A SET OF TRANSITION SEASON REFERENCE ATMOSPHERES

atmospheres also extend to 90 km. Therefore the integration of Groves'
atmospheres, layer by layer, supplies a set of adjustments to pressure values
at each latitude, for each level and each midseasonal month represented in
this study.

The uneven distribution of station observations, both geographically and
seasonally, justifies a second adjustment to the results which is minor in
comparison with the first. This adjustment is also based upon Groves' model,
and it affects the density and temperature. It is calculated by entering
Groves' model values of density into the regression equations and then com-
paring the predicted density at the top of the layer with Groves' model. The
departures are applied as corrections to the generated densities at levels
from 60 km to 90 km. As may be seen in Figure 7, these corrections are usually
under one percent except in high latitudes, where they may reach five percent.
In practice, this adjustment does not cause a duplication of Groves' model, but
it utilizes information available in Groves' model to produce an improved
result. Temperature, computed from the equation of state, is affected slightly
by the density adjustment.

Summarizing, the extrapolation method is to use high correlations of
pressure with density at 8-km steps to predict the density at the top of a
layer by regression; to integrate through the layer by the hydrostatic approxi-
mation to find the pressure at the top; to adjust the pressure and density,
using corrections based upon reference atmosphere climatology; and to compute
the temperature at the top by the equation of state.
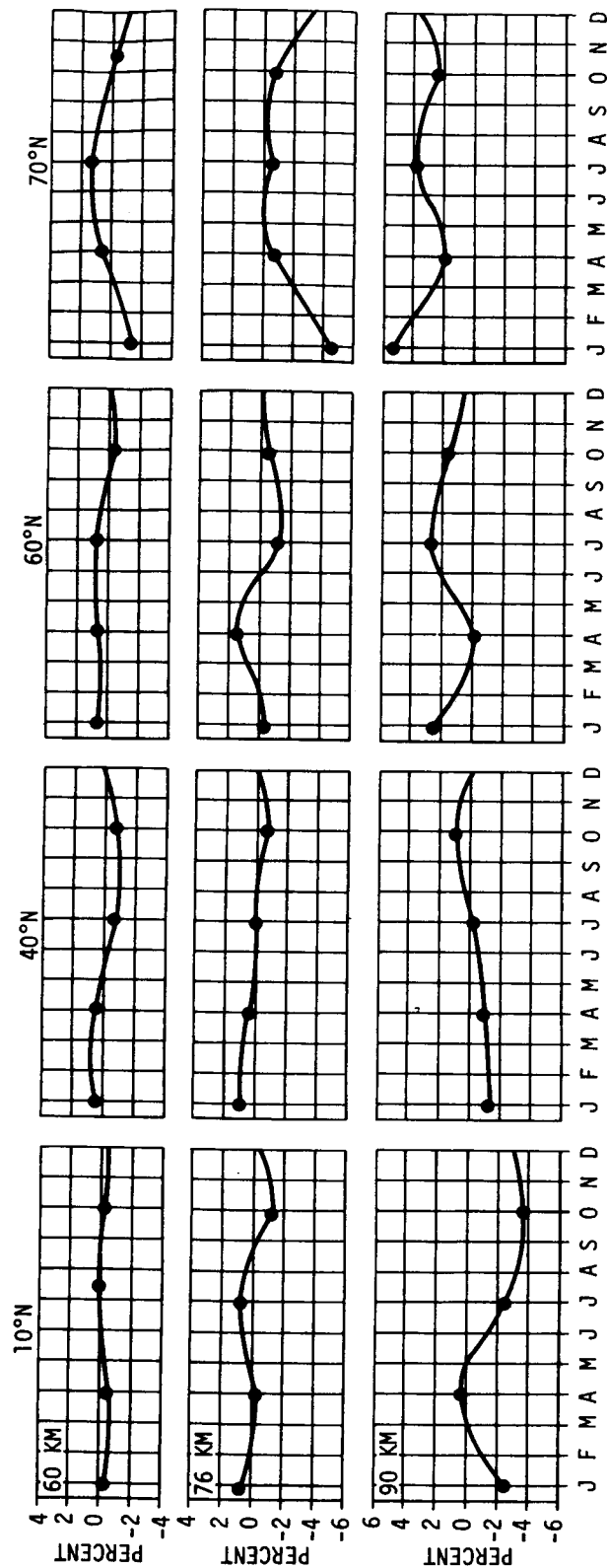
Figure 7. DENSITY ADJUSTMENTS BASED UPON GROVES' MODEL

14

Section III

INVESTIGATION OF ERRORS

The outcome of the extrapolation, in terms of mean error, rms error, bias, and 99 percentiles of negative and positive errors, is displayed in Figures 8 through 10. where the number of cases of grenade data decreased with height in accordance with Table 1. Figure 8 for density shows no systematic error at 60 km or 68 km, about 1 percent at 76 km, 3 percent at 84 km, and 1 percent at 90 km. The rms errors range from less than 3 percent at 60 km to about 16 percent at 90 km. Those errors falling near the upper and lower error bounds have been investigated individually, and are found to be connected with unusual temperature profiles which are not suspect of any internal inconsistency. The results for temperature, Figure 9, show very little bias, the rms error ranging from 4 percent to 10 percent and the extreme errors ranging from less than 10 percent at 60 km to about 25 percent at 90 km. The curves for pressure, Figure 10, are not unlike those for density.

The correlation coefficient $r(\hat{\rho}, \rho)$ between estimated and predicted density values is displayed in the righthand graph of Figure 11. Its rate of decrease becomes greater as one proceeds upward through the mesosphere, but substantial correlations of 0.83 at 84 km and 0.55 at 90 km are attained.

Curves corresponding to those of Figures 8 through 10 should be presented for independent data samples from high-level rocket soundings. However, such data subsequent to 1969 are not known to be available, so we have proceeded with the extrapolation technique and the regression coefficients which led to these figures, keeping in mind that a test on independent data would be desirable at the earliest opportunity.

Since density is the most important variable being estimated, one may question the choice of a bootstrapping regression technique over a direct extrapolation from 52 km to each of the other five levels ranging up to 90 km. The errors of direct extrapolation are given in Figure 11, along with the
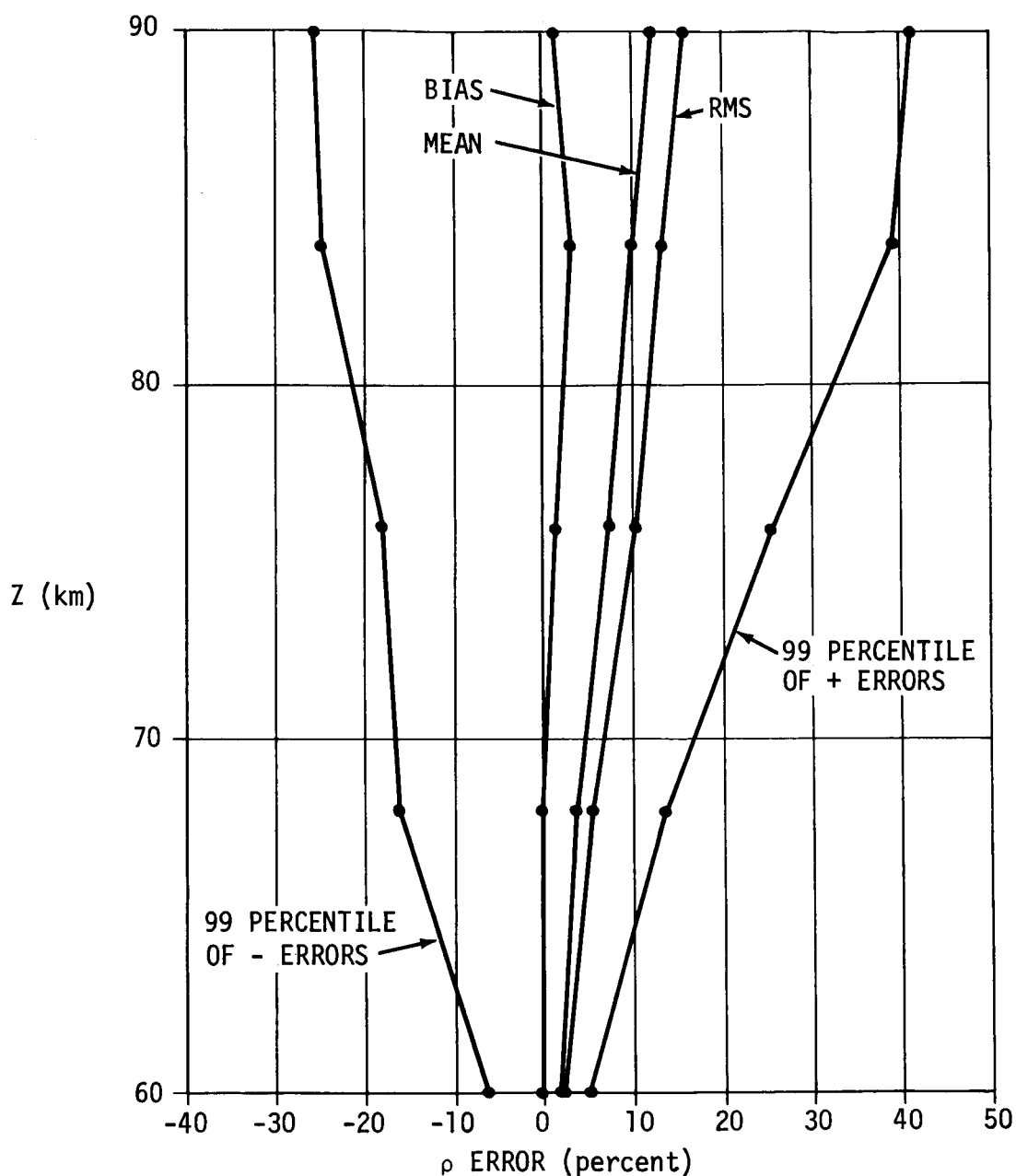
Figure 8. HEIGHT PROFILES OF VARIOUS ERROR QUANTITIES FOR THE EXTRAPOLATION
OF ρ FROM 52 KM, USING GRENADE DATA. MEAN ERROR IS FOUND BY EQ. 3,
RMS ERROR BY EQ. 4, AND BIAS BY EQ. 5. 99 PERCENTILES OF POSITIVE
AND NEGATIVE ERRORS ARE ALSO SHOWN.
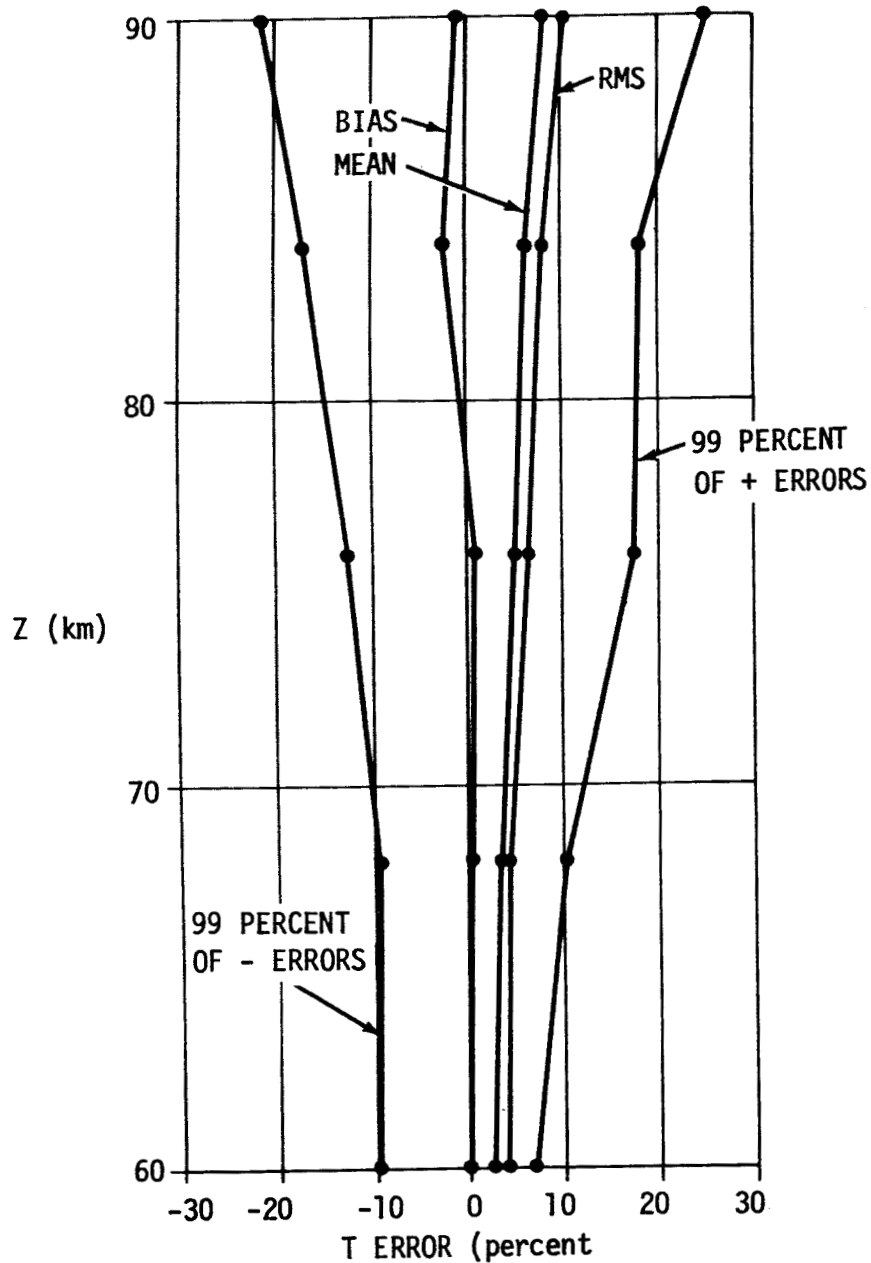
Figure 9. HEIGHT PROFILES OF VARIOUS ERROR QUANTITIES FOR THE EXTRAPOLATION OF T FROM 52 KM, USING GRENADE DATA. MEAN ERROR IS FOUND BY EQ. 3, RMS ERROR BY EQ. 4, AND BIAS BY EQ. 5. 99 PERCENTILES OF POSITIVE AND NEGATIVE ERRORS ARE ALSO SHOWN.
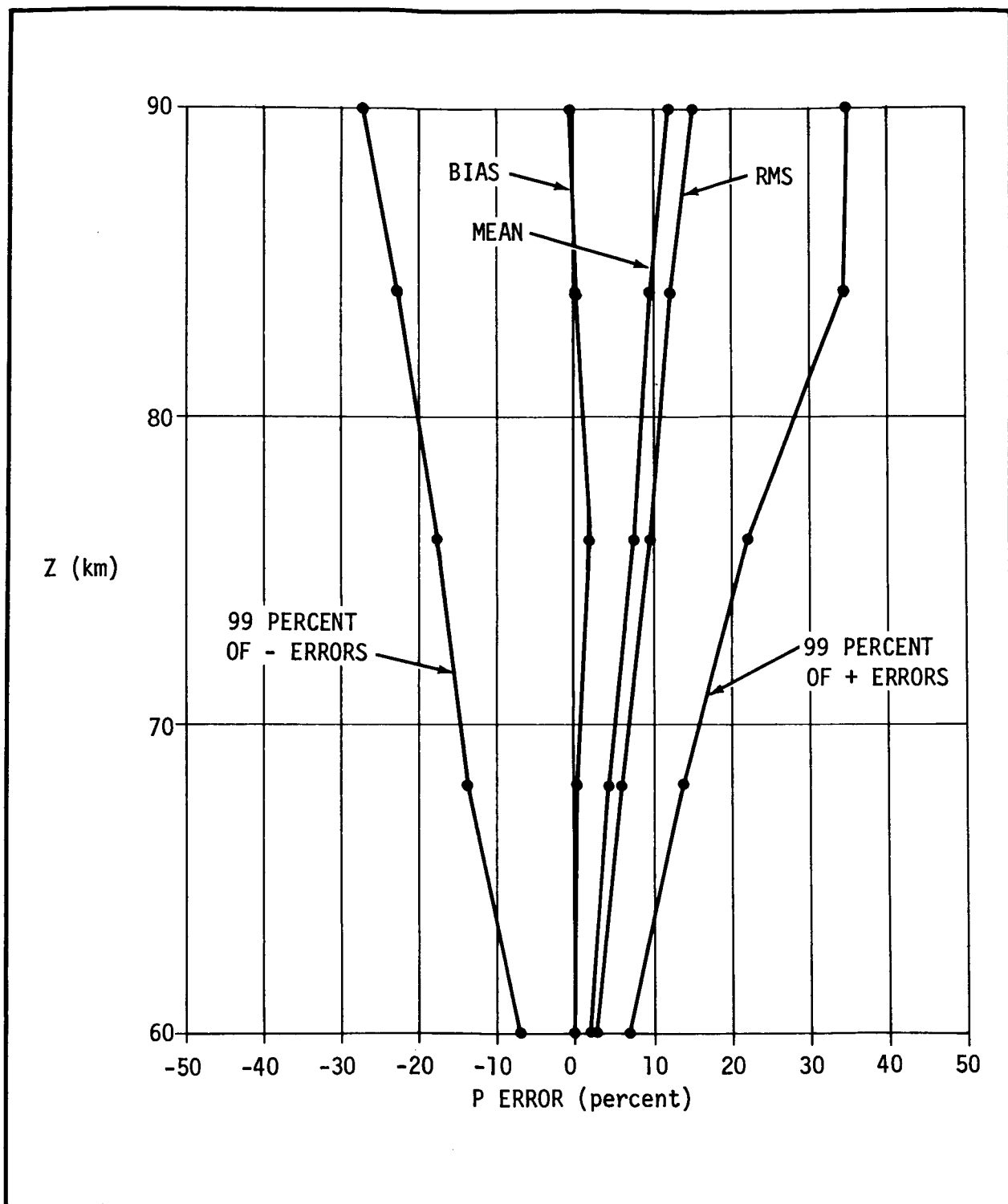
Figure 10. HEIGHT PROFILES OF VARIOUS ERROR QUANTITIES FOR THE EXTRAPOLATION OF P FROM 52 KM, USING GRENADE DATA. MEAN ERROR IS FOUND BY EQ. 3, RMS ERROR BY EQ. 4, AND BIAS BY EQ. 5. 99 PERCENTILES OF POSITIVE AND NEGATIVE ERRORS ARE ALSO SHOWN.
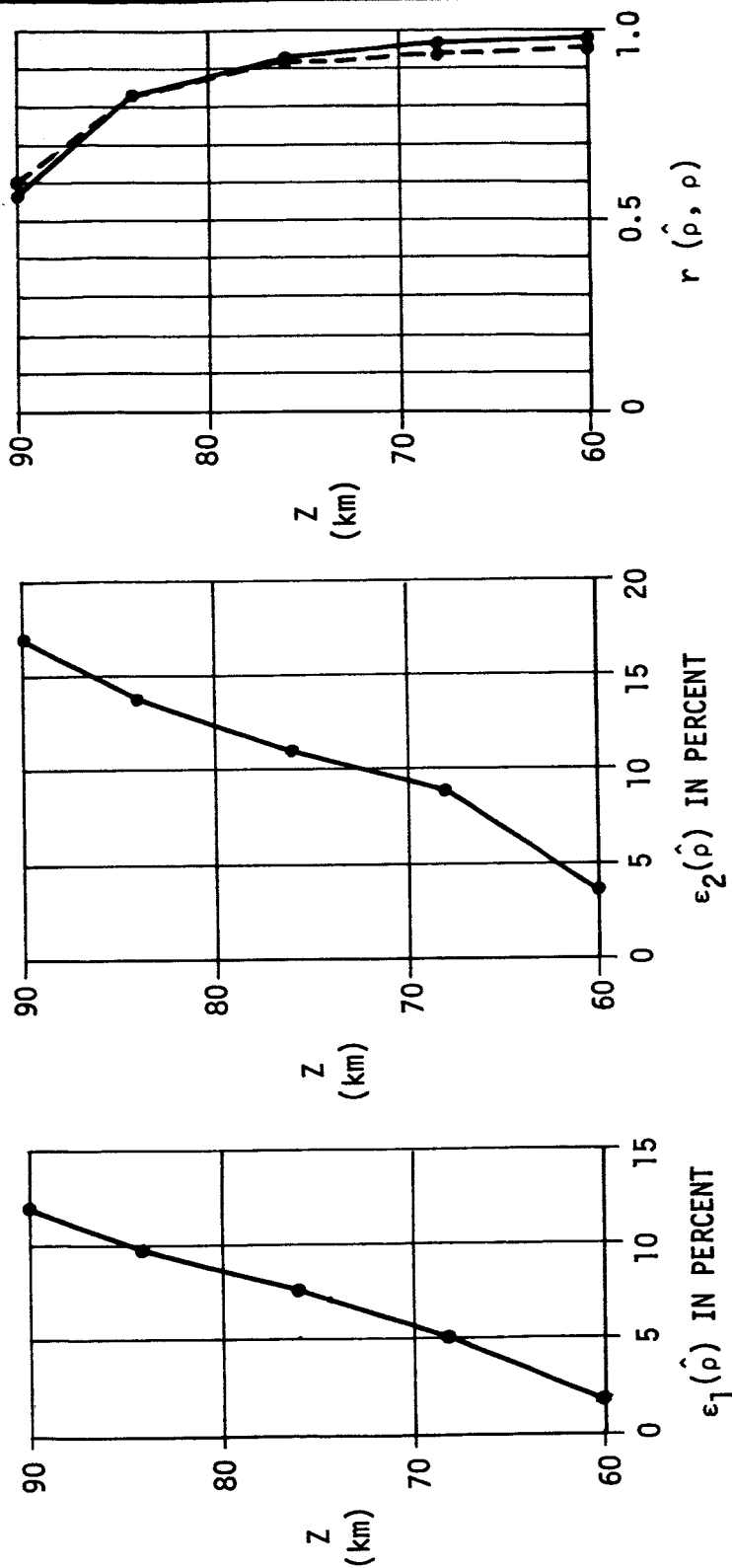
Figure 11. ACCURACY OF ESTIMATING ρ BY DIRECT EXTRAPOLATION, USING GRENADE DATA. MEAN ERROR ϵ_1 IS FOUND BY EQ. 3 AND RMS ERROR BY EQ. 4. $r(\hat{\rho}, \rho)$ IS THE CORRELATION COEFFICIENT BETWEEN ESTIMATED AND OBSERVED QUANTITIES AT THE DESIGNATED LEVELS. THE BROKEN CURVE IS FOR DIRECT EXTRAPOLATION AND THE CONTINUOUS CURVE IS FOR STEPWISE EXTRAPOLATION.

correlation coefficients between predicted and observed density at the various levels after direct extrapolation. There is a remarkable coincidence between the error curves, comparable pairs being within 1 percent at all levels. Although the density is easily obtained by direct regression, the computation of P and T must be carried on the same as before. In view of this, the absence of any improvement in the error quantities evidently rules out direct extrapolation in favor of step-by-step bootstrapping.

A second comparison test uses Groves' model (ref. 13), which lists internally consistent mean latitudinal values of ρ, T, and P at each 10 degrees latitude and each month of the year at 5-km intervals through the atmospheric zones being considered here. For each variable, there is a fairly constant rms error (Figures 12 through 14). When the final rms error results are placed upon these graphs, one sees an improvement of more than 10 percent over Groves' model at 60 km in ρ, and P falling to only 1 or 2 percent at 90 km. The temperature curves (Figure 13) are within 2 percent of each other all the way up. Of course, Groves' model does not give any longitudinal variation in any of the variables, so the closeness of the comparison curves at 90 km is not sufficient cause to throw out the extrapolation technique at that level. Rather, one may say that the extrapolation technique is capable of representing the variables over a 90-km chart with some uncertainty in the patterns, but with far more information content than Groves' model can produce.

Another experiment introduced an artificial temperature error at the base level of 52 km to note its effect upon outputs at higher levels (Figures 15 through 17). When integrating to get P at the top of a layer, the adjustment based upon US62 Standard Atmosphere was used throughout these calculations. Regarding ρ and P, it was found that most of the error incurred by artificially inducing a -10 percent or +10 percent error in T at 52 km integrates out as one proceeds upward, and nearly disappears at 90 km. In fact, when predicting temperature itself, most of the induced error is gone by the time one reaches 70 km. This performance is characteristic of a stable scheme which can tolerate some temperature uncertainty in the input data.

20
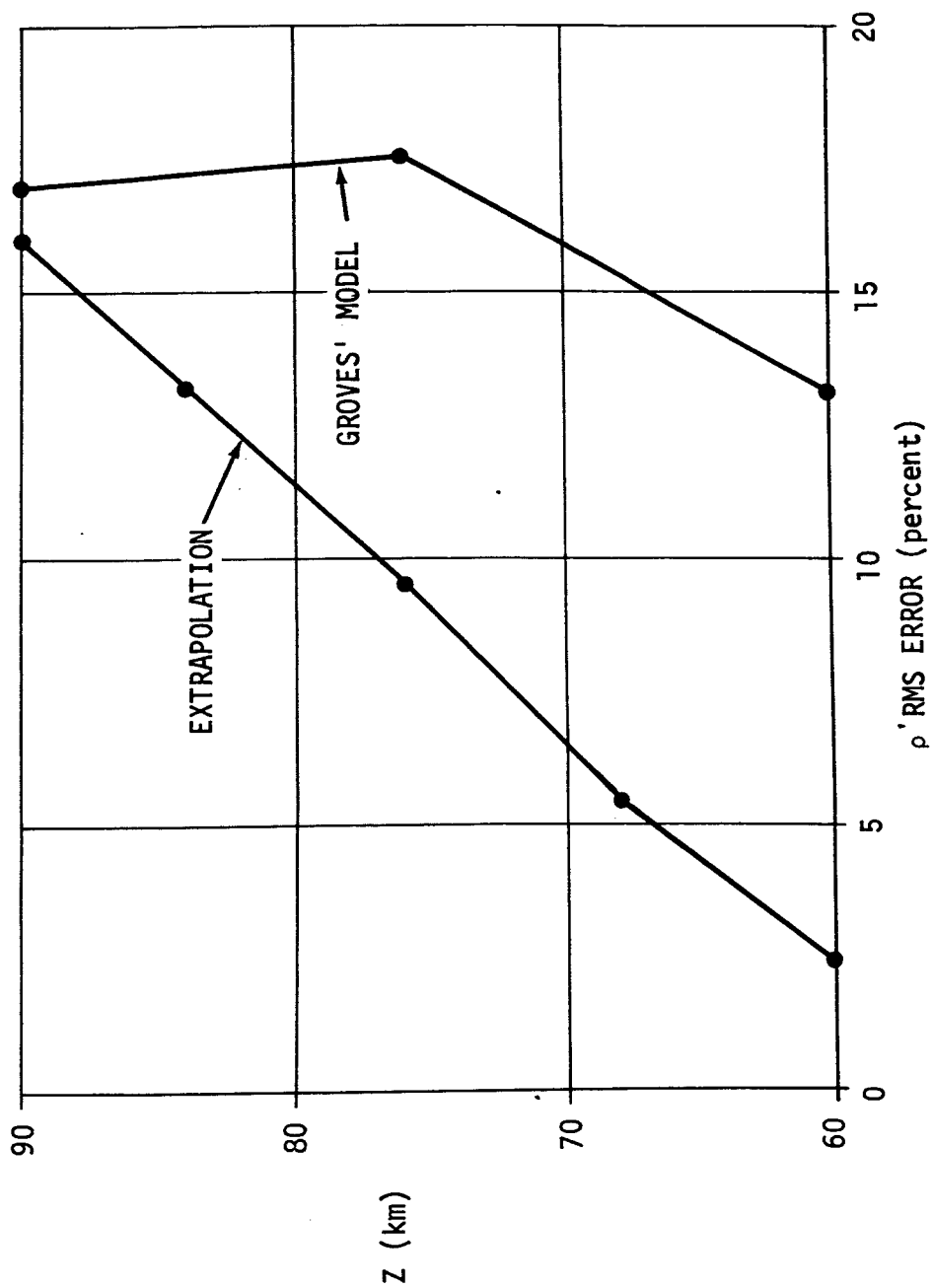
Figure 12. COMPARISON OF RMS ERROR IN ρ RESULTING FROM THE EXTRAPOLATION TECHNIQUE OF FIGURE 2 AND THE EMPLOYMENT OF GROVES' MODEL TO ESTIMATE ρ, USING GRENADE DATA
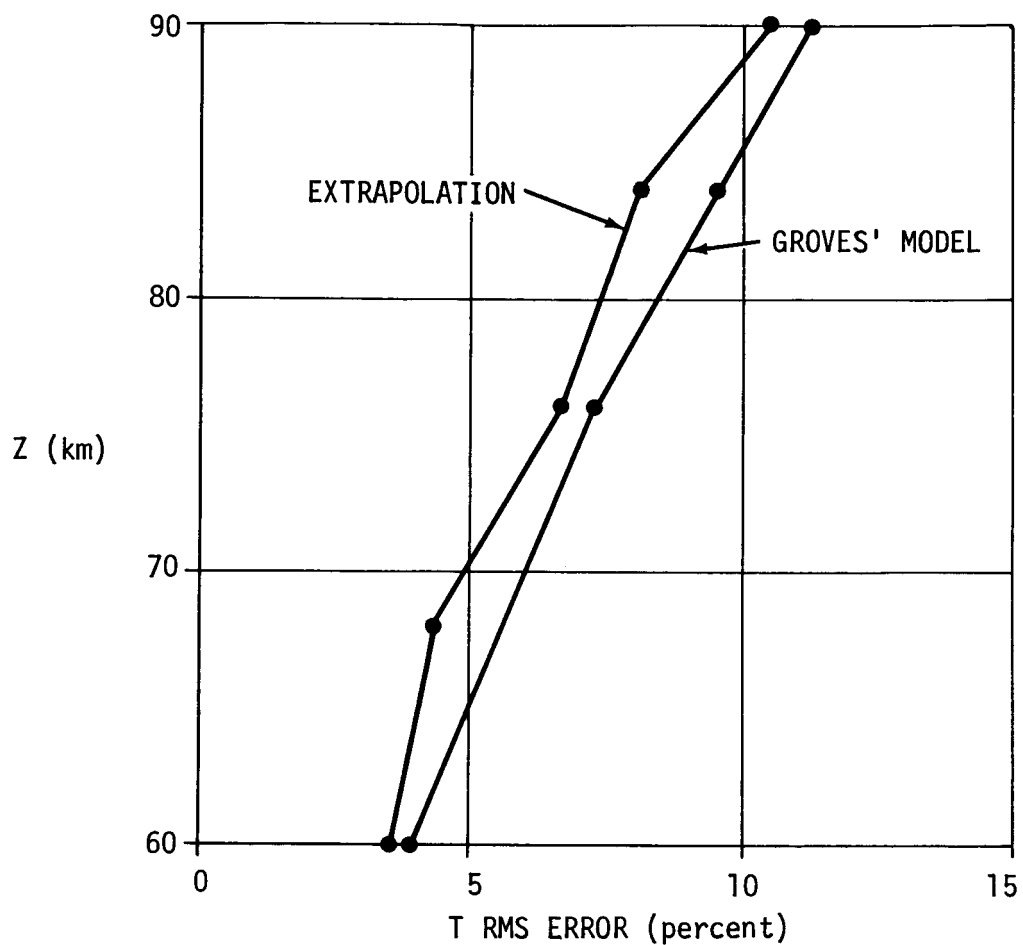
Figure 13. COMPARISON OF RMS ERROR IN T RESULTING FROM THE EXTRAPOLATION TECHNIQUE OF FIGURE 2 AND THE EMPLOYMENT OF GROVES' MODEL TO ESTIMATE T, USING GRENADE DATA
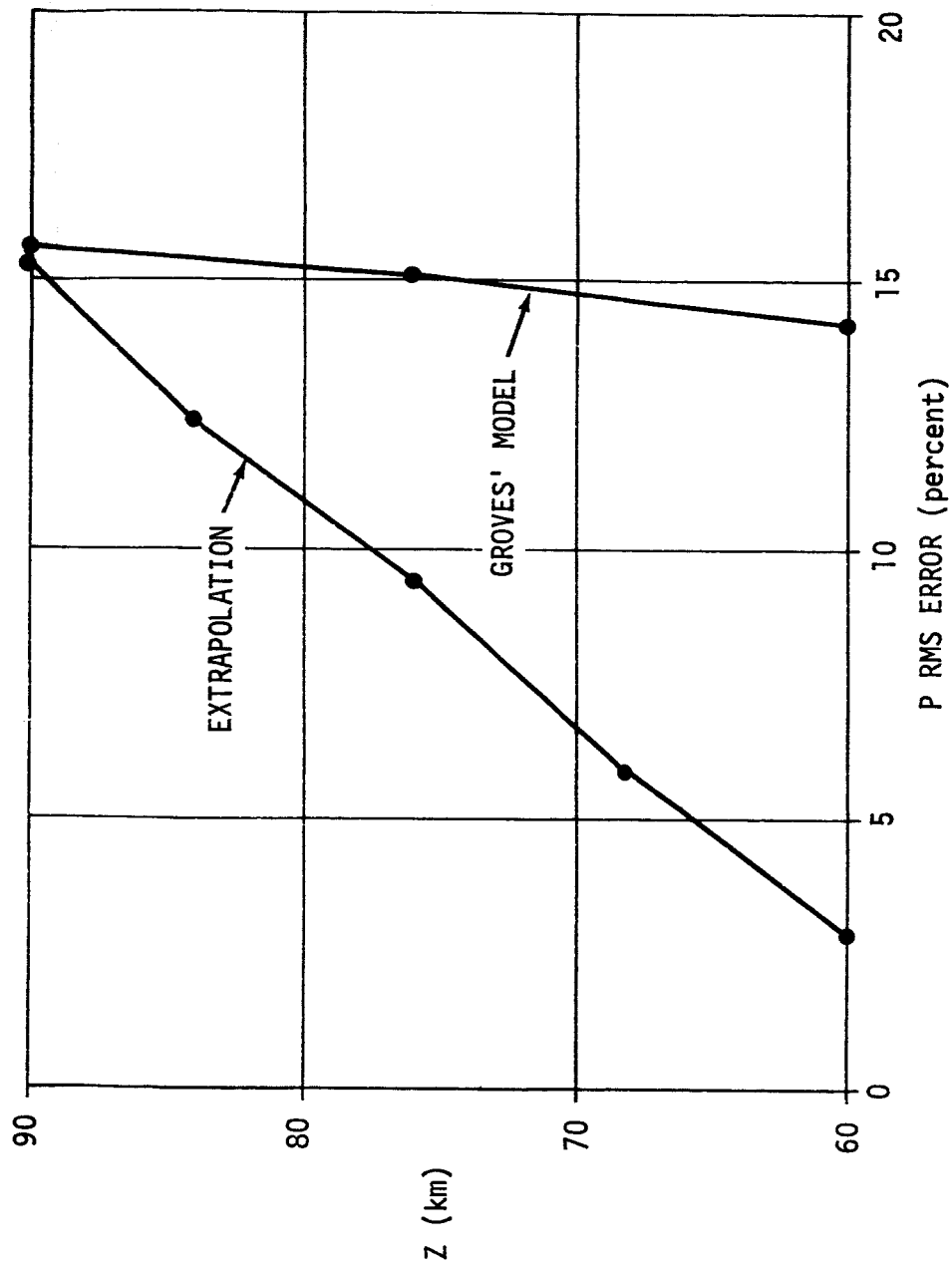
Figure 14. COMPARISON OF RMS ERROR IN P RESULTING FROM THE EXTRAPOLATION
TECHNIQUE OF FIGURE 2 AND THE EMPLOYMENT OF GROVES' MODEL TO
ESTIMATE P, USING GRENADE DATA

23
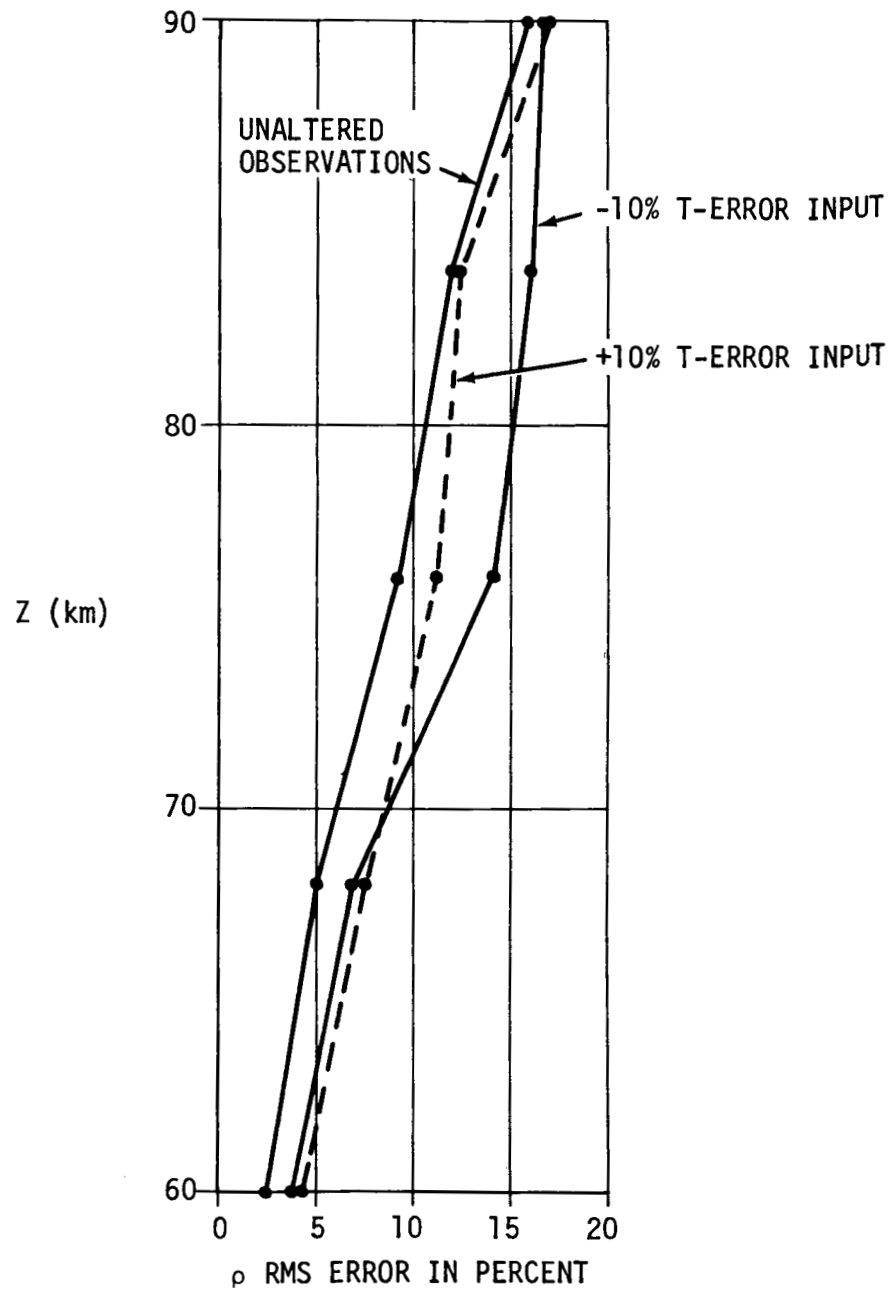
Figure 15.   EFFECT ON ρ OF INTRODUCING ERRORS OF -10% AND +10% IN T AT THE BASE
LEVEL OF 52 KM, USING GRENADE DATA
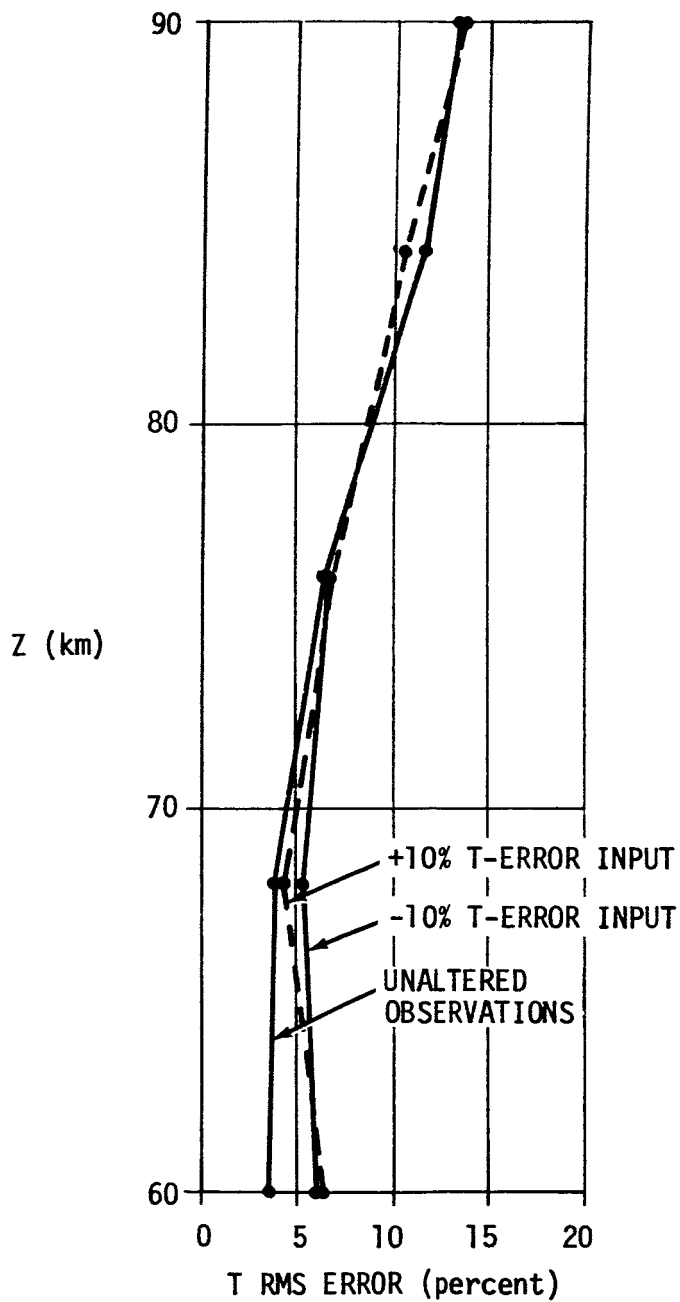
Figure 16.   EFFECT ON T OF INTRODUCING ERRORS OF -10% AND +10% IN T AT THE BASE
LEVEL OF 52 KM, USING GRENADE DATA
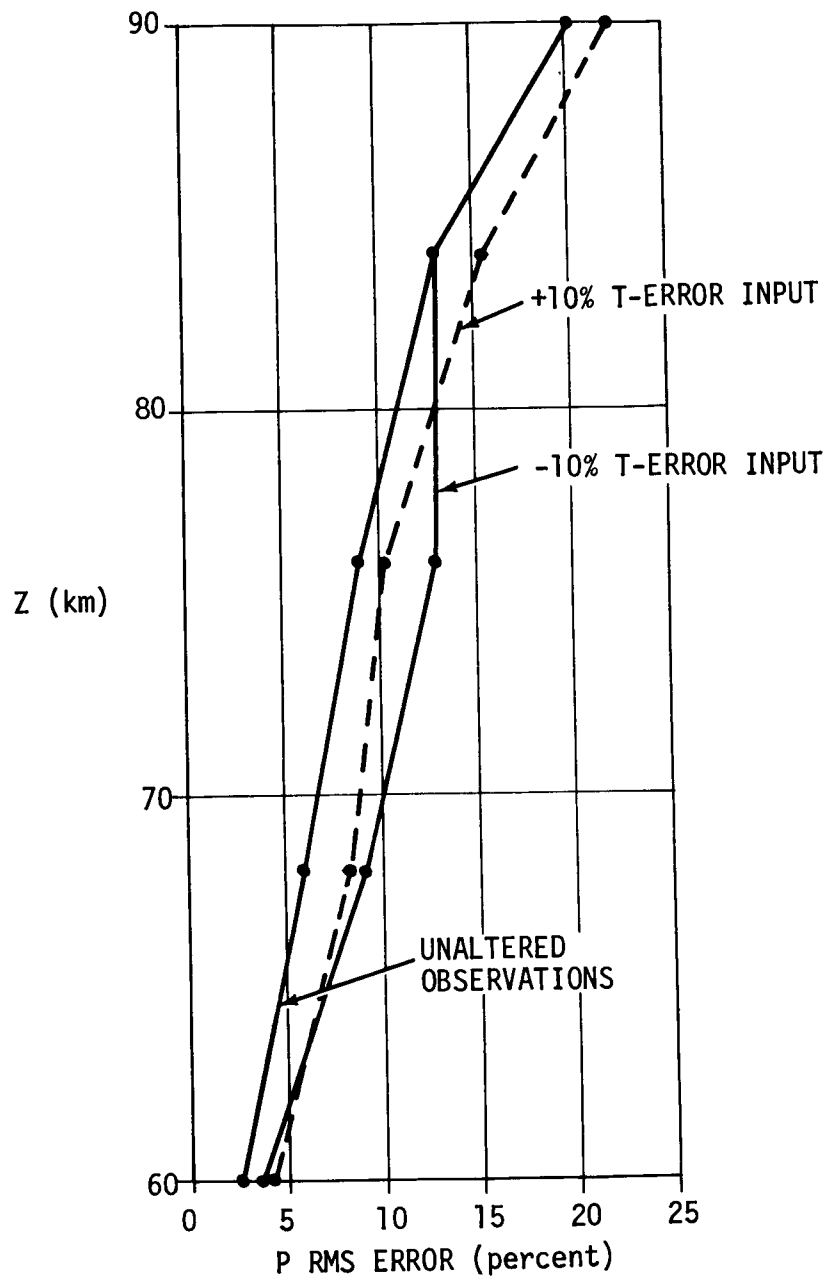
Figure 17. EFFECT ON P OF INTRODUCING ERRORS OF -10% AND +10% IN T AT THE BASE LEVEL OF 52 KM, USING GRENADE DATA.

Section IV

APPLICATION TO SECTIONAL NORTH AMERICAN CHARTS

The sectional North American charts referred to in the Introduction were
prepared by the Staff of the Upper Air Branch, National Meteorological Center
for the quiet solar period from 1964 to 1966 (ref. 14), and they include 50
weekly midseasonal maps for North America and adjacent oceans. Chart analyses
were carried out by that group at 5, 2, and 0.4-mb levels, and grid values
were supplied the authors for geopotential height and temperature. The grid
area extends from 40 degrees west longitude to 170 degrees east longitude, and
from 10 degrees north latitude to the North Pole. The spacing in both grid
directions is 5 degrees.

Estimates of the error in the height data at the 5-mb, 2-mb, and 0.4-mb
levels are difficult to make. However, Johnson (ref. 15) reports a root-mean-
square height difference of 90 meters and 2.4 degrees C at 10 mb over North
America. He also states that a large part of the 10-mb error is due to off-
level extrapolated reports. If we assume a similar error for the 5-mb, 2-mb,
and 0.4-mb analyses, then the gridded map data would be comparable to station
sounding data where there is a random error due to the uncertainty in the
height of the rawinsonde instrument from which the base pressure for the rocket-
sonde or grenadesonde is obtained. If one assumes the map analysis errors
are random, then mean values obtained from the grid data should compare in
accuracy with the means of the station data.

A computer program developed by Miller (ref. 16) is capable of interpo-
lating among the three map levels to give density (ρ), pressure (P), and
temperature (T) estimates at selected heights. These estimates are obtained
through the use of a model temperature profile based upon T values at map
levels and the thickness of the intervening layer. The interpolation program
is modified somewhat in this study in that the model temperature profile is
used to obtain the mean temperature between the constant pressure surface and
the maximum or minimum temperature at the midpoint of the layer. This mean
temperature is then used with the isothermal form of the hydrostatic equation,

equation (6), to compute the pressure at the midpoint of the layer. This refinement of the interpolation procedure reduces the error in the pressure estimates by 40 percent. The comparison test is based on a sample of 112 rocket soundings taken at Cape Kennedy. Table 2 gives the relative differences in percent between the estimates of ρ, P, and T obtained from the interpolation program and the observed values in the Cape Kennedy sample. The mean errors for levels between 36 km and 56 km are as follows: ρ, 0.85 percent; P, 0.26 percent; T, 0.79 percent. The maximum errors for more than 2000 comparisons between observed and derived quantities are: ρ, 5.7 percent; P, 1.7 percent; and T, 6.7 percent.

Since 52 km has been selected as the base level for extrapolation, the magnitudes of the error quantities at this level are especially interesting. For the Cape Kennedy data, the mean errors are as follows: ρ, 1.22 percent; P, 0.35 percent; T, 1.21 percent. The maximum errors are: ρ, 4.0 percent; P, 1.3 percent; T, 3.84 percent.

The above comparisons accept the observed values as true, thus they include the unknown random and systematic errors of measurement. For T, these errors are reported by Smith, Theon, Katchen, and Swartz (ref. 4) to be 0.4 percent to 2.0 percent at 50 km. Comparing the latter values with those given above for the interpolation model, one may conclude that approximately half of the error lies in the measurement and half is in the model.

Fortunately, the pressure, which is the variable with the greatest weight in the extrapolation to higher levels, is the most accurate parameter obtained from the interpolation program. At the base level of 52 km, its error values are indeed small.

Example of January 8, 1964. To illustrate the application of the technique described in Section II to produce stratospheric and mesospheric synoptic charts, a case study of January 8, 1964 data will now be presented. Figures 18 and 19 show the 2-mb and 0.4-mb constant pressure levels from which the 52-km constant height level is produced. The major synoptic features of the 2-mb level are a deep low east of Greenland with a trough extending

Table 2. DIFFERENCE BETWEEN INTERPOLATED AND OBSERVED VALUES IN
PERCENT FOR 112 SOUNDINGS AT CAPE KENNEDY

HEIGHT (meters)	MEAN PRESSURE ERROR (%)	RMS PRESSURE ERROR (%)	MEAN DENSITY ERROR (%)	RMS DENSITY ERROR (%)	MEAN TEMPERATURE ERROR (%)	RMS TEMPERATURE ERROR (%)
36000.00	.00	.00	.01	.01	.00	.00
37000.00	.21	.24	.67	.86	.73	.94
38000.00	.28	.33	.58	.73	.66	.88
39000.00	.22	.27	.69	.83	.75	.89
40000.00	.21	.26	.72	.92	.70	.88
41000.00	.25	.30	.80	1.04	.73	.94
42000.00	.18	.22	.57	.77	.54	.71
43000.00	.02	.07	.11	.48	.08	.42
44000.00	.20	.24	.89	1.33	.83	1.24
45000.00	.30	.36	1.06	1.40	.97	1.30
46000.00	.33	.41	1.00	1.32	1.00	1.30
47000.00	.34	.44	.76	1.06	.78	1.02
48000.00	.33	.44	.77	1.12	.77	1.09
49000.00	.36	.48	1.18	1.54	1.14	1.46
50000.00	.37	.48	1.38	1.65	1.16	1.39
51000.00	.37	.48	1.35	1.68	1.11	1.39
52000.00	.35	.44	1.22	1.50	.98	1.21
53000.00	.29	.38	1.14	1.42	.94	1.19
54000.00	.32	1.07	.89	1.20	.76	1.05
55000.00	.10	.15	.44	.63	.38	.57
56000.00	.00	.00	.07	.09	.00	.00
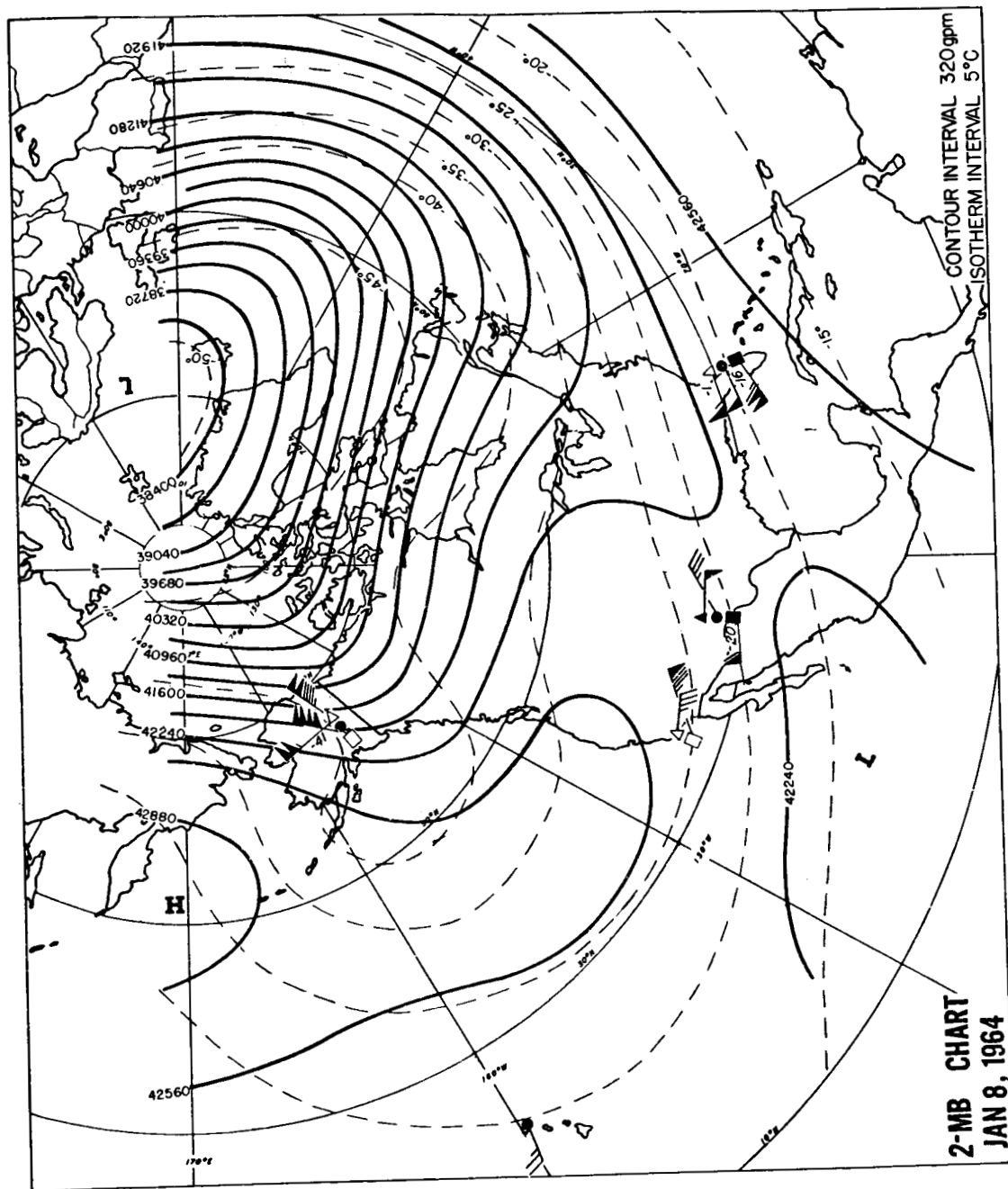
Figure 18.   NATIONAL METEOROLOGICAL CENTER 2-MB GEOPOTENTIAL HEIGHT AND
TEMPERATURE ANALYSES

30

0.4-MB CHART
JAN 8, 1964

CONTOUR INTERVAL 320gpm
ISOTHERM INTERVAL 5°C
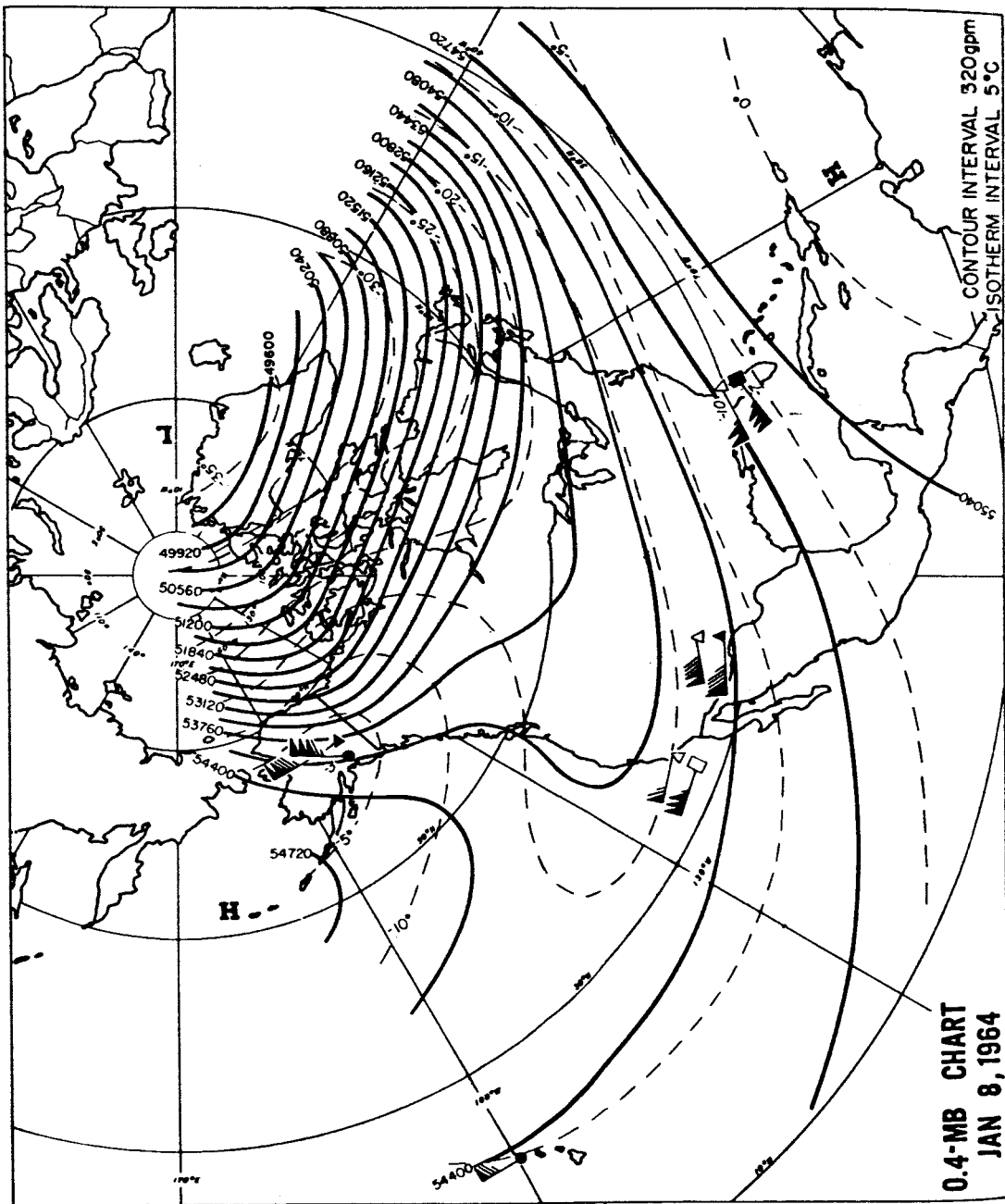
Figure 19. NATIONAL METEOROLOGICAL CENTER 0.4-MB GEOPOTENTIAL HEIGHT AND
TEMPERATURE ANALYSES

31

southwestward to Texas and a ridge extending from the Eastern Pacific to the Pacific Coast. The most interesting feature in the 2-mb temperature field is the strong thermal trough over western Canada and Alaska which extends into the Gulf of Alaska.

The contour patterns at the 0.4-mb surface are similar to those at 2-mb, except that the trough through the United States is displaced westward and the ridge of high pressure from the Pacific is less pronounced and is farther north. The thermal trough at 2 mb over Alaska is replaced by a strong thermal ridge at the 0.4-mb level. The height of the 2-mb surface is approximately 43 km in the center of the Pacific high cell and 39 km in the low near Greenland. The corresponding heights of the 0.4-mb surface are approximately 55 km and 50 km.

For each 5 degrees latitude and 5 degrees longitude, the geopotential height and temperature for the 2-mb and 0.4-mb surfaces are the data inputs to the computer program. The program converts the geopotential height to geometric height, correcting the acceleration of gravity for both altitude and latitude at each grid point. The interpolation program discussed in Section II then produces pressure, temperature, and density values over the grid for the 52-km height surface, which is required for extrapolation to higher levels. Figure 20 shows the fields of temperature and pressure for the 52-km level based on the grid values for January 8, 1964. The corresponding density field is shown in Figure 21.

The 52-km pressure pattern is very similar to the 0.4-mb contour field, which illustrates the strong mutual dependence of pressure and height. At this level, a change of 10 meters in the height of the 0.4-mb pressure surface is equivalent to a change of 0.001 mb in the pressure at 52 km. The isobars on the 52-km pressure chart are drawn for an interval of 0.031 mb, which is a change of about 5 percent of the US62 Standard Atmosphere. Thus the isobars are labeled in percent departure from US62 as well as in millibars. The 52-km pressure ranges from 0.640 to 0.295 mb, which is a departure of +3 percent to −53 percent in relation to the US62 Standard Atmosphere.

32
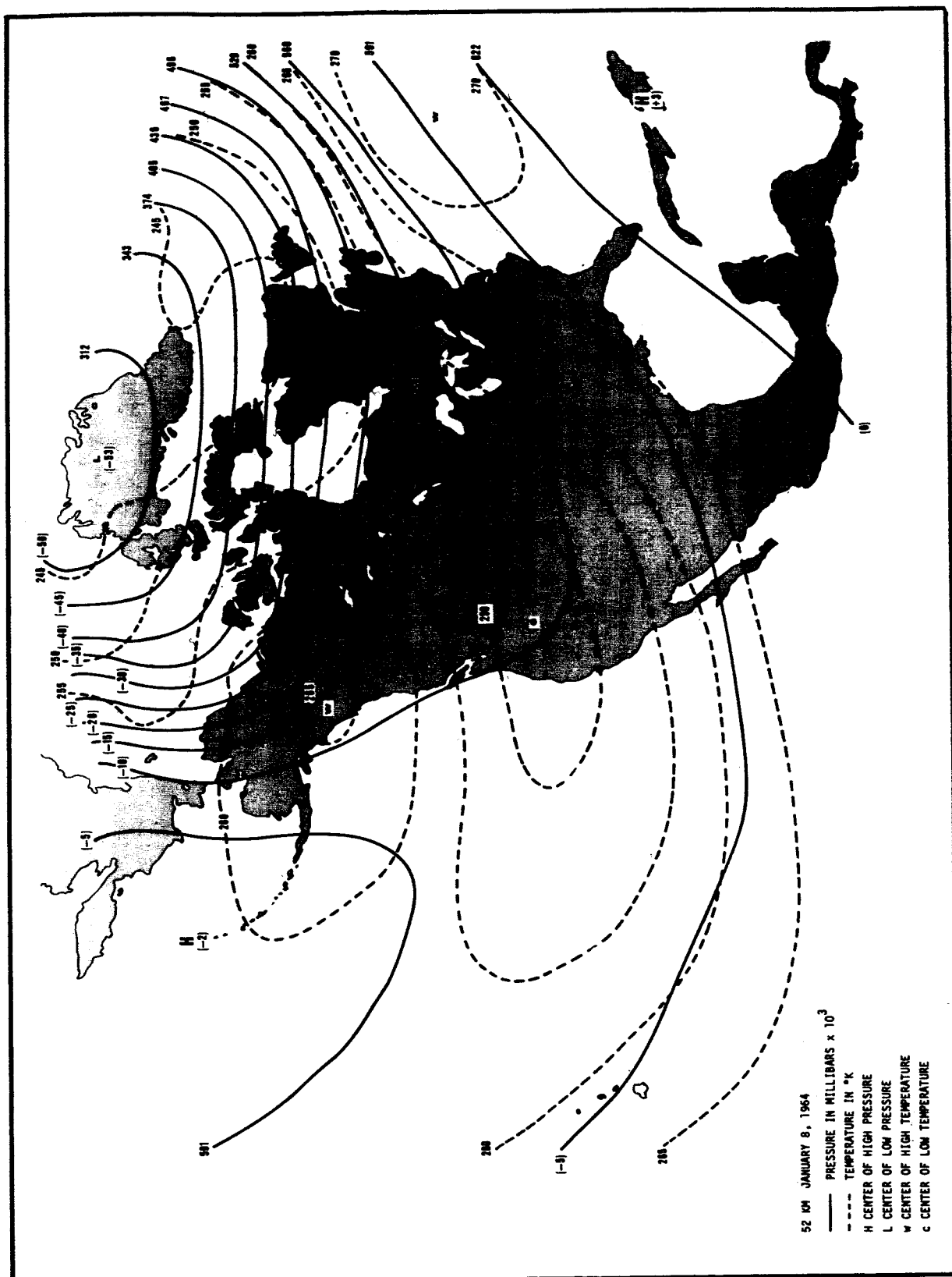
Figure 20. 52-KILOMETER PRESSURE AND TEMPERATURE ANALYSES

52 KM JANUARY 8, 1964

——— PRESSURE IN MILLIBARS × 10³
– – – – TEMPERATURE IN °K
H CENTER OF HIGH PRESSURE
L CENTER OF LOW PRESSURE
w CENTER OF HIGH TEMPERATURE
c CENTER OF LOW TEMPERATURE
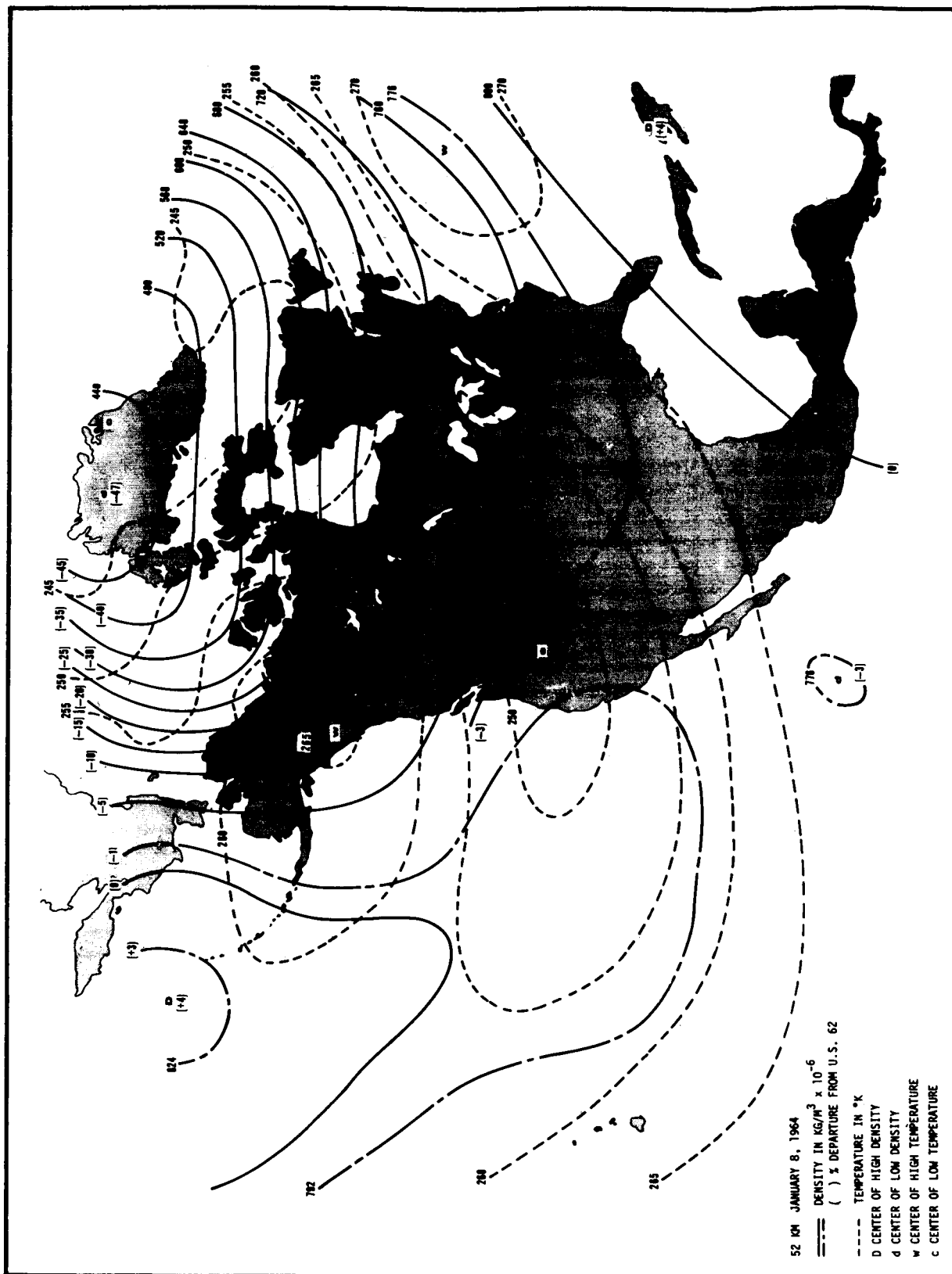
Figure 21. 52-KILOMETER DENSITY AND TEMPERATURE ANALYSES

52 KM JANUARY 8, 1964

DENSITY IN KG/M³ x 10⁻⁶
( ) % DEPARTURE FROM U.S. 62

TEMPERATURE IN °K
D CENTER OF HIGH DENSITY
d CENTER OF LOW DENSITY
W CENTER OF HIGH TEMPERATURE
c CENTER OF LOW TEMPERATURE

The 52-km temperature field resembles more closely the 0.4-mb temperature field than the 2-mb level. Since the 52-km surface intersects the 0.4-mb pressure surface, this is to be expected.

The 52-km density chart illustrates two facts reported earlier by Quiroz (ref. 17) and by Quiroz and Miller (ref. 10). First, pressure dominates over temperature in determining the density at a level, with the latter variable contributing to the minor detail in the density structure. An example of the temperature influence in Figure 21 is the ridging in the density pattern from the Pacific Coast to the Great Lakes. Note that whereas the pressure at 52 km has a deviation of +3 percent to -53 percent from the US62 Standard Atmosphere, the 52-km density has a deviation ranging from +4 percent to -47 percent.

Second, the correlation between the pressure and density at the same level is less than that between density and the pressure at an altitude which is one scale height less. This is illustrated by the almost exact correspondence between the 52-km density field and the ridge of high pressure from the Pacific Ocean to the West Coast on the 2-mb chart (Figure 18). The height of the latter chart is about one scale height below 52 km.

At 60 km, the density pattern (Figure 22) is quite similar to the 0.4-mb pressure pattern. In fact, the 60-km density field is generally more like the 0.4-mb pattern than the 52-km pressure pattern, from which the density at 60-km is derived by regression. Again, this illustrates the high dependence of density on height and pressure. It also illustrates the fact that in areas of weak pressure gradient and strong temperature gradient, the temperature term in the bivariate regression changes the density pattern at the higher level from that of the pressure at the lower level, where the extrapolation begins. This is shown in the 60-km density field in the Pacific Northwest.

The 60-km temperature field shows little correlation with the 60-km density field and only a partial correlation with the 52-km temperature field. The Alaskan thermal ridge persists, and a similar thermal pattern is seen in the low latitudes. However, the cold pocket at 52-km over Greenland disappears, and is replaced by a warm center over Northern Greenland.
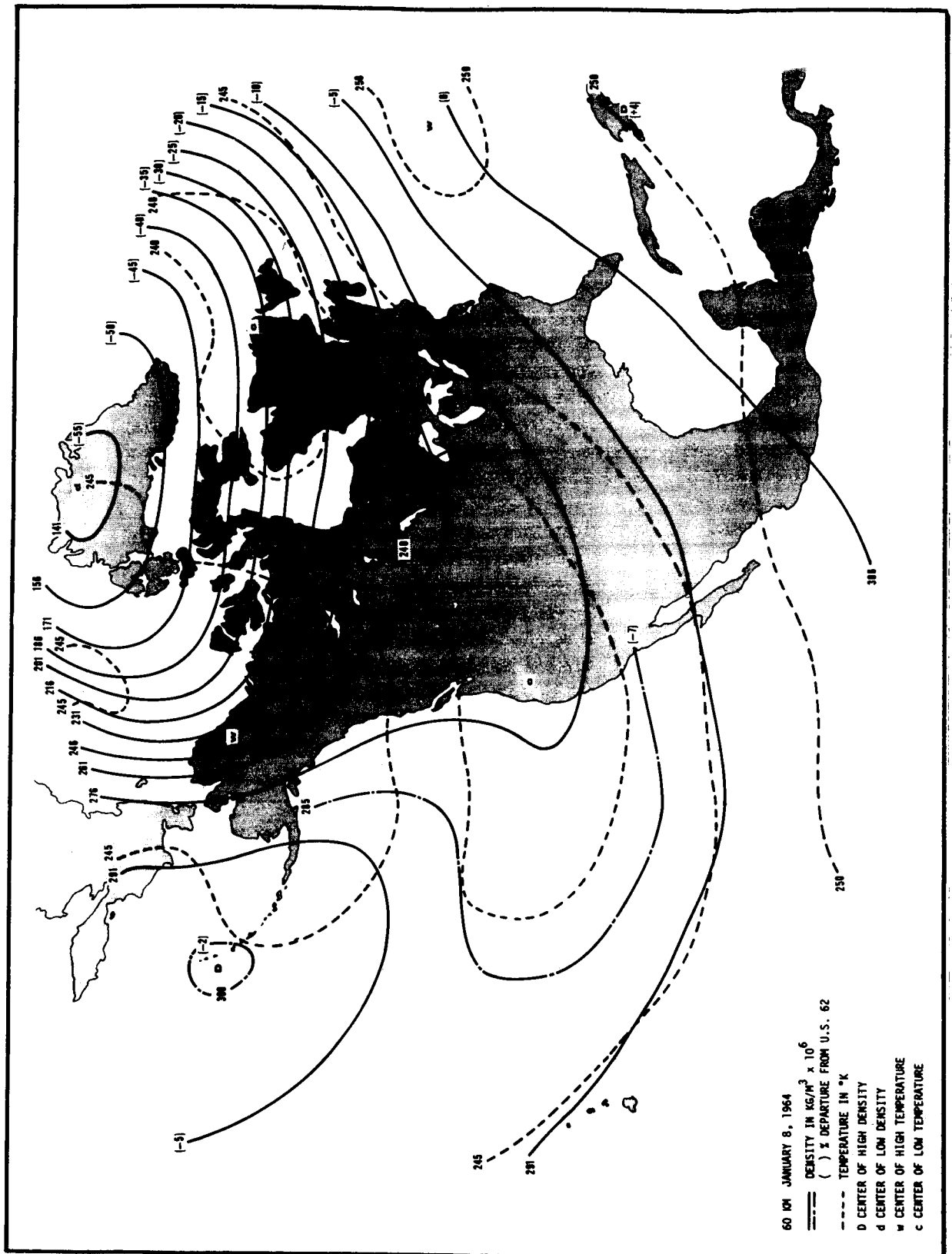
Figure 22. 60-KILOMETER DENSITY AND TEMPERATURE ANALYSES

60 KM JANUARY 8, 1964

DENSITY IN KG/M³ x 10⁶
( ) % DEPARTURE FROM U.S. 62
TEMPERATURE IN °K

D CENTER OF HIGH DENSITY
d CENTER OF LOW DENSITY
W CENTER OF HIGH TEMPERATURE
c CENTER OF LOW TEMPERATURE

Related to the US62 Standard Atmosphere, the density at 60 km has a high of +4 percent near Haiti and a low of -55 percent over Greenland. Great variation in the density gradient is indicated by the contrast between wide spacing of the contours over the western United States and tight packing north of Siberia and Alaska.

At 90 km, the density pattern (Figure 23) is similar to that at 60 km. With reference to the US62 Standard Atmosphere, the highest densities are found near Haiti (+13 percent) and in the Bering Sea (+10 percent). The major low density center is located near Greenland (-39 percent).

The 90-km temperature field (Figure 23) exhibits a reversal from the 52-km pattern, with cold temperatures now to the south and warm temperatures to the north, with the exception of the Greenland area where a cold pocket remains. The maximum temperature difference from north to south is 14 degrees K, which is about 54 percent of the value given by Groves' model interpolated to January 8. This can easily be explained as the variation from the mean in an individual case. A 3 percent decrease in temperature at 15 degrees N and a 5 percent increase at 70 degrees N would produce a latitudinal variation in excess of Groves' model.

Example of January 3, 1968. The data sample from 1964-1966 does not include a major stratospheric warming. However, this kind of anomaly in the structure parameters appears in the published charts for 5, 2, and 0.4 mb (ref. 18) on January 3, 1968. Therefore, the geopotential heights and temperatures have been read from those charts and processed by the extrapolation program.

Discussions of this case by Williams and Miers (ref. 19), Quiroz (ref. 20), and others indicate that the warming began over Greenland at 45 km about December 12, 1967 and largely disappeared by January 10, 1968. A very warm stratosphere is evident over Central Canada at 36 km (Figure 24), with the center of high temperature being nearly 50°C greater than our mean value for January, and 4 to 5 standard deviations greater than our statistical value for January (Section V). The warm center is found near the Pacific Coast at

Figure 23. 90-KILOMETER DENSITY AND TEMPERATURE ANALYSES

90 KM JANUARY 8, 1964

—— DENSITY IN KG/M^3 x 10^8

( ) % DEPARTURE FROM U.S. 62

– – – TEMPERATURE IN °K

D CENTER OF HIGH DENSITY

d CENTER OF LOW DENSITY

W CENTER OF HIGH TEMPERATURE

c CENTER OF LOW TEMPERATURE
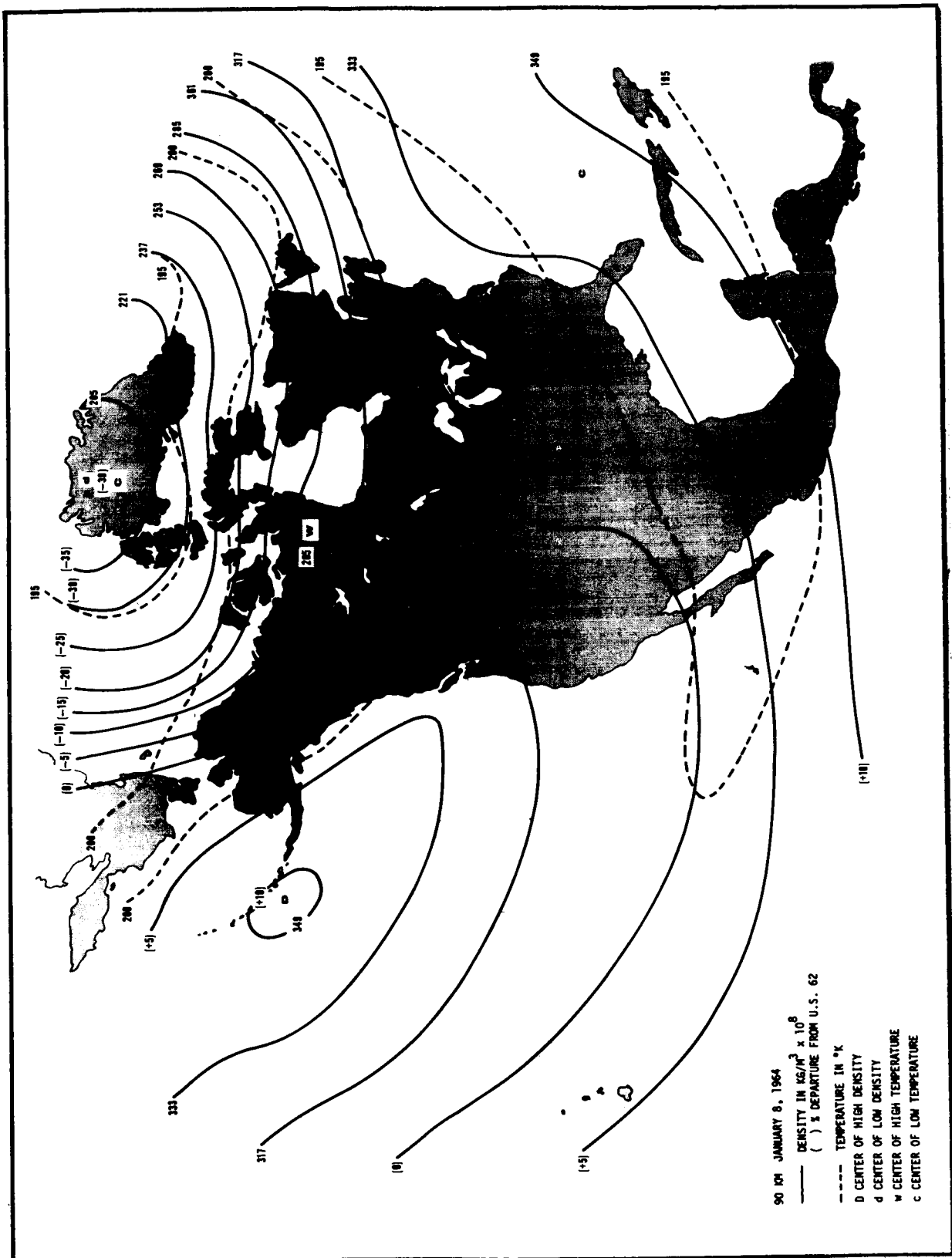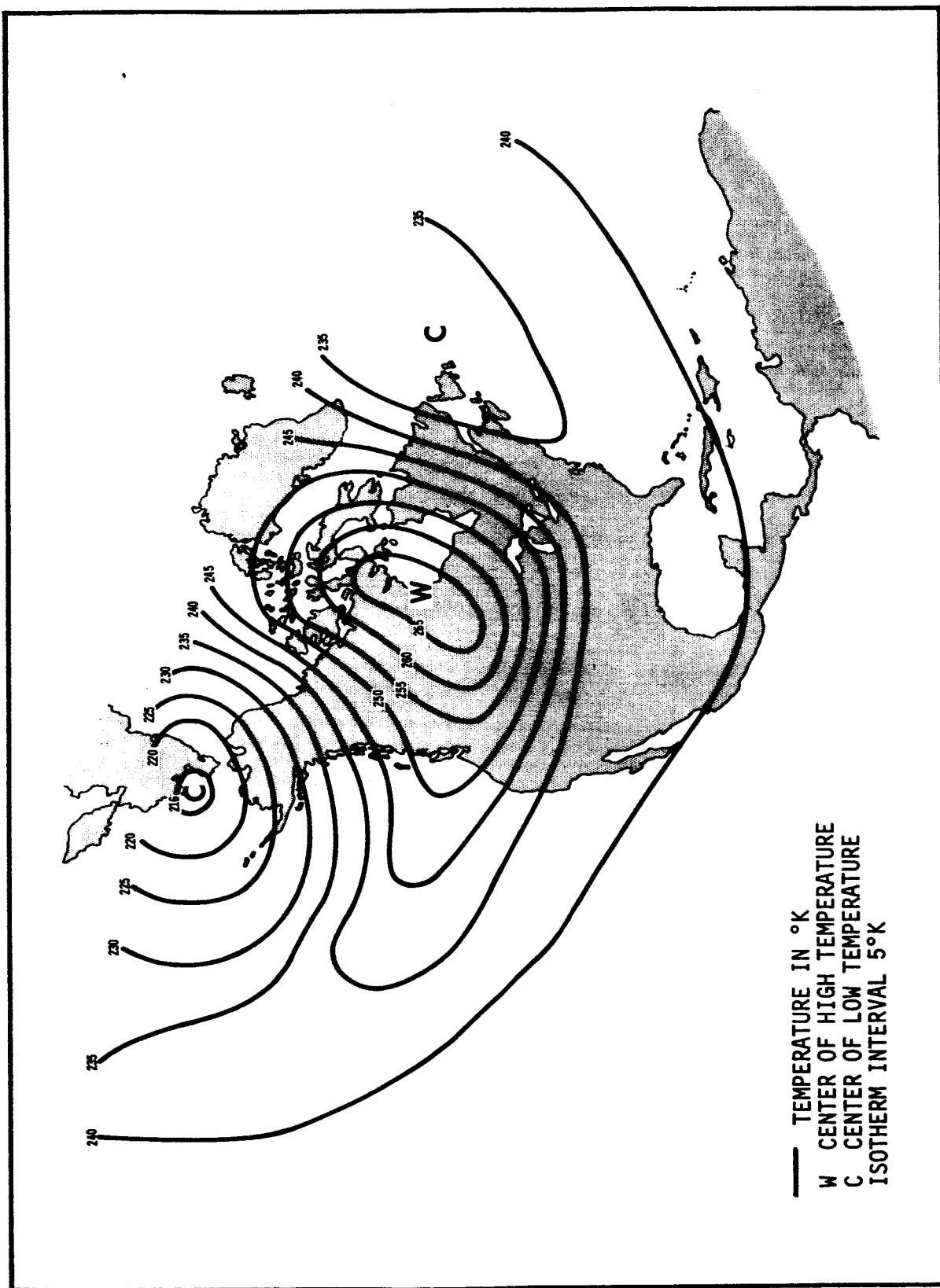
Figure 24. 36-KILOMETER TEMPERATURE ANALYSIS FOR STRATOSPHERIC WARMING CASE, 3 JANUARY 1968

TEMPERATURE IN °K
W CENTER OF HIGH TEMPERATURE
C CENTER OF LOW TEMPERATURE
ISOTHERM INTERVAL 5°K

44 km in a weaker state (Figure 25), and relatively cool air predominates at mesospheric levels over this region (Figures 26, 27).

Each of the density charts for 36 km (Figure 28) and 44 km (Figure 29) has a low center over Canada which corresponds to a temperature maximum at the same level. At greater altitudes, the density field becomes somewhat flat at 52 km (Figure 30), then attains very strong gradients higher in the mesosphere (Figure 31), especially on the northern side of the Pacific high density area.

Since 52 km is the base level for vertical extrapolation, the 52-km pressure chart is also shown (Figure 32). As in the previous example, this chart is very similar to the 0.4-mb geopotential height field, and its deep trough pattern over the continent again resembles the density field one scale height higher (Figure 33) more than the density field at the same level. The indicated flow is basically west to east at 52 km, but the 5-mb chart (ref. 18) shows a disruption of this flow in mid-stratosphere.

The 90 km charts for density (Figure 34), pressure (Figure 35) and temperature (Figure 36) contain the uncertainties of a regression-extrapolation scheme operating upon very anomalous data. The density field is not unlike that of the previous example at 90 km (Figure 23), but the densities are 5-10 percent greater throughout. The pressure pattern is nearly circumpolar in the wintertime sense on the poleward side of 50 degrees N, but complex elsewhere. The temperature chart has a discontinuous warm band centered at 65 degrees N, so one may conclude that the estimated values at the base of the thermosphere produce different patterns than are found in the mesosphere or stratosphere. Above the site of the stratospheric warming, there is a tendency to top a cold mesosphere with a warm thermosphere, but the extrapolation method does not provide support for conclusive statements about the thermosphere.

The straight line drawn in Figure 36 gives the position of a cross-section through the stratospheric warming zone. The anomalies in temperature and density for eight grid points along this line are analyzed in Figures 37 and 38, respectively. These anomalies represent departures from the mean values for January which are presented in the following section.
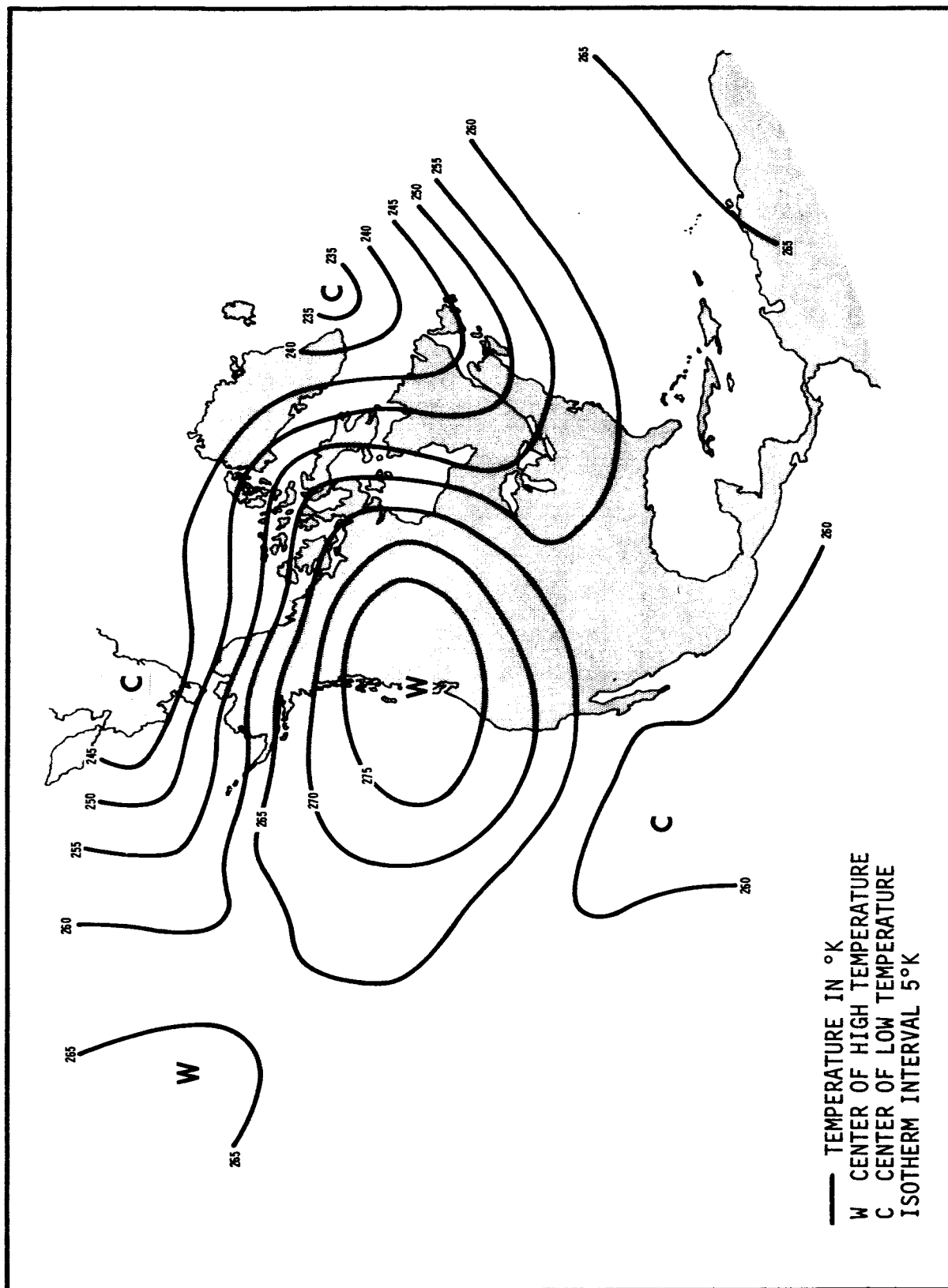
Figure 25. 44-KILOMETER TEMPERATURE ANALYSIS FOR STRATOSPHERIC WARMING CASE, 3 JANUARY 1968

TEMPERATURE IN °K
W CENTER OF HIGH TEMPERATURE
C CENTER OF LOW TEMPERATURE
ISOTHERM INTERVAL 5°K
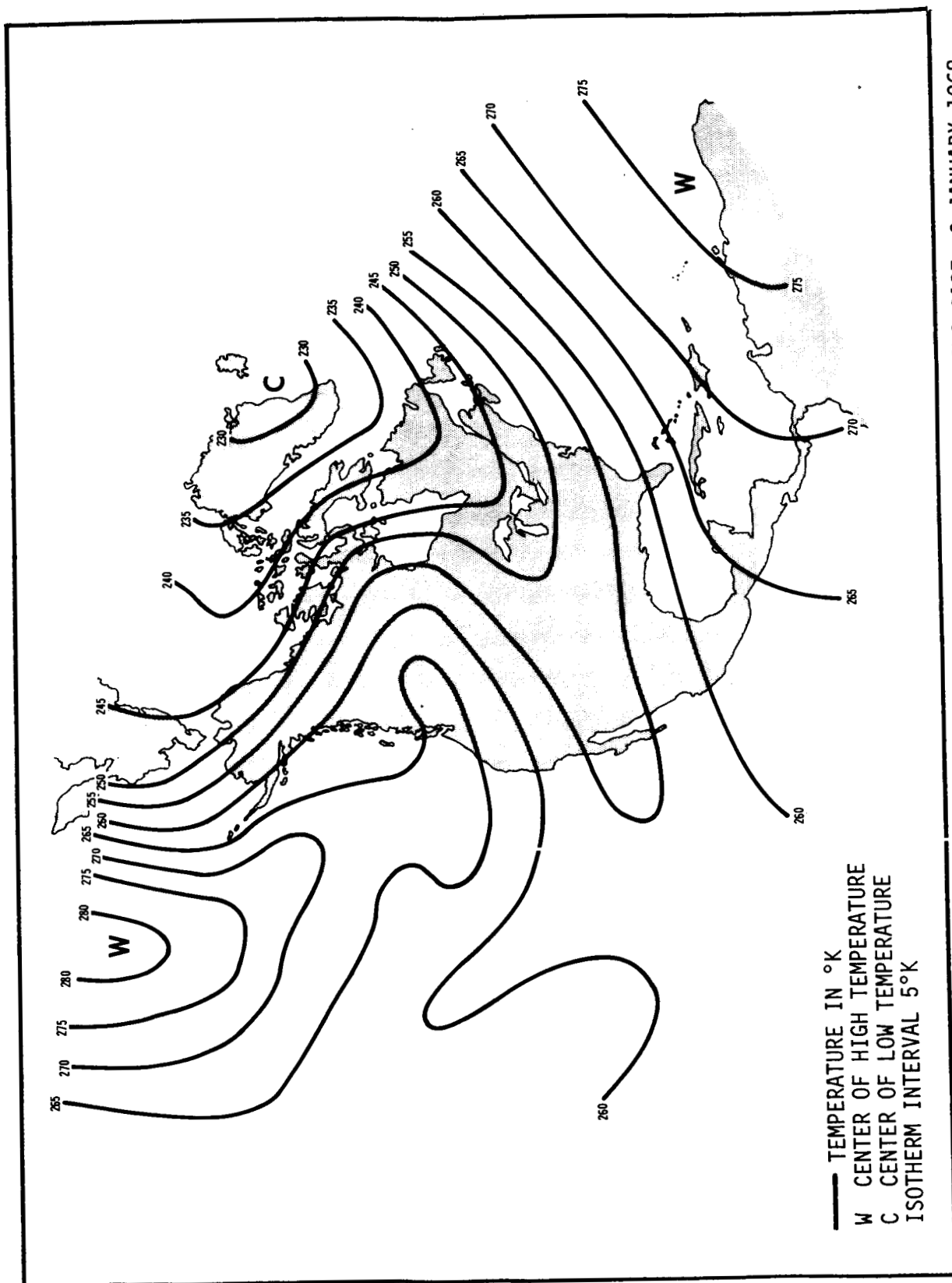
Figure 26. 52-KILOMETER TEMPERATURE ANALYSIS FOR STRATOSPHERIC WARMING CASE, 3 JANUARY 1968

TEMPERATURE IN °K
W CENTER OF HIGH TEMPERATURE
C CENTER OF LOW TEMPERATURE
ISOTHERM INTERVAL 5°K
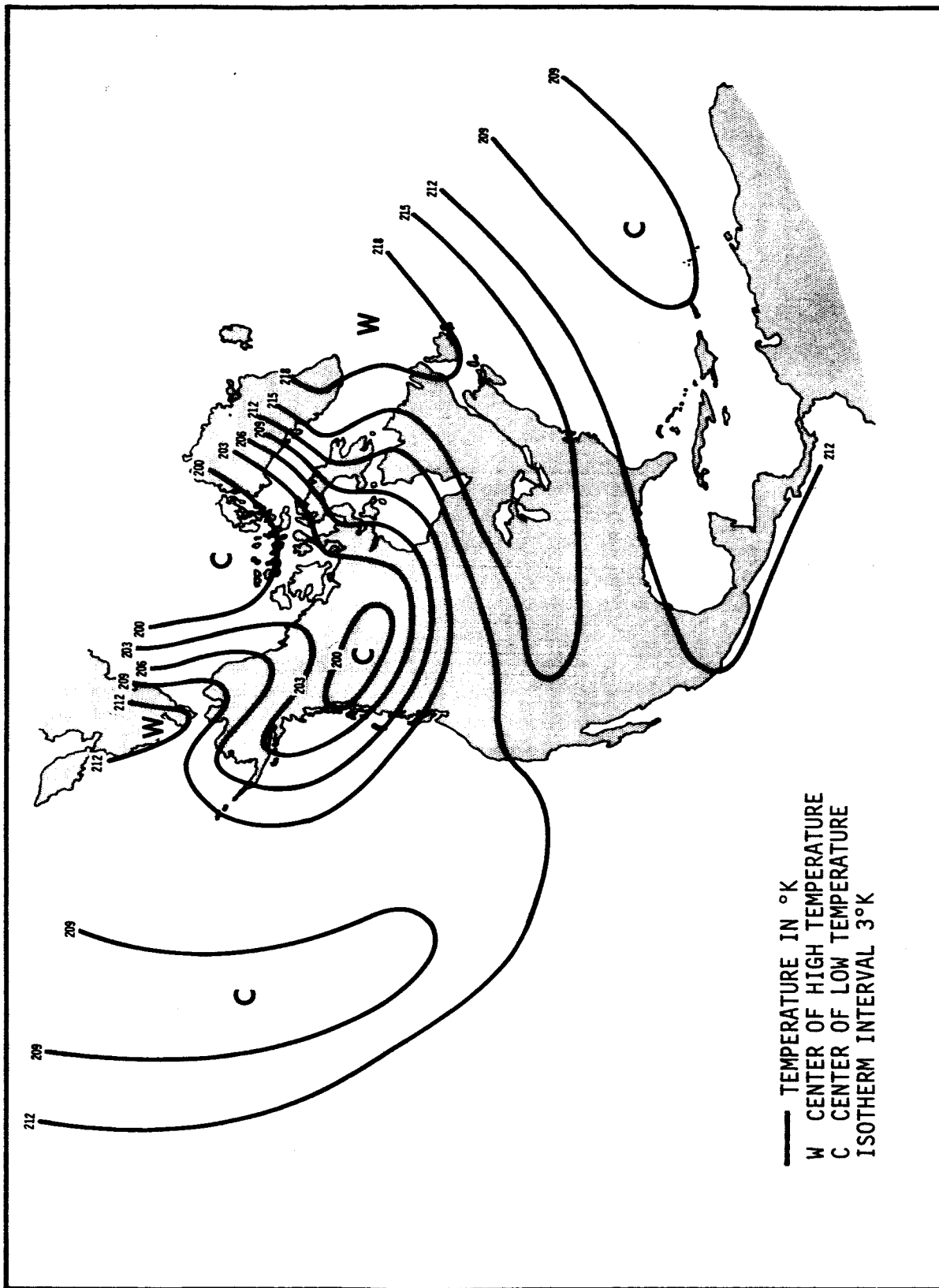
Figure 27. 76-KILOMETER TEMPERATURE ANALYSIS FOR STRATOSPHERIC WARMING CASE, 3 JANUARY 1968
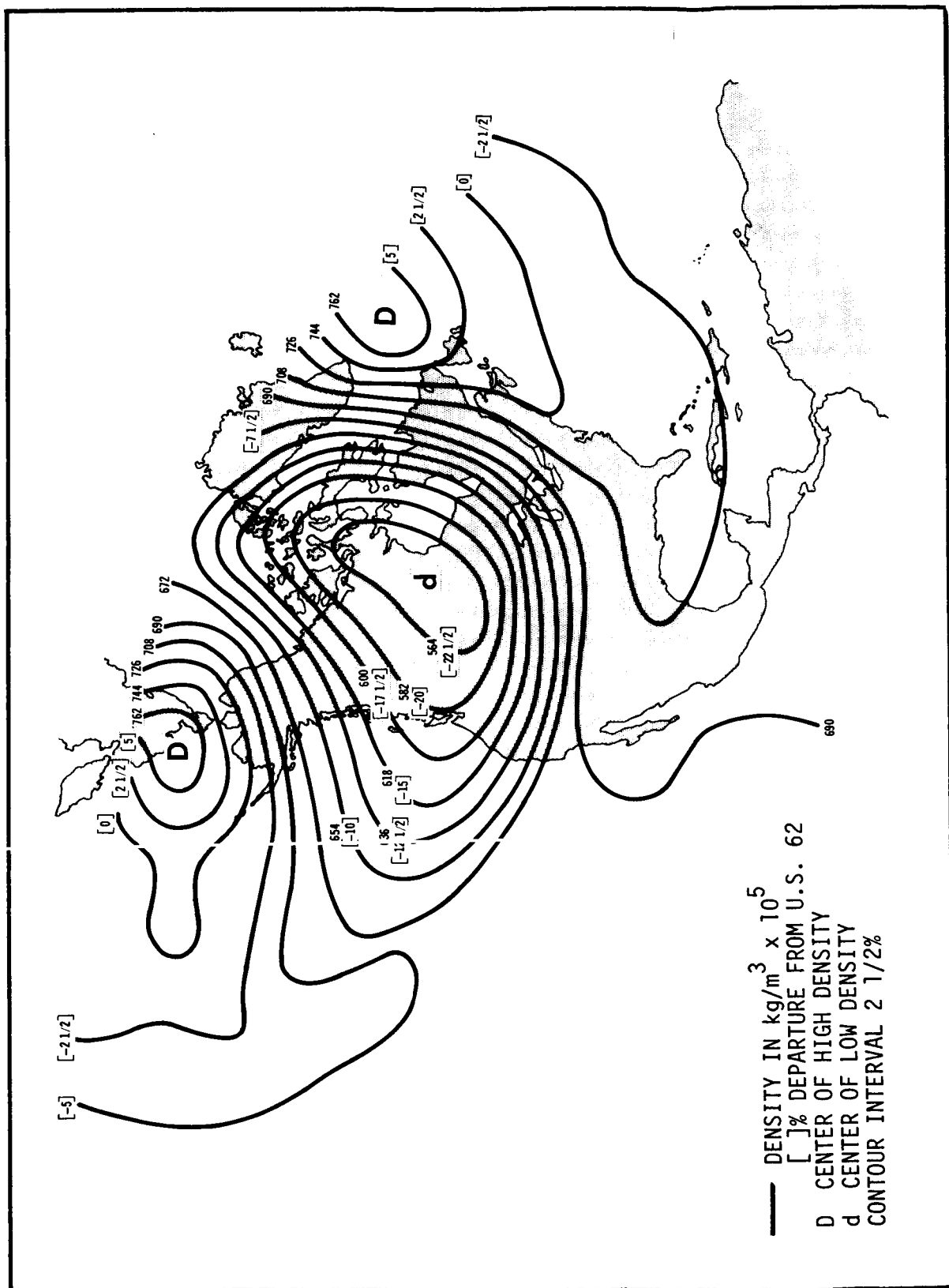
Figure 28. 36-KILOMETER DENSITY ANALYSIS FOR STRATOSPHERIC WARMING CASE, 3 JANUARY 1968

DENSITY IN kg/m³ x 10⁵
[ ]% DEPARTURE FROM U.S. 62
D CENTER OF HIGH DENSITY
d CENTER OF LOW DENSITY
CONTOUR INTERVAL 2 1/2%

44
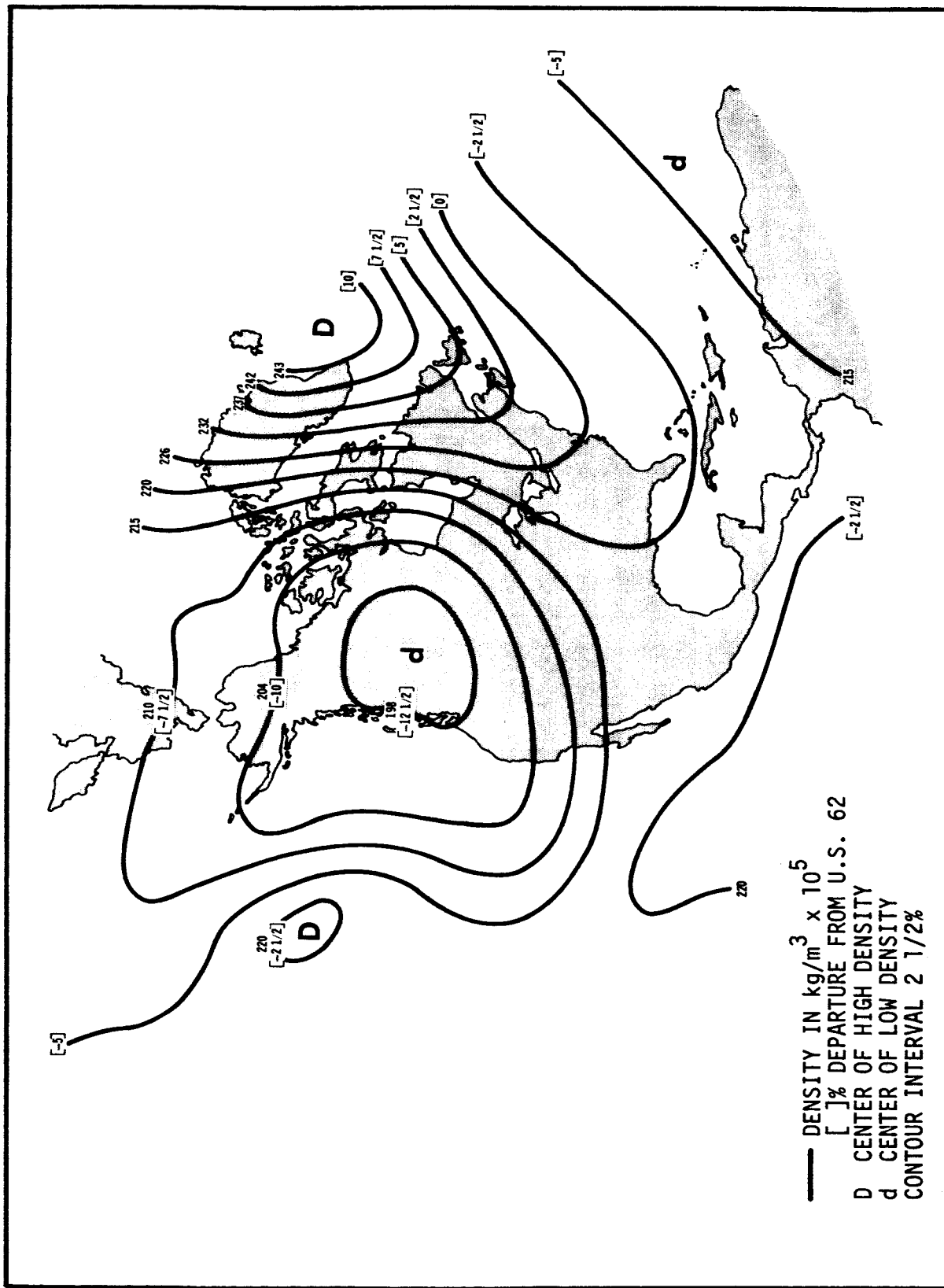
Figure 29. 44-KILOMETER DENSITY ANALYSIS FOR STRATOSPHERIC WARMING CASE, 3 JANUARY 1968

DENSITY IN kg/m^3 x 10^5
[ ]% DEPARTURE FROM U.S. 62
D CENTER OF HIGH DENSITY
d CENTER OF LOW DENSITY
CONTOUR INTERVAL 2 1/2%

45
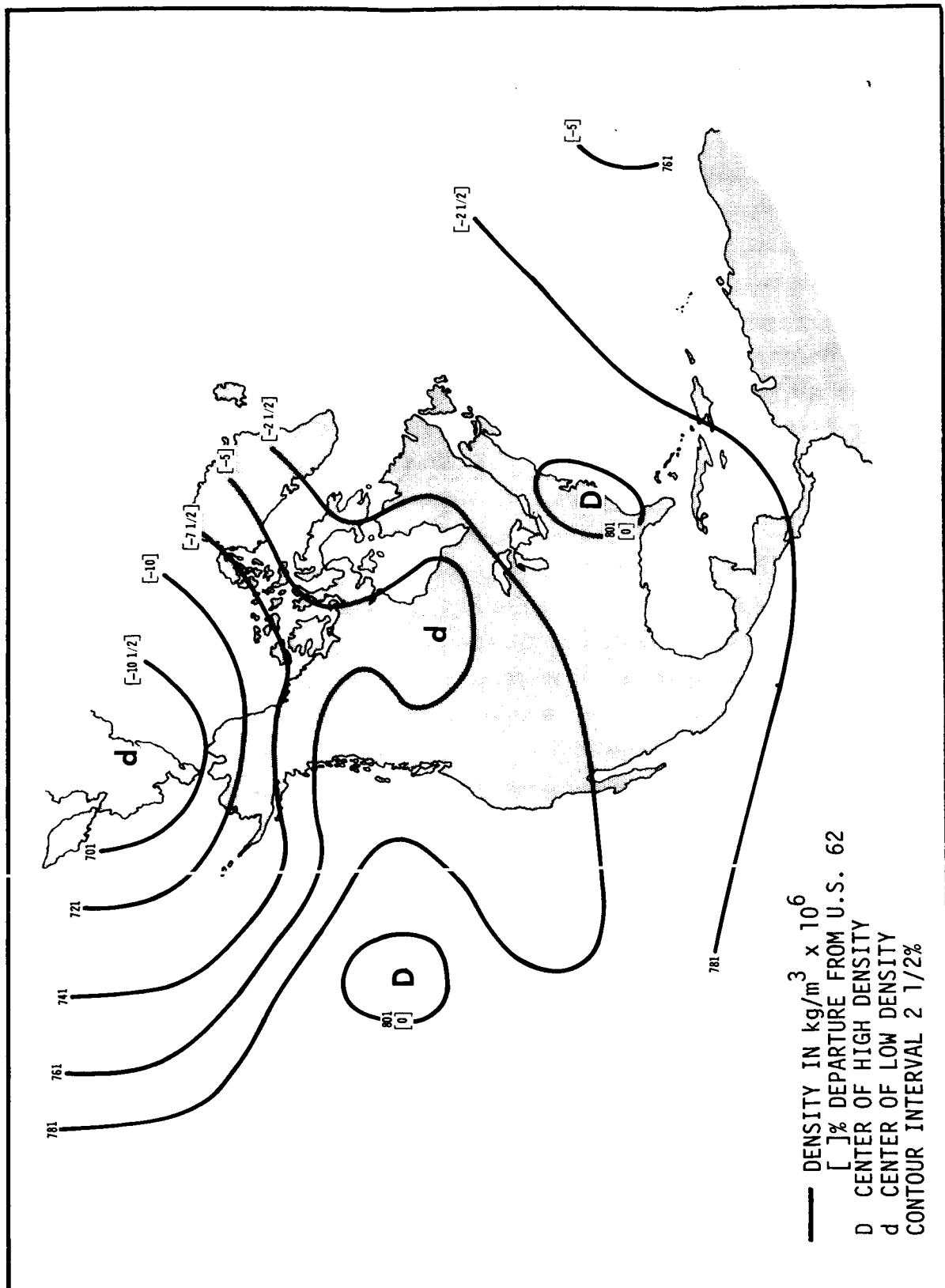
Figure 30. 52-KILOMETER DENSITY ANALYSIS FOR STRATOSPHERIC WARMING CASE, 3 JANUARY 1968

DENSITY IN kg/m³ x 10⁶
[ ]% DEPARTURE FROM U.S. 62
D CENTER OF HIGH DENSITY
d CENTER OF LOW DENSITY
CONTOUR INTERVAL 2 1/2%
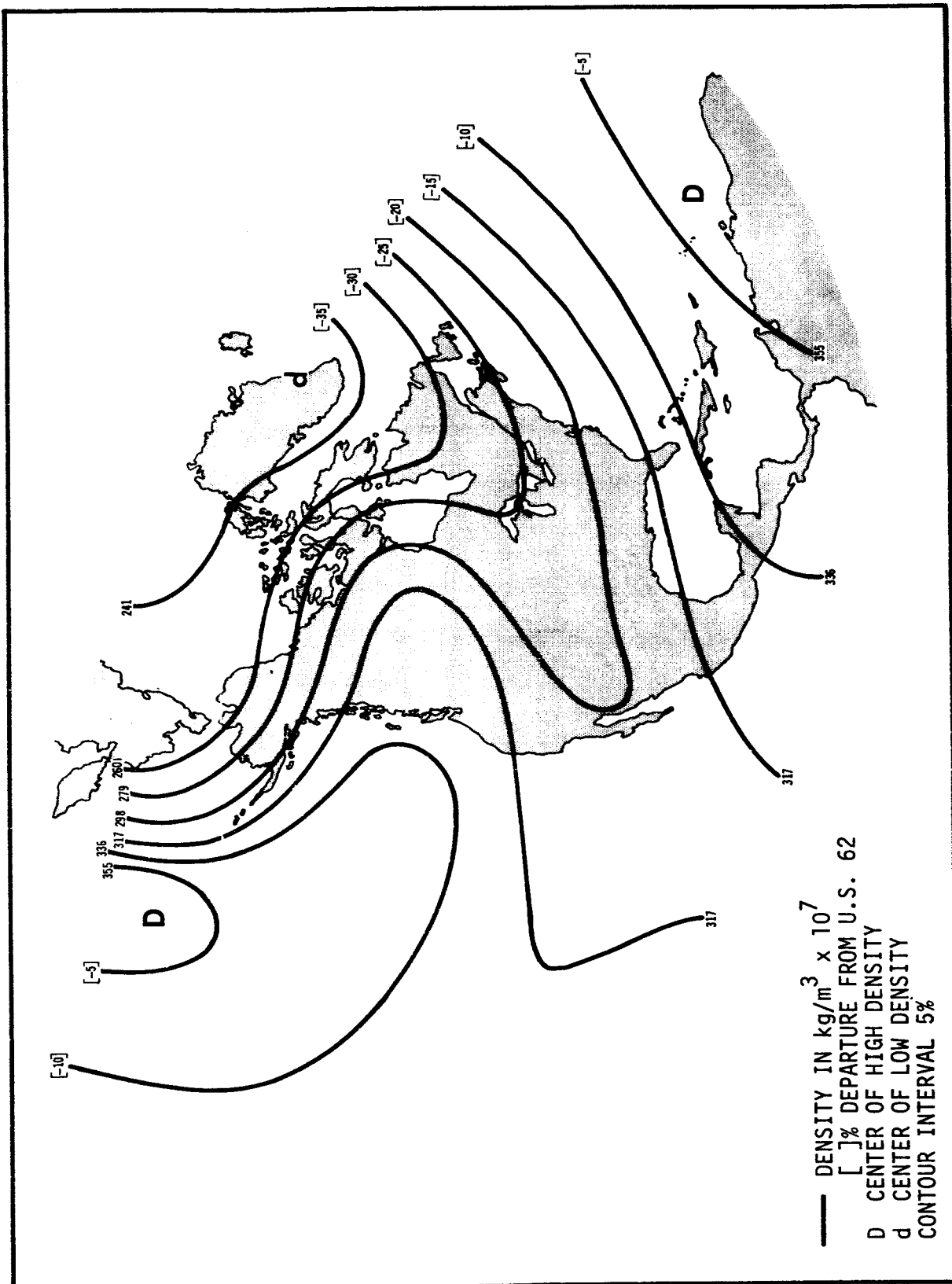
Figure 31. 76-KILOMETER DENSITY ANALYSIS FOR STRATOSPHERIC WARMING CASE, 3 JANUARY 1968

——— DENSITY IN kg/m^3 x 10^7
[ ]% DEPARTURE FROM U.S. 62
D CENTER OF HIGH DENSITY
d CENTER OF LOW DENSITY
CONTOUR INTERVAL 5%

Figure 32. 52-KILOMETER PRESSURE ANALYSIS FOR STRATOSPHERIC WARMING CASE, 3 JANUARY 1968

PRESSURE IN mb x 10
[ ]% DEPARTURE FROM U.S. 62
H CENTER OF HIGH PRESSURE
L CENTER OF LOW PRESSURE
CONTOUR INTERVAL 2 1/2%
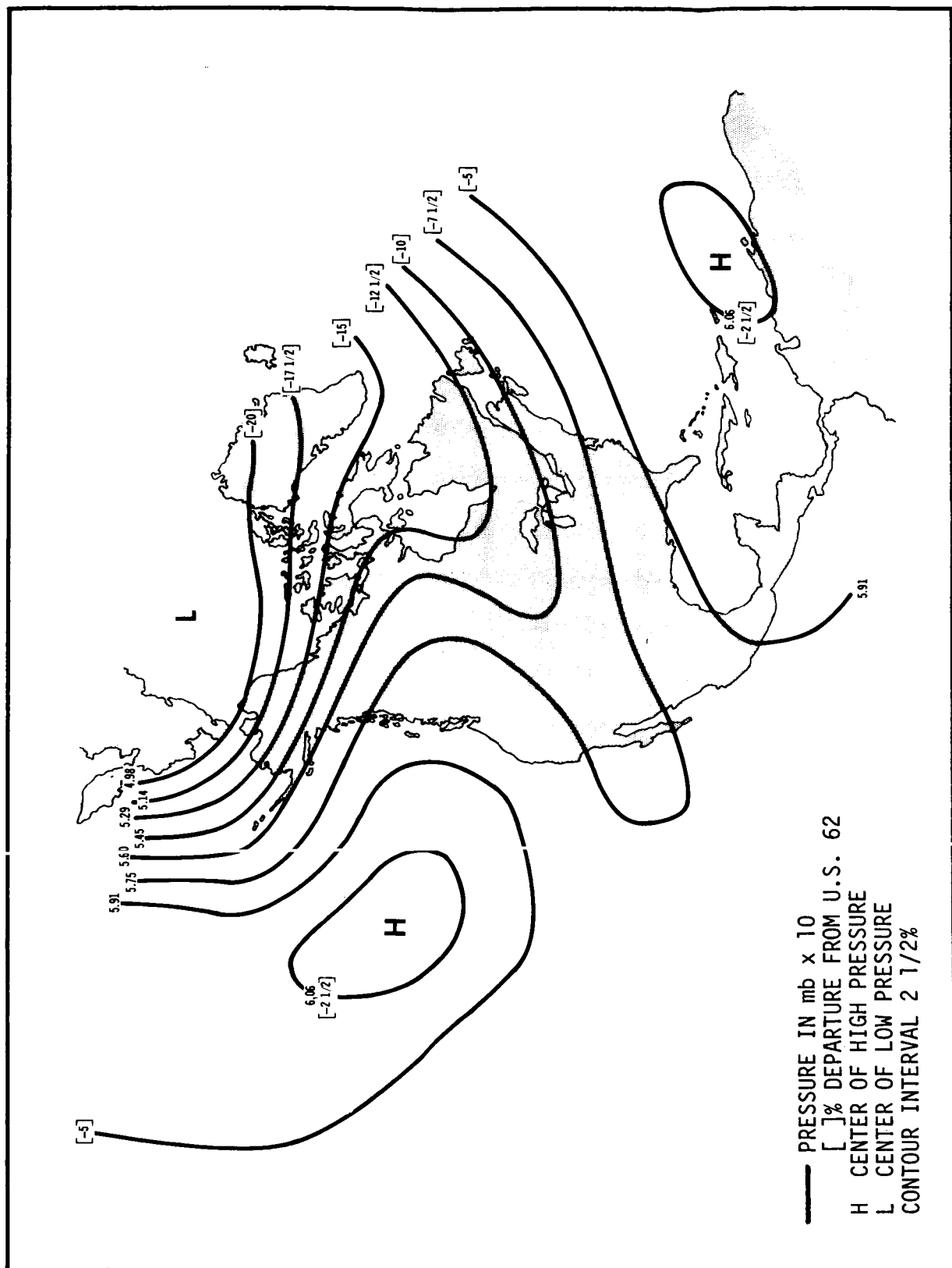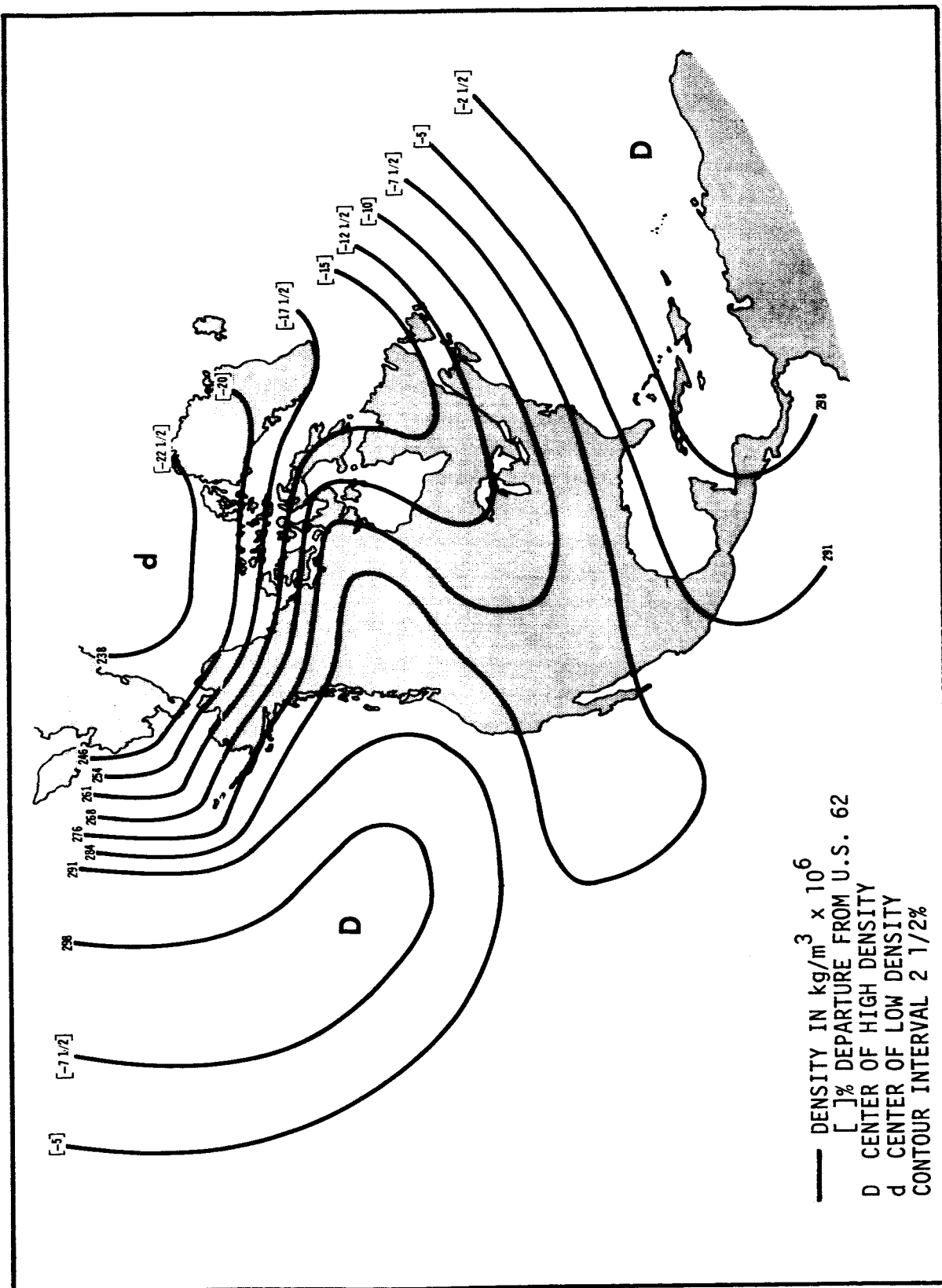
Figure 33. 60-KILOMETER DENSITY ANALYSIS FOR STRATOSPHERIC WARMING CASE, 3 JANUARY 1968

DENSITY IN kg/m³ × 10⁶
[ ]% DEPARTURE FROM U.S. 62
D CENTER OF HIGH DENSITY
d CENTER OF LOW DENSITY
CONTOUR INTERVAL 2 1/2%
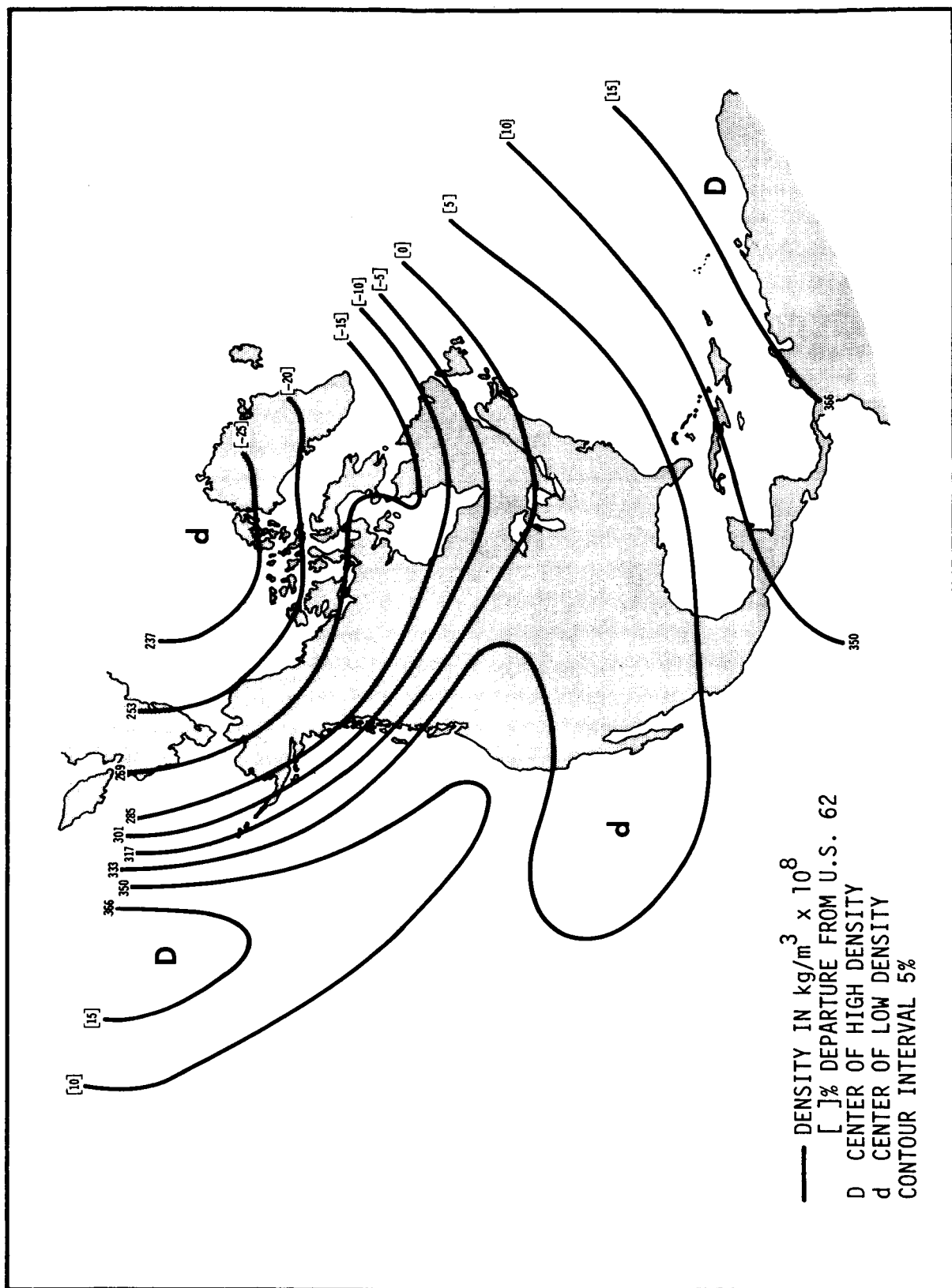
Figure 34. 90-KILOMETER DENSITY ANALYSIS FOR STRATOSPHERIC WARMING CASE, 3 JANUARY 1968

DENSITY IN kg/m³ x 10⁸
[ ]% DEPARTURE FROM U.S. 62
D CENTER OF HIGH DENSITY
d CENTER OF LOW DENSITY
CONTOUR INTERVAL 5%

50
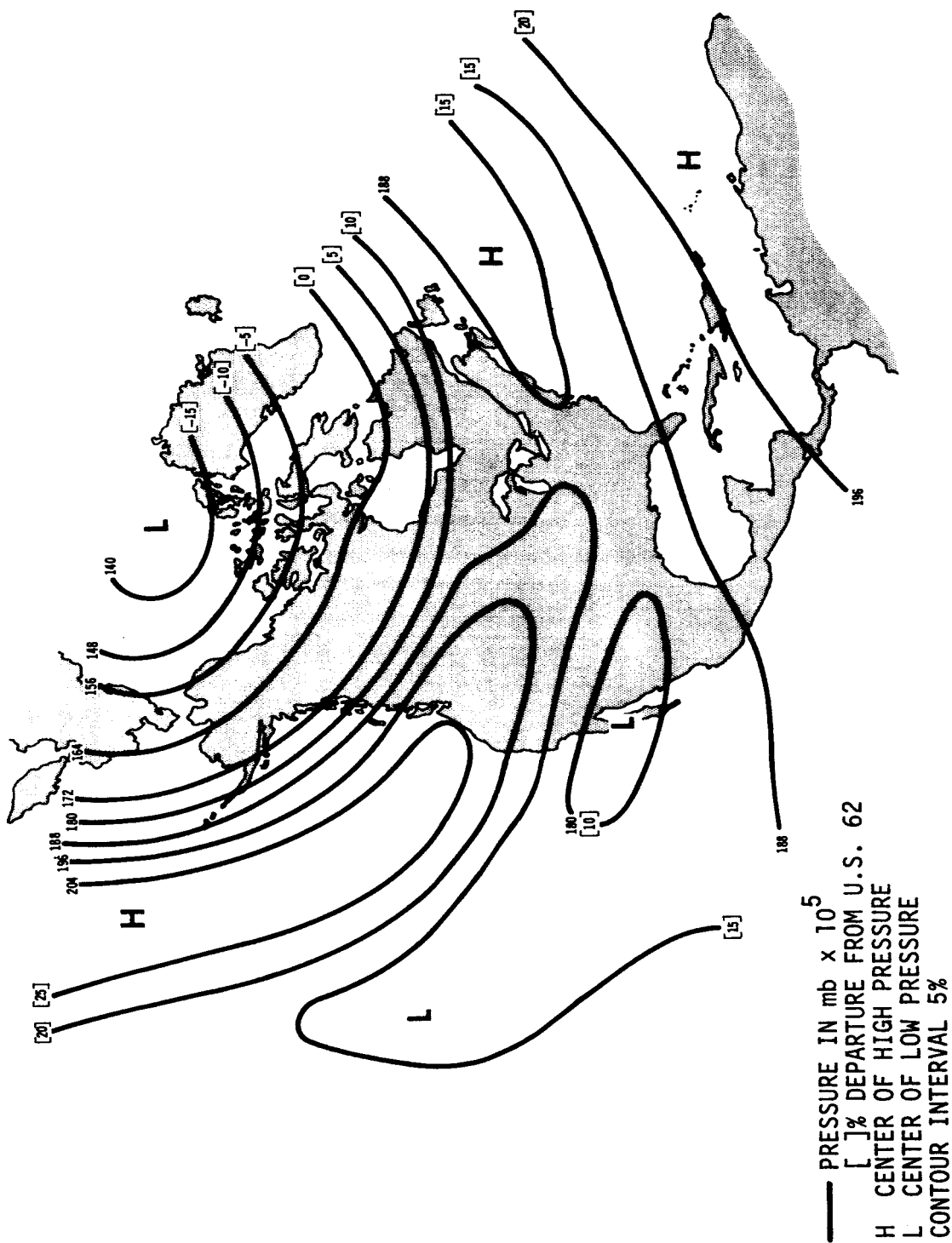
Figure 35. 90-KILOMETER PRESSURE ANALYSIS FOR STRATOSPHERIC WARMING CASE, 3 JANUARY 1968

PRESSURE IN mb x 10^5
[ ]% DEPARTURE FROM U.S. 62
H CENTER OF HIGH PRESSURE
L CENTER OF LOW PRESSURE
CONTOUR INTERVAL 5%
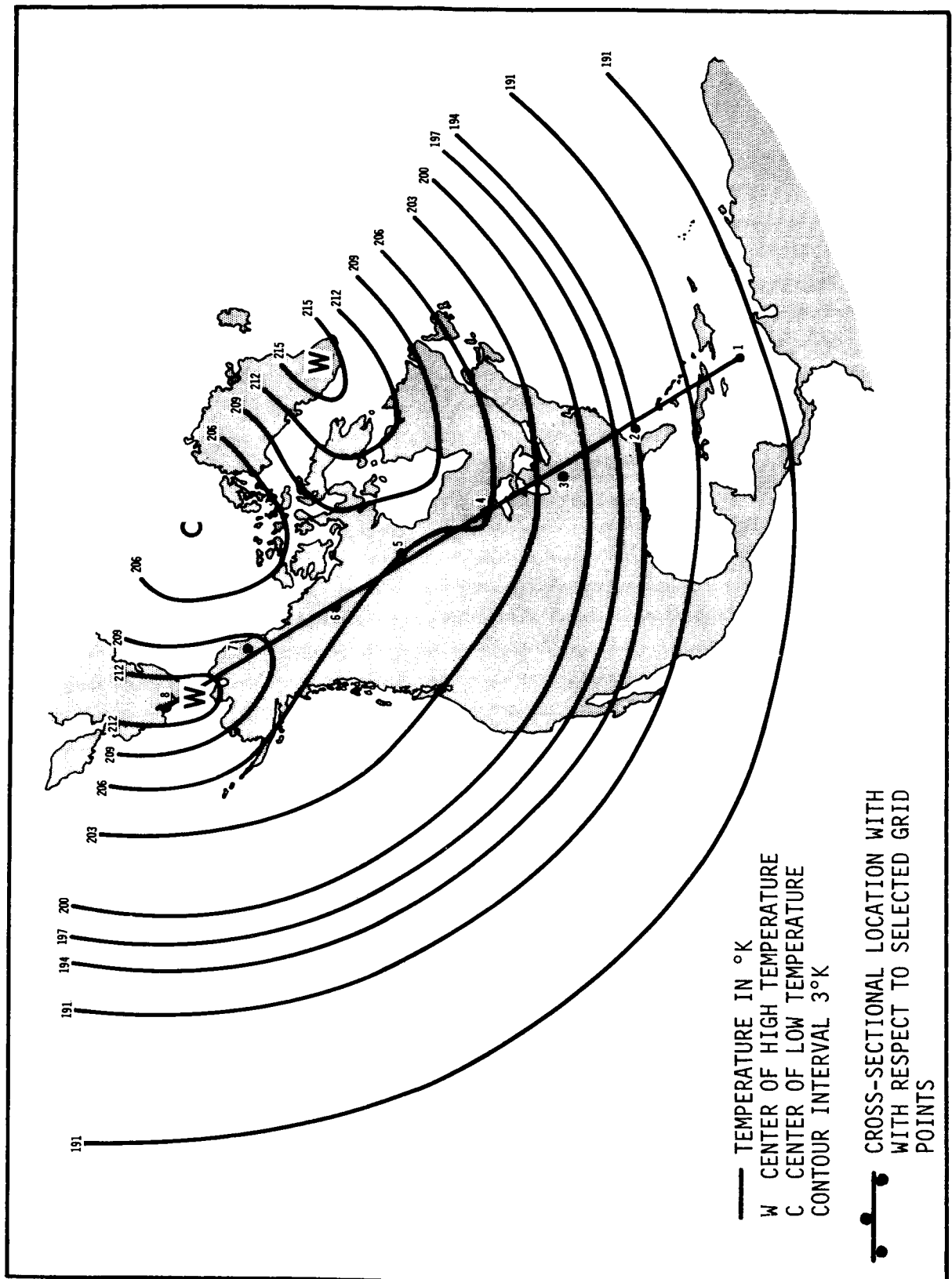
Figure 36. 90-KILOMETER TEMPERATURE ANALYSIS AND CROSS-SECTIONAL LINE FOR STRATOSPHERIC WARMING CASE, 3 JANUARY 1968

—— TEMPERATURE IN °K
W CENTER OF HIGH TEMPERATURE
C CENTER OF LOW TEMPERATURE
CONTOUR INTERVAL 3°K

CROSS-SECTIONAL LOCATION WITH
WITH RESPECT TO SELECTED GRID
POINTS

52
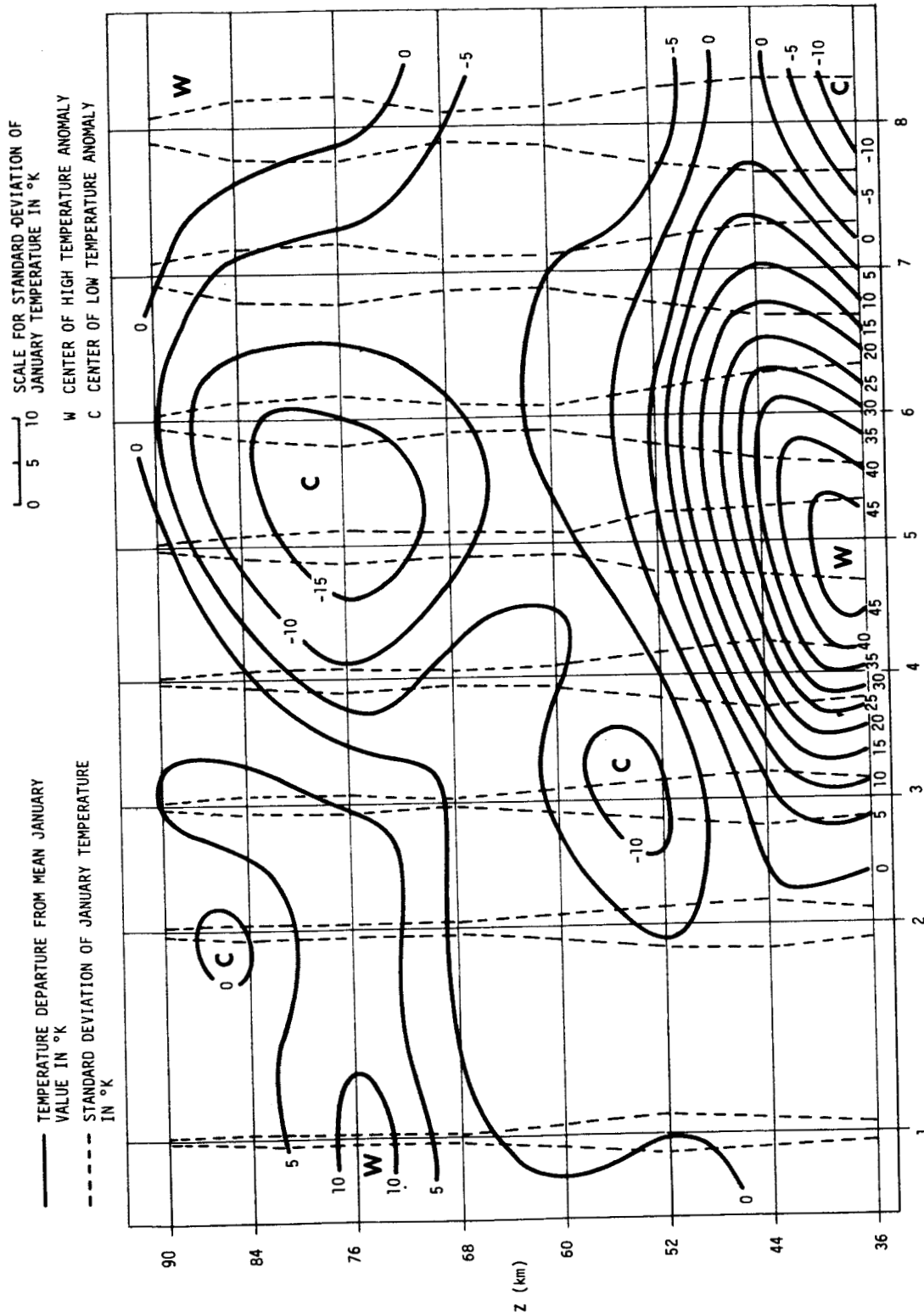
Figure 37. CROSS-SECTION ALONG LINE IN FIGURE 36. TEMPERATURE ANALYSIS AND STANDARD DEVIATION OF BASE DATA FOR STRATOSPHERIC WARMING CASE, 3 JANUARY 1968

53
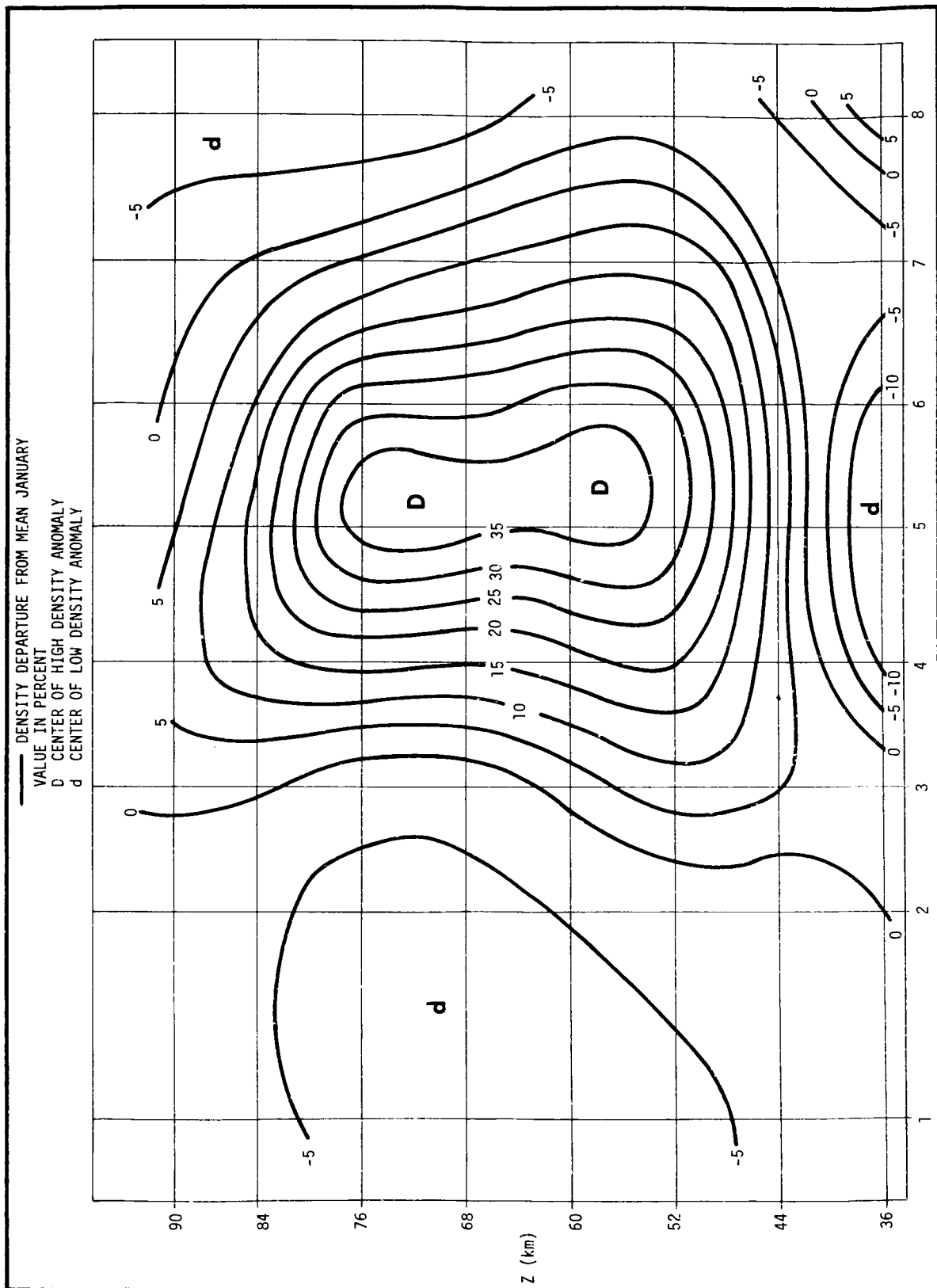
Figure 38. CROSS-SECTION ALONG LINE IN FIGURE 36. DENSITY ANALYSIS FOR STRATOSPHERIC WARMING CASE, 3 JANUARY 1968

— DENSITY DEPARTURE FROM MEAN JANUARY
VALUE IN PERCENT
D CENTER OF HIGH DENSITY ANOMALY
d CENTER OF LOW DENSITY ANOMALY

Z (km)

Prominently displayed in Figure 37 is the stratospheric warming center, which is located near Ft. Churchill, Manitoba at 38 km or possibly lower. Strong anomaly gradients exist on the sides and the top of this warm center, and the mesosphere has a cold center about 4 latitude degrees to the northwest at 78 km altitude. A second cold center at 55 km is a full 20 degrees to the south, and is not believed to be associated with the warming. With this configuration of anomalies, the stratopause and mesopause levels above the warming zone appear to be well below their normal heights.

The density anomaly chart has low values at the same level as the stratospheric warming, with strong gradients up to the first positive anomaly center near 58 km. This is some 20 km above the temperature anomaly center, in agreement with the 1967 case discussed by Quiroz (ref. 20). The high density center is dual-lobed, with the upper center being located near 72 km. This upper center is doubtful, however, because of a tendency to overestimate density in the mesosphere above an anomalously warm stratosphere. This kind of error is noted in extrapolated density values for Pt. Barrow on 4 February 1969, when a minor warming occurred at 40 km, and if it were removed the density cross-section would show substantially reduced values above 60 km in the neighborhood of the warming center. The trough at 76 km (Figure 31) would also be displaced a few degrees westward. Aside from these known shortcomings in the regressed densities, the two cross-sections match hydrostatically in a qualitative sense, giving credence to the extrapolated results in this anomalous case.

Section V

STATISTICS FOR EXTRAPOLATED DATA

The 50 sectional North American charts of Section IV are tabulated by midseasonal months in Table 3. Density, pressure, and temperature data at 36, 44, 52, 60, 68, 76, 84, and 90 km have been generated for each of these cases and they have been recorded upon magnetic tape.

Table 3. FREQUENCY OF CHARTS BY MONTHS

MONTH	NUMBER OF CHARTS
January	12
April	13
July	13
October	12
Total	50

The following statistical quantities have been computed for each seasonal set of charts, for density, temperature, and pressure, for each level enumerated above in Section IV.

(1) Arithmetic mean value at each grid point.

(2) Standard deviation, based upon grid point mean values, at each grid point.

(3) Coefficient of variation for (1) and (2), at each grid point.

(4) Arithmetic mean value for each 5 degrees of latitude from 10 degrees north to the North Pole, based upon the same field as Groves' model, namely, 70 degrees west to 160 degrees west. This cuts off 30 degrees on each side of our data field.

(5) Standard deviation for the smaller field, based upon the latitudinal mean values, at each grid point.

(6) Coefficient of variation for (4) and (5), at each grid point.

All of the statistics in (1) through (6) have been placed upon magnetic tape.

The latitudinal variation of the second kind of arithmetic mean value (4) for pressure, temperature, and density at the levels of 52, 60, 76, and 90 km are presented in Figures 39-41. To show the longitudinal variation as well,

56
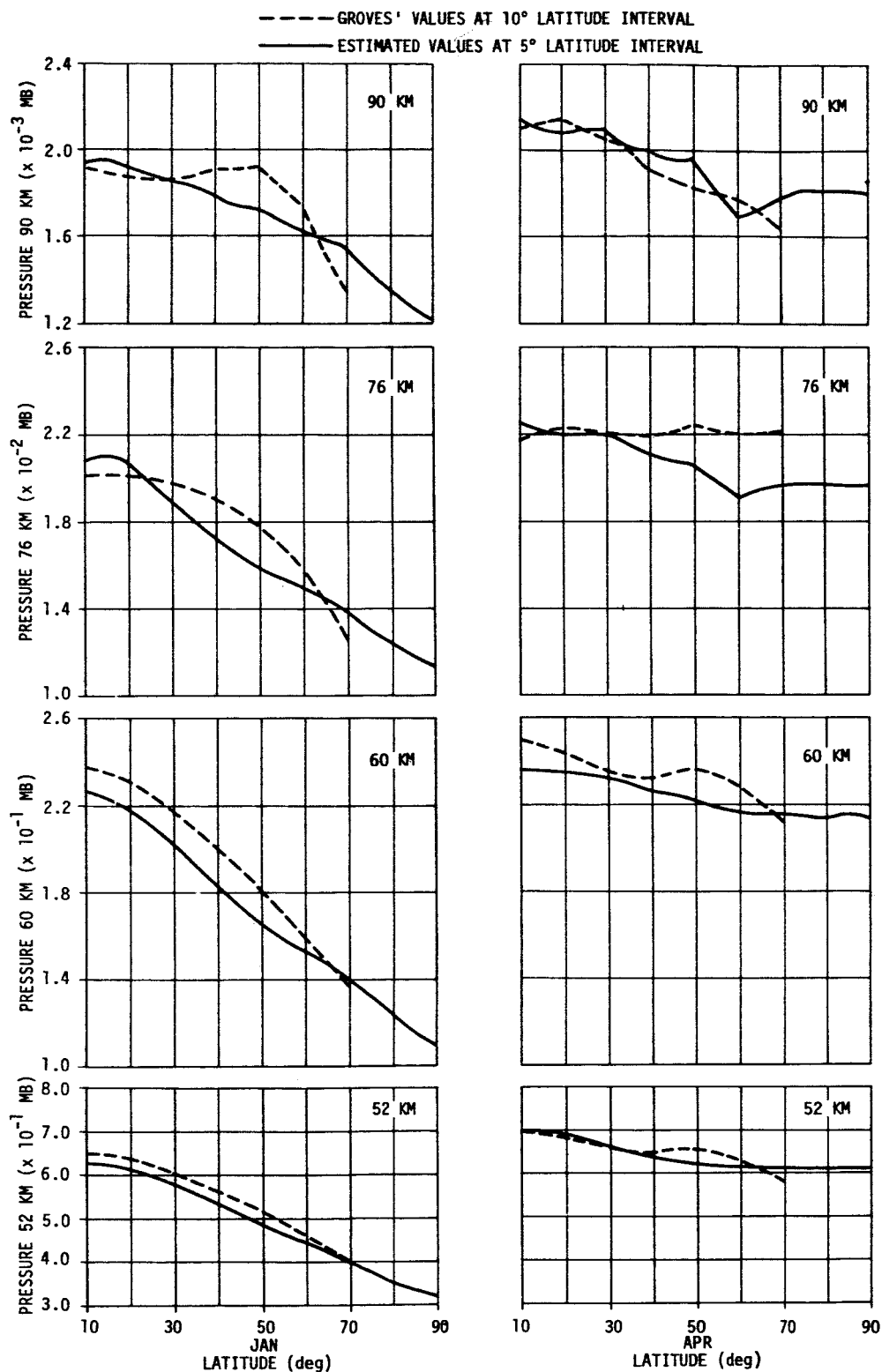
Figure 39a.   COMPARISON OF THE MEAN LATITUDINAL PRESSURE DISTRIBUTION WITH
             GROVES' MODEL
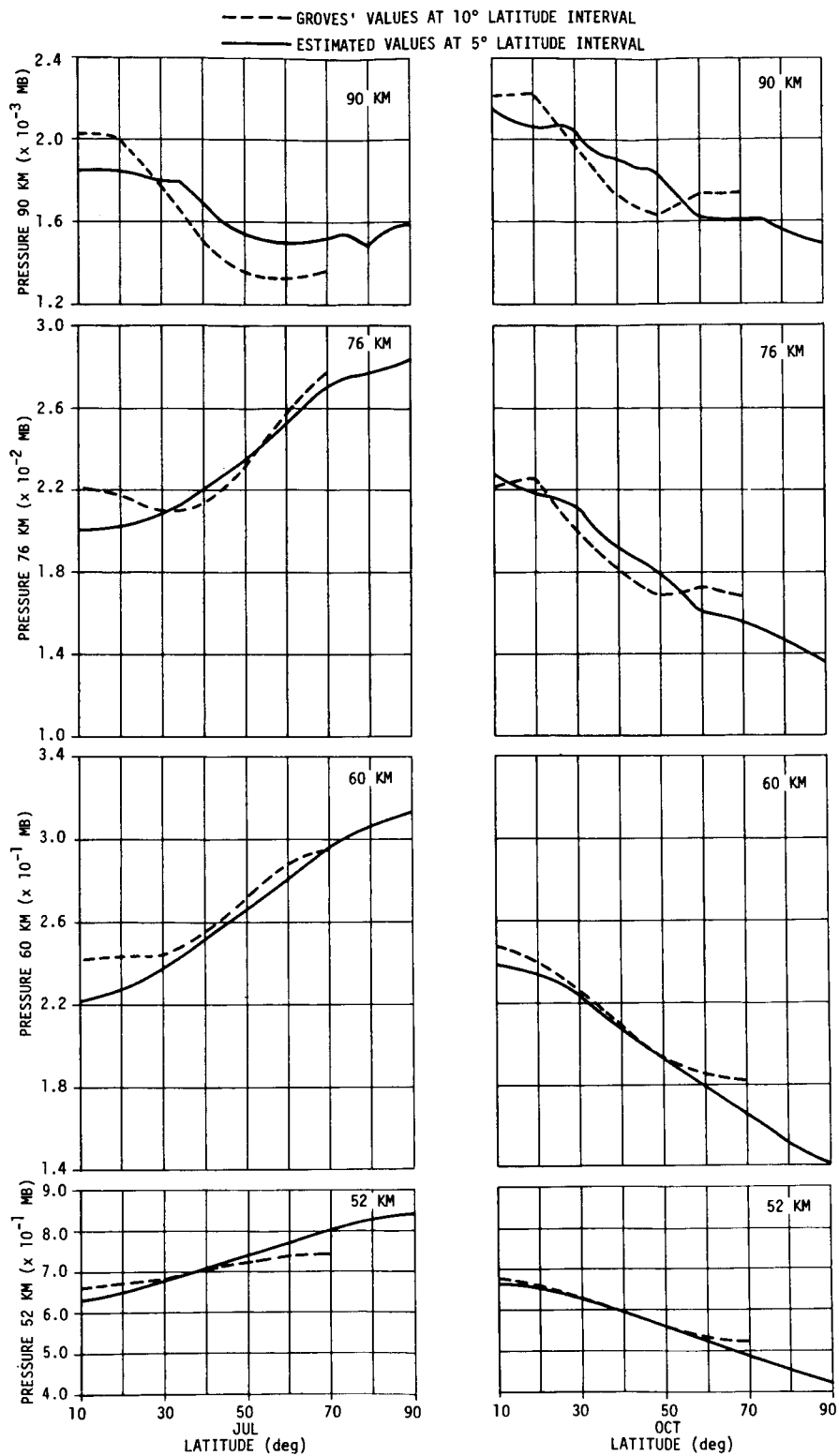
Figure 39b.   COMPARISON OF THE MEAN LATITUDINAL PRESSURE DISTRIBUTION WITH
GROVES' MODEL

58
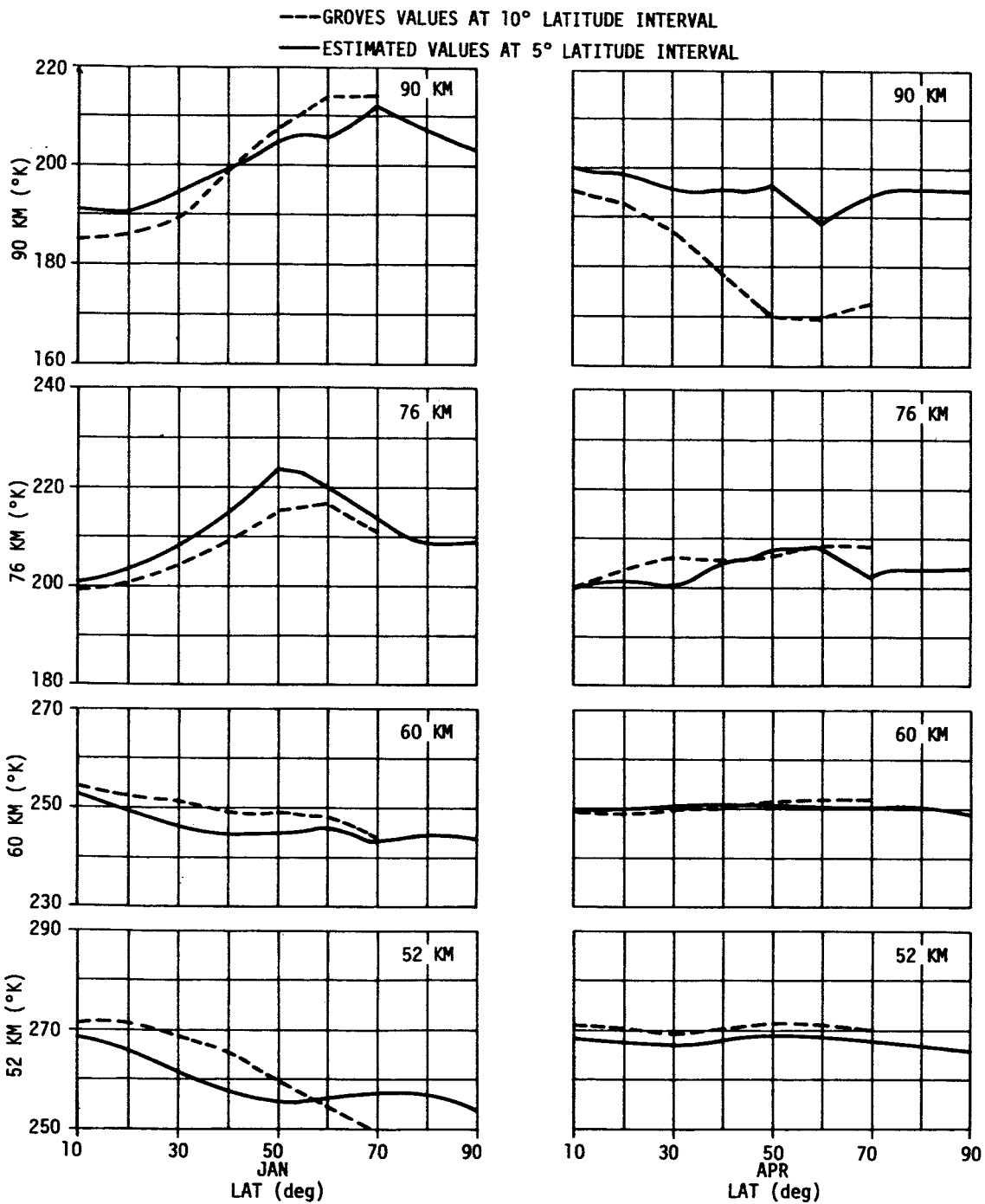
Figure 40a. COMPARISON OF THE MEAN LATITUDINAL TEMPERATURE DISTRIBUTION WITH GROVES' MODEL
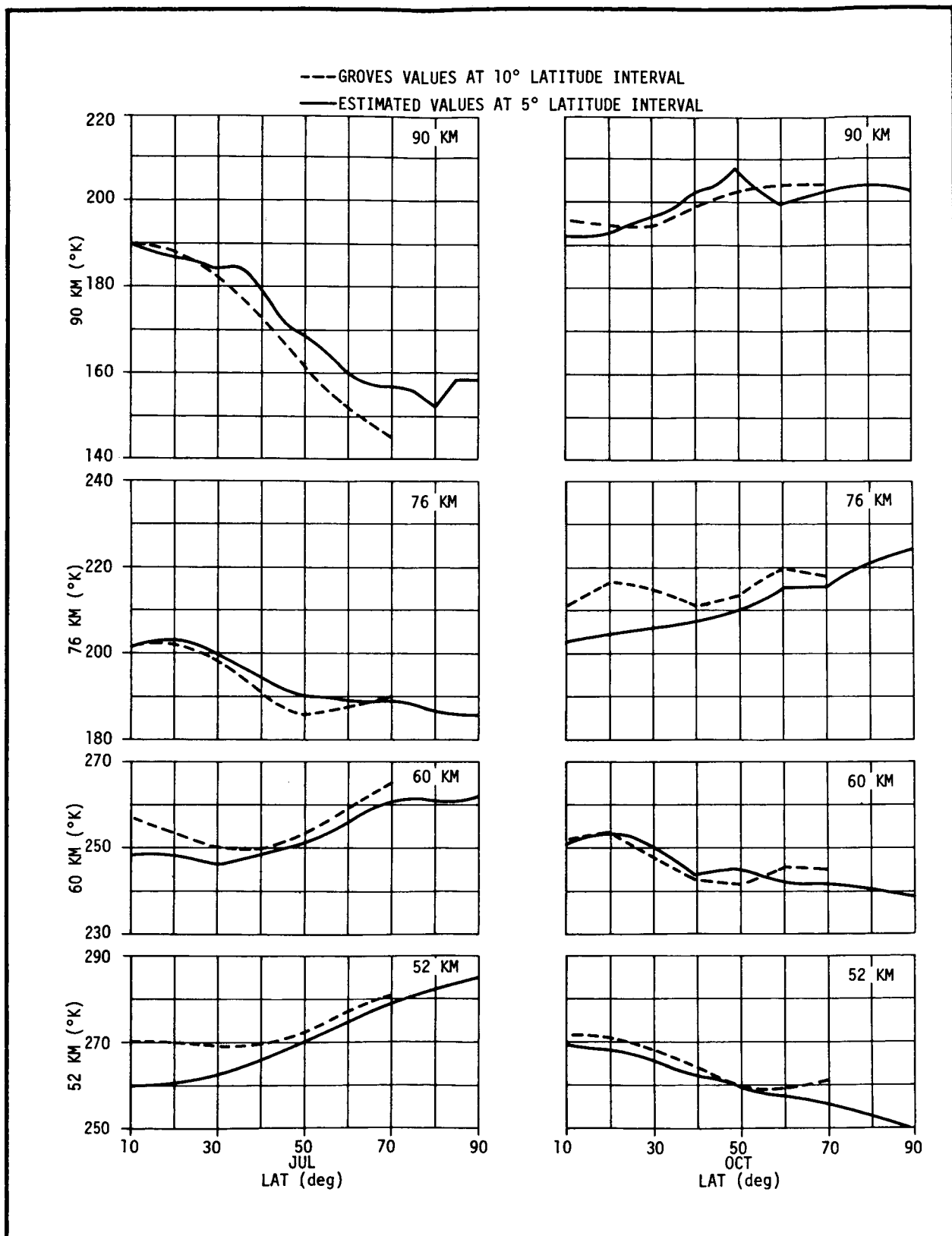
Figure 40b.   COMPARISON OF THE MEAN LATITUDINAL TEMPERATURE DISTRIBUTION WITH GROVES' MODEL
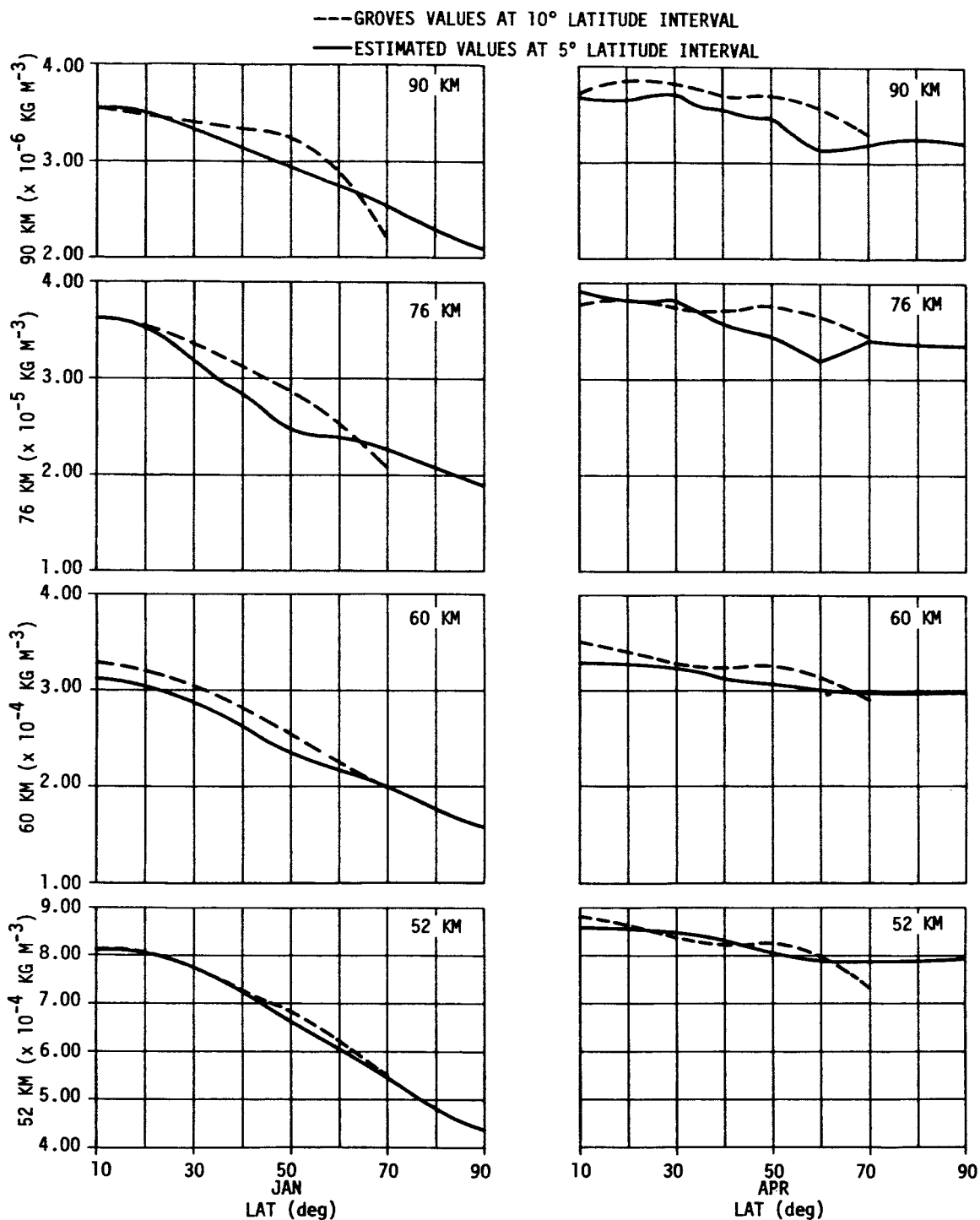
Figure 41a. COMPARISON OF THE MEAN LATITUDINAL DENSITY DISTRIBUTION WITH GROVES' MODEL

61
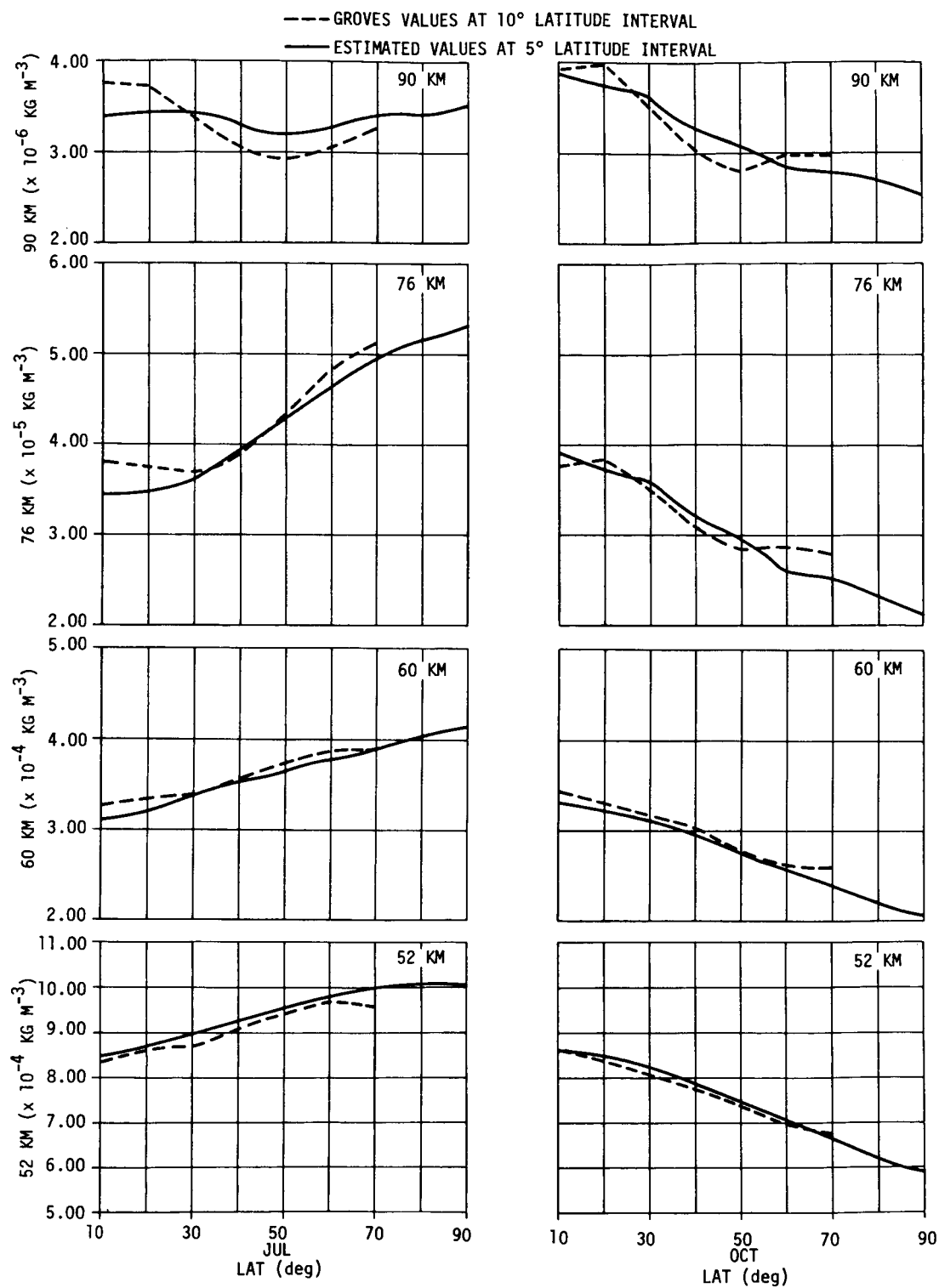
Figure 41b. COMPARISON OF THE MEAN LATITUDINAL DENSITY DISTRIBUTION WITH GROVES' MODEL

some charts for the first kind of arithmetic mean value (1) and standard deviation (2) are added in Figures 42-61.

Four of the eight mean fields for density in January are displayed in Figures 42-45, together with the standard deviation of density. At 44 km, the mean field resembles the high-level wintertime pressure fields which are published in reference 18. The main features are a minimum in density over the Greenland area, a broad trough from Greenland southwestward, a flat field in the Eastern Pacific, and relatively strong density gradients over the Arctic and much of Canada. At higher levels, the density gradients over the United States are notably stronger than at 44 km. The field showing the standard deviation of density has a maximum over the Siberian-Alaskan region at all four levels, but it reaches a peak at 76 km, where the value attains fully 20 percent of the mean value in this region. Over the United States mainland, the variability of density is small for the cases contained in the sample, with the sole exception being the Pacific Northwest area in winter.

The two October charts (Figures 46, 47) have a minimum density center somewhat offset from the North Pole as in January, but the trough and ridge features are not present. Density gradients are much less in this month at high latitudes, but there is a notable buildup of the south-north density gradient with height across the United States and Southern Canada.

The April chart at 44 km (Figure 48) is that of a flat mean density field which retains much of its wintertime variability. In July, the time fluctuations are small (Figure 49). At higher levels in these months (not shown), a thin band of minimum density is found at 50 to 60 degrees north latitude with increasing values to the north and south throughout the fields.

The mean fields of temperature for the same four levels in January are presented in Figures 50-53. At 44 km, a cold center dominates the Alaskan region. This center diminishes with height, being replaced by a warm ridge over the same area at 90 km. The standard deviation of temperature surpasses 10°K at 44 km, and again approaches this amount in the mid-mesosphere at 76 km, but is much smaller at 60 km and 90 km. The July charts for
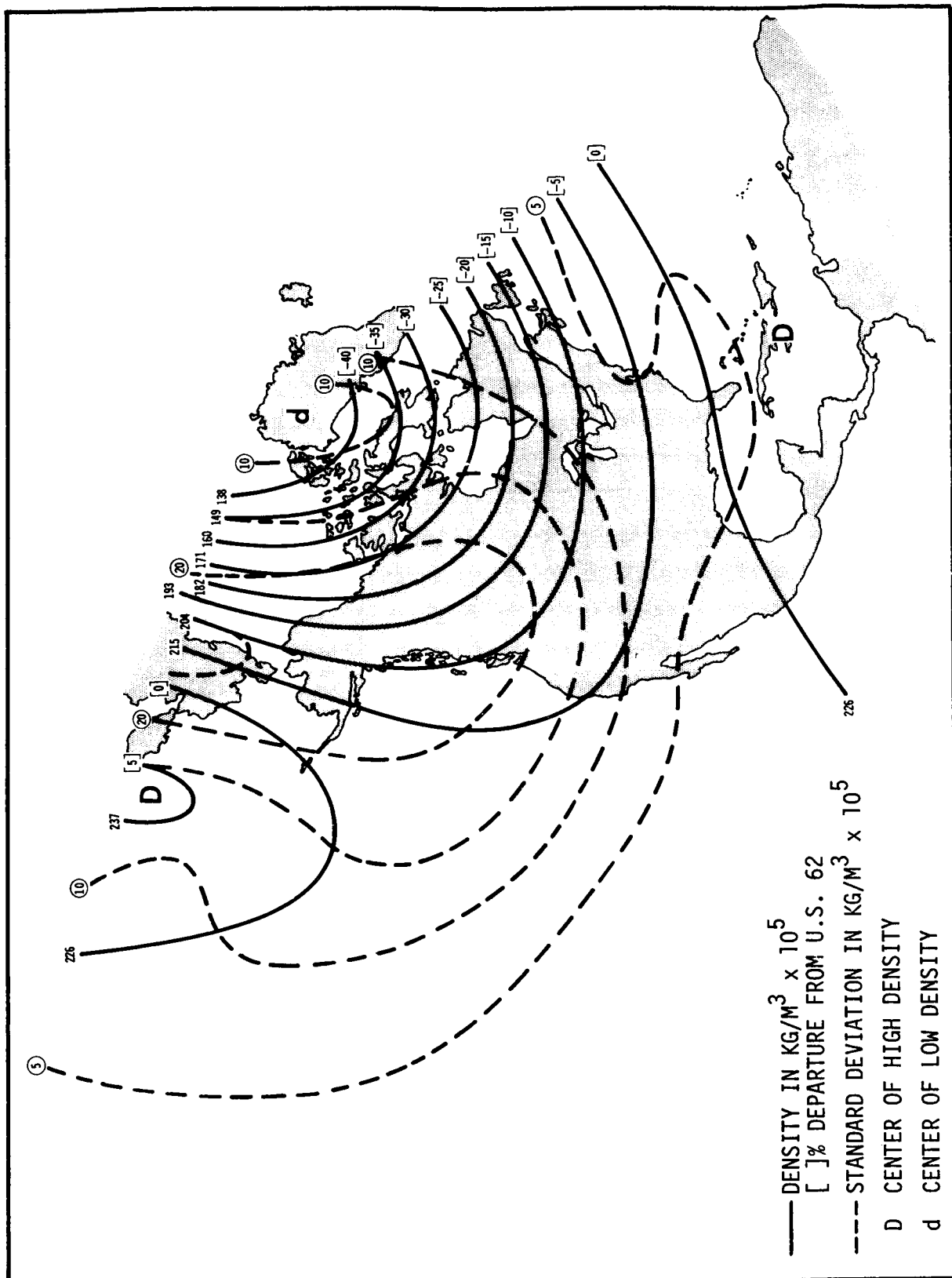
Figure 42. MONTHLY MEAN DENSITY AND STANDARD DEVIATION FOR JANUARY, 44 KM ALTITUDE

DENSITY IN KG/M³ × 10⁵
[ ]% DEPARTURE FROM U.S. 62
STANDARD DEVIATION IN KG/M³ × 10⁵
D CENTER OF HIGH DENSITY
d CENTER OF LOW DENSITY
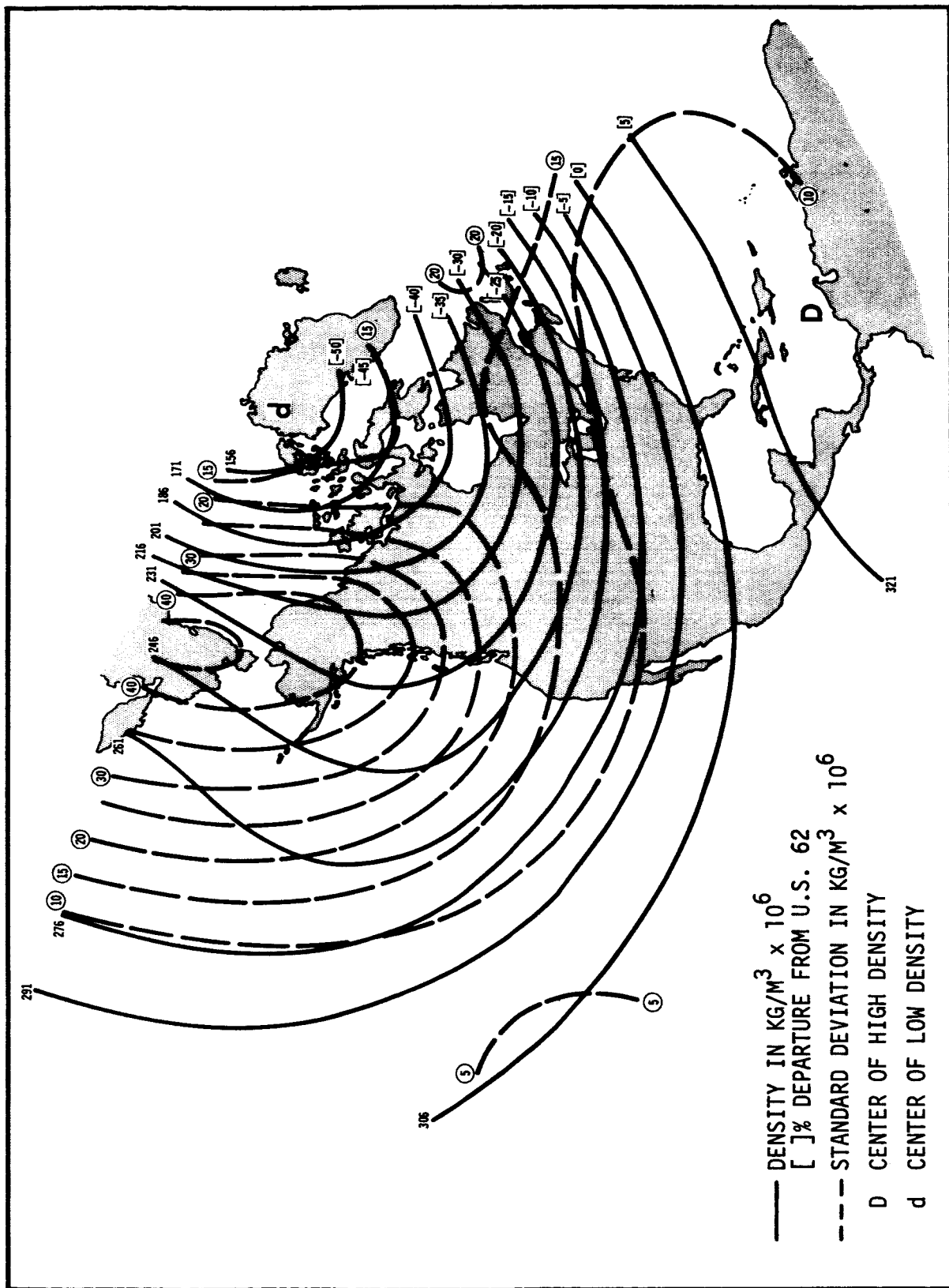
Figure 43. MONTHLY MEAN DENSITY AND STANDARD DEVIATION FOR JANUARY, 60 KM ALTITUDE

DENSITY IN KG/M^3 x 10^6
[ ]% DEPARTURE FROM U.S. 62

STANDARD DEVIATION IN KG/M^3 x 10^6

D CENTER OF HIGH DENSITY

d CENTER OF LOW DENSITY
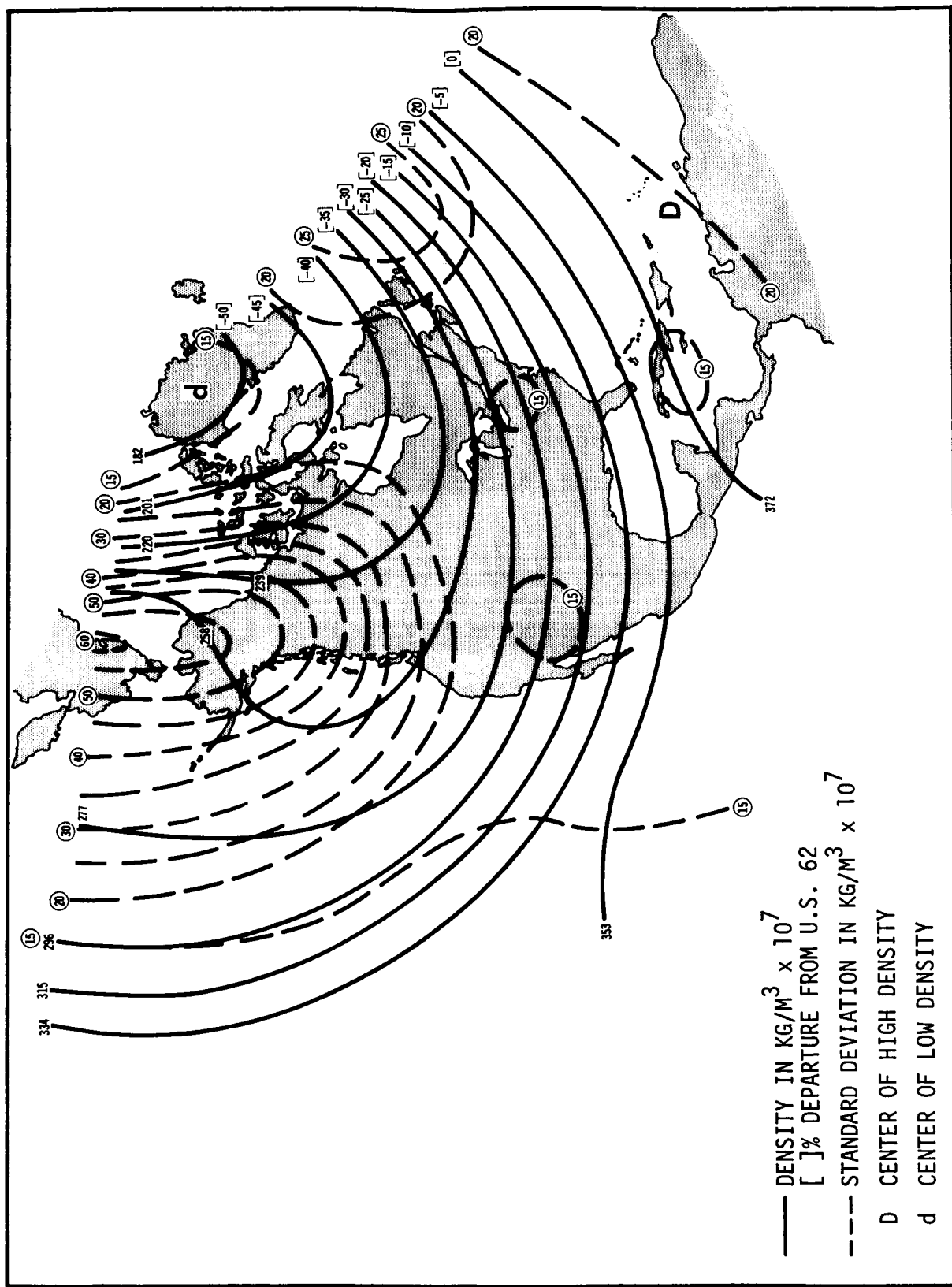
Figure 44. MONTHLY MEAN DENSITY AND STANDARD DEVIATION FOR JANUARY, 76 KM ALTITUDE

——— DENSITY IN KG/M^3 x 10^7
[ ]% DEPARTURE FROM U.S. 62
– – – STANDARD DEVIATION IN KG/M^3 x 10^7
D   CENTER OF HIGH DENSITY
d   CENTER OF LOW DENSITY
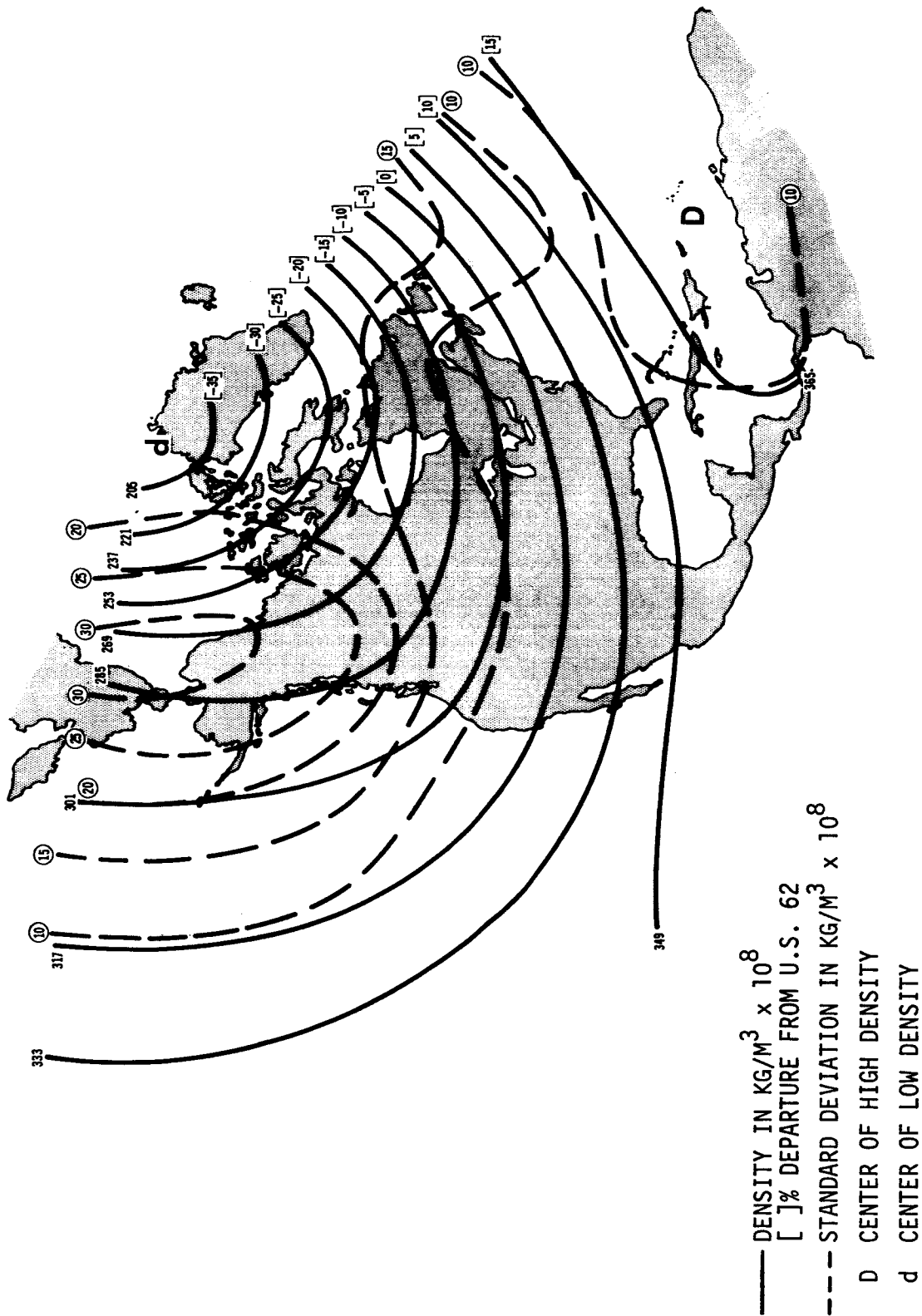
Figure 45. MONTHLY MEAN DENSITY AND STANDARD DEVIATION FOR JANUARY, 90 KM ALTITUDE

DENSITY IN KG/M³ x 10⁸
[ ]% DEPARTURE FROM U.S. 62
STANDARD DEVIATION IN KG/M³ x 10⁸
D CENTER OF HIGH DENSITY
d CENTER OF LOW DENSITY

67
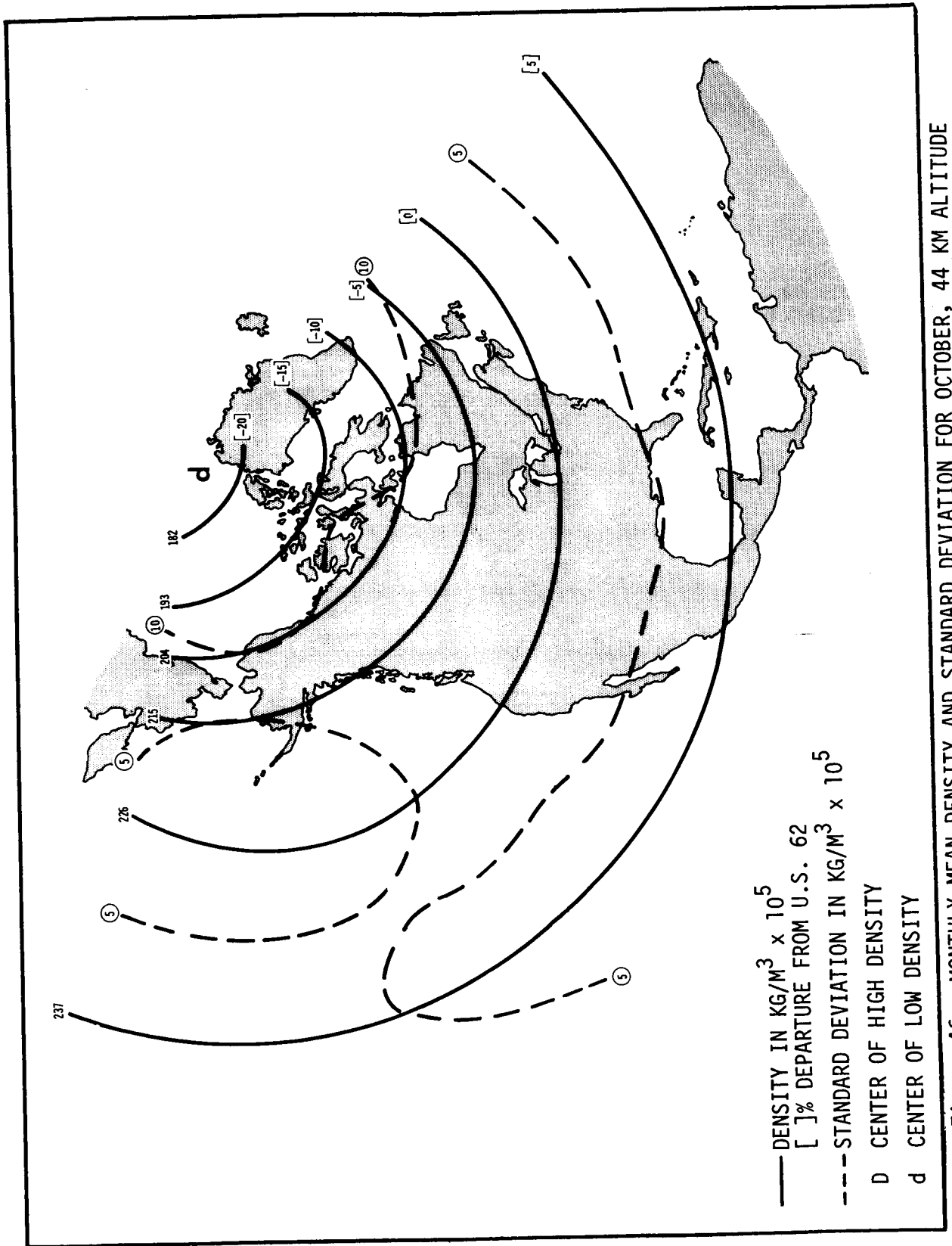
Figure 46. MONTHLY MEAN DENSITY AND STANDARD DEVIATION FOR OCTOBER, 44 KM ALTITUDE

DENSITY IN KG/M^3 x 10^5
[ ]% DEPARTURE FROM U.S. 62
STANDARD DEVIATION IN KG/M^3 x 10^5
D   CENTER OF HIGH DENSITY
d   CENTER OF LOW DENSITY
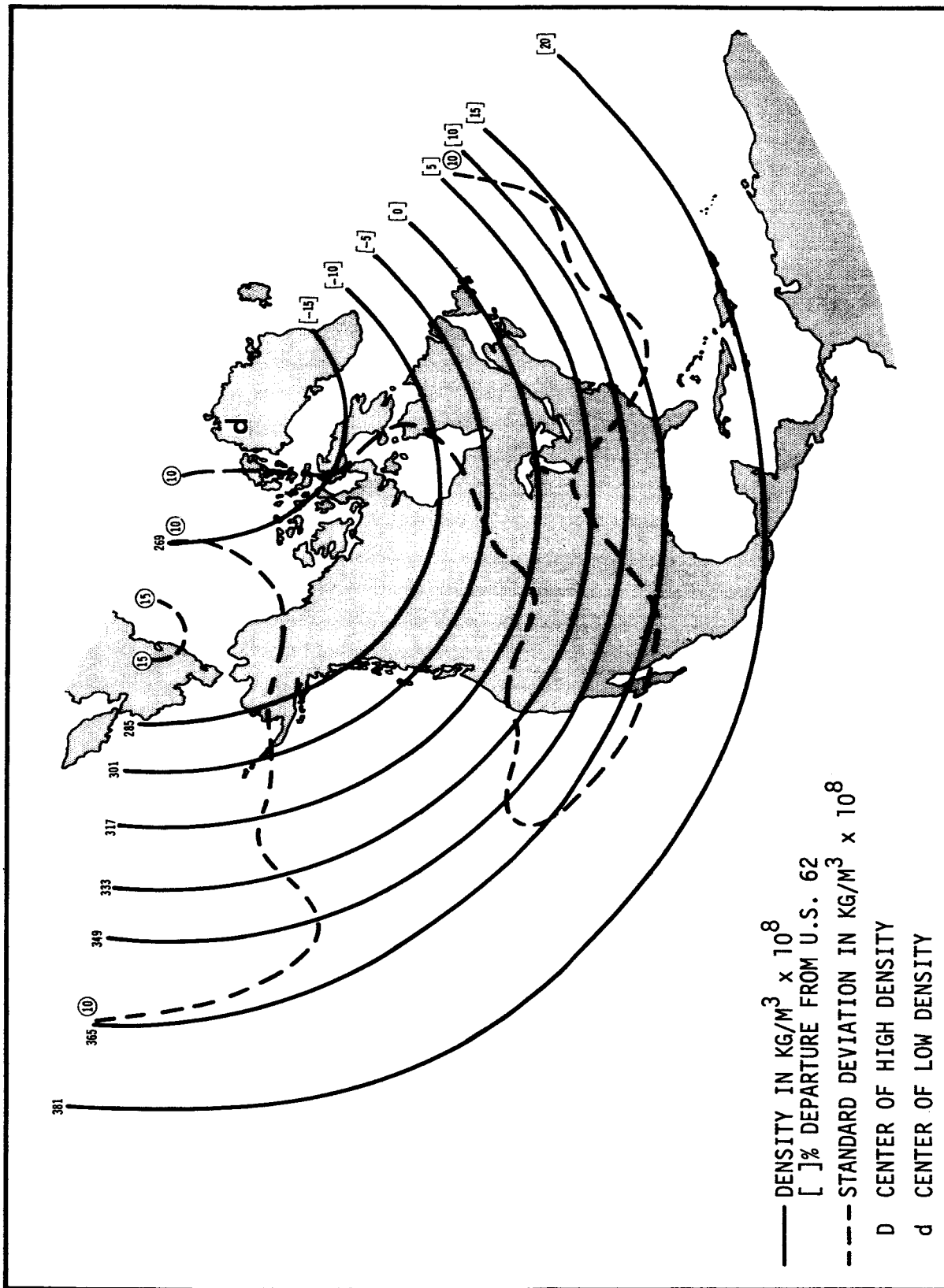
Figure 47. MONTHLY MEAN DENSITY AND STANDARD DEVIATION FOR OCTOBER, 90 KM ALTITUDE

DENSITY IN KG/M^3 x 10^8
[ ]% DEPARTURE FROM U.S. 62
STANDARD DEVIATION IN KG/M^3 x 10^8
D   CENTER OF HIGH DENSITY
d   CENTER OF LOW DENSITY
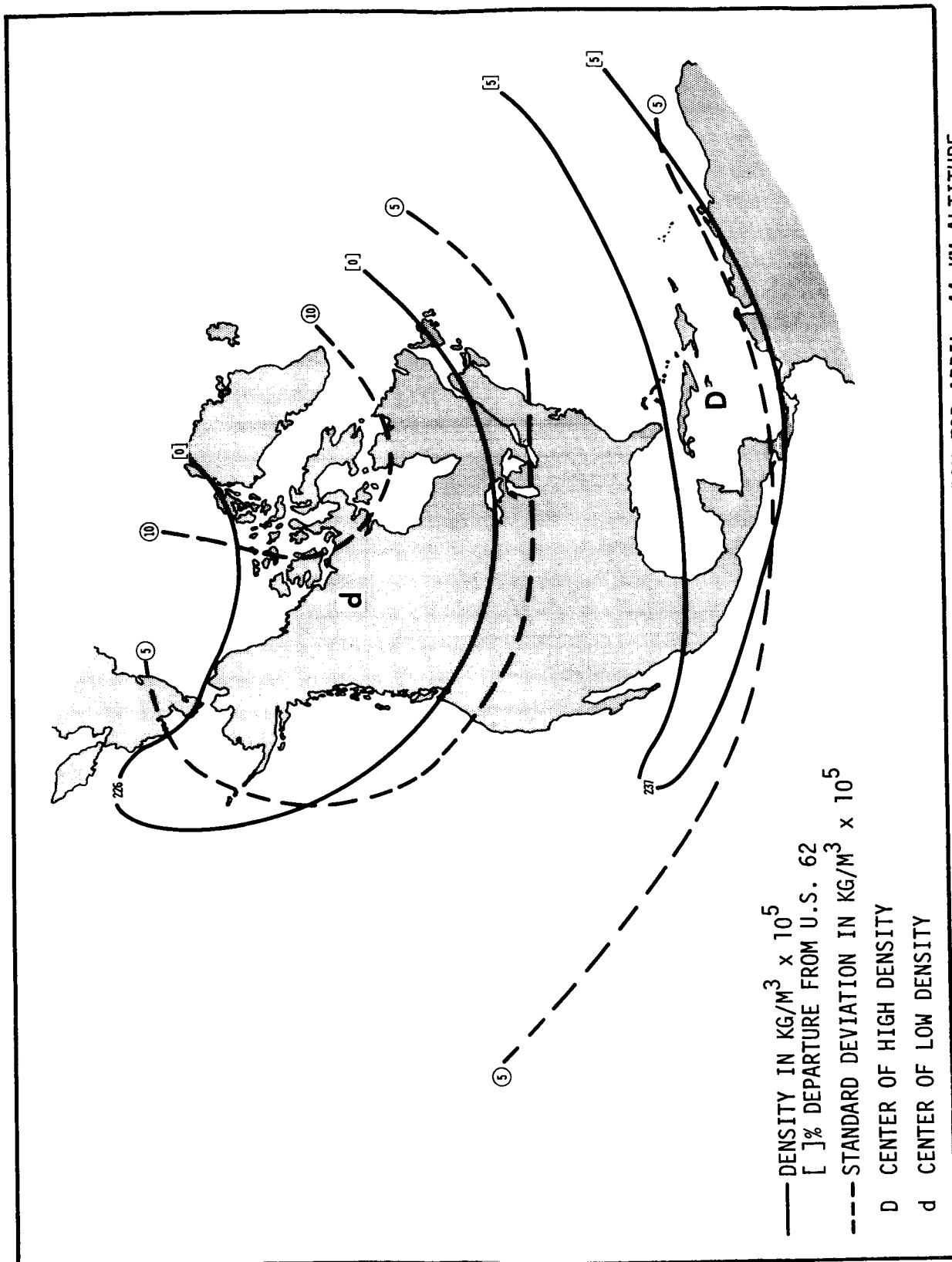
Figure 48. MONTHLY MEAN DENSITY AND STANDARD DEVIATION FOR APRIL, 44 KM ALTITUDE

DENSITY IN KG/M³ x 10⁵
[ ]% DEPARTURE FROM U.S. 62
STANDARD DEVIATION IN KG/M³ x 10⁵
D   CENTER OF HIGH DENSITY
d   CENTER OF LOW DENSITY

DENSITY IN KG/M^3 x 10^5
[ ]% DEPARTURE FROM U.S. 62
STANDARD DEVIATION IN KG/M^3 x 10^5
D   CENTER OF HIGH DENSITY
d   CENTER OF LOW DENSITY
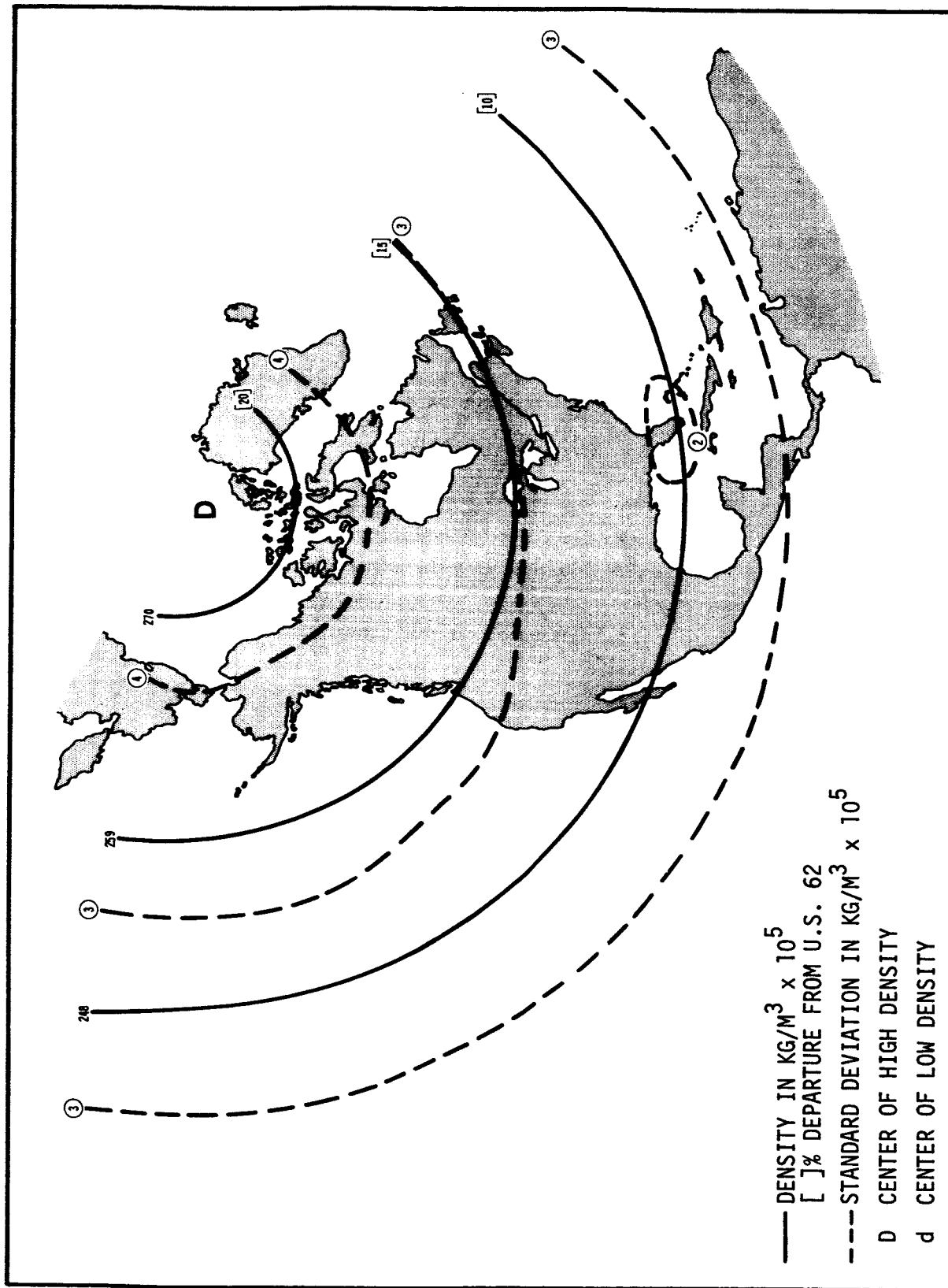
Figure 49.   MONTHLY MEAN DENSITY AND STANDARD DEVIATION FOR JULY, 44 KM ALTITUDE

71
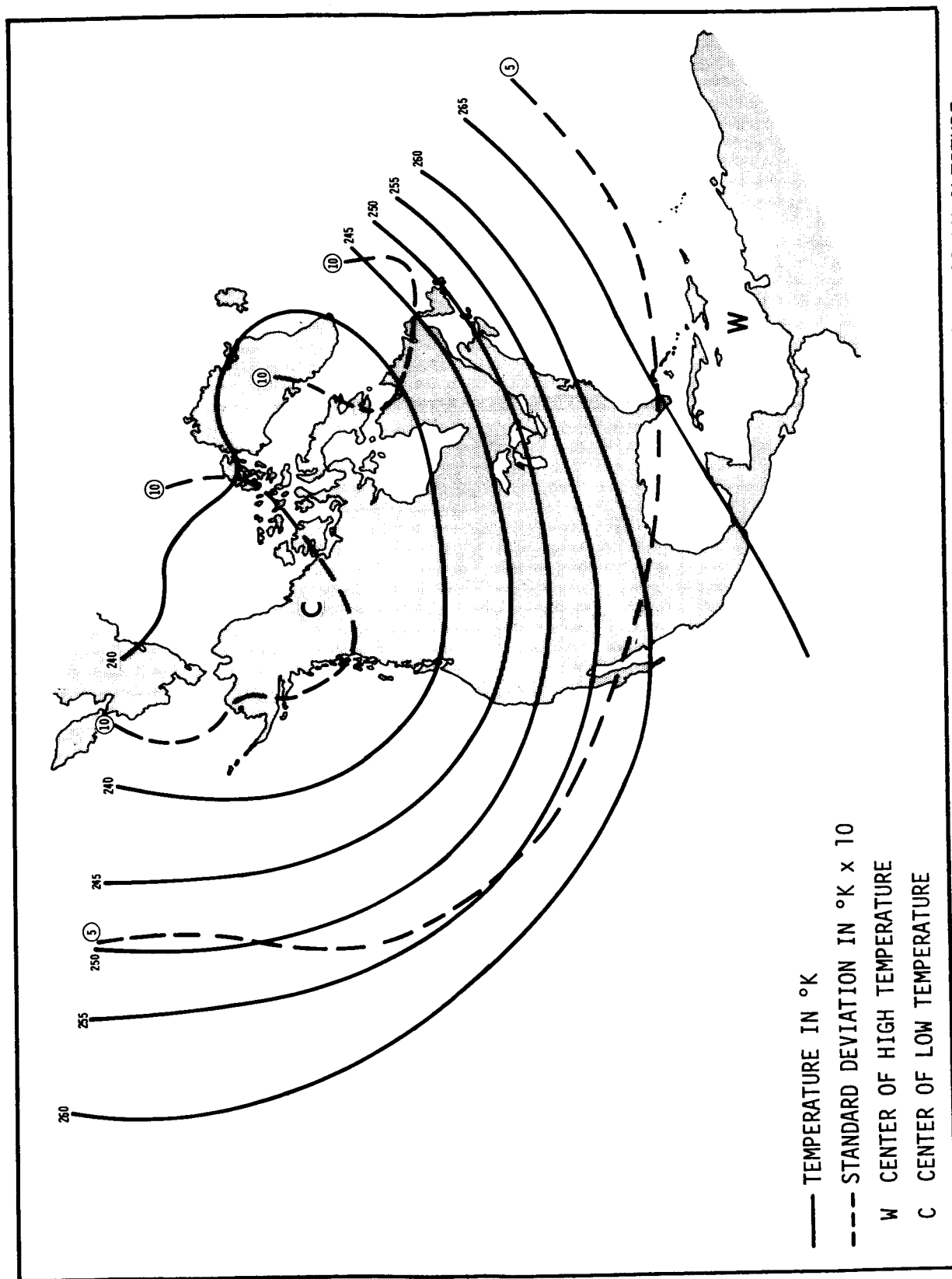
Figure 50. MONTHLY MEAN TEMPERATURE AND STANDARD DEVIATION FOR JANUARY, 44 KM ALTITUDE

——— TEMPERATURE IN °K

- - - STANDARD DEVIATION IN °K x 10

W CENTER OF HIGH TEMPERATURE

C CENTER OF LOW TEMPERATURE
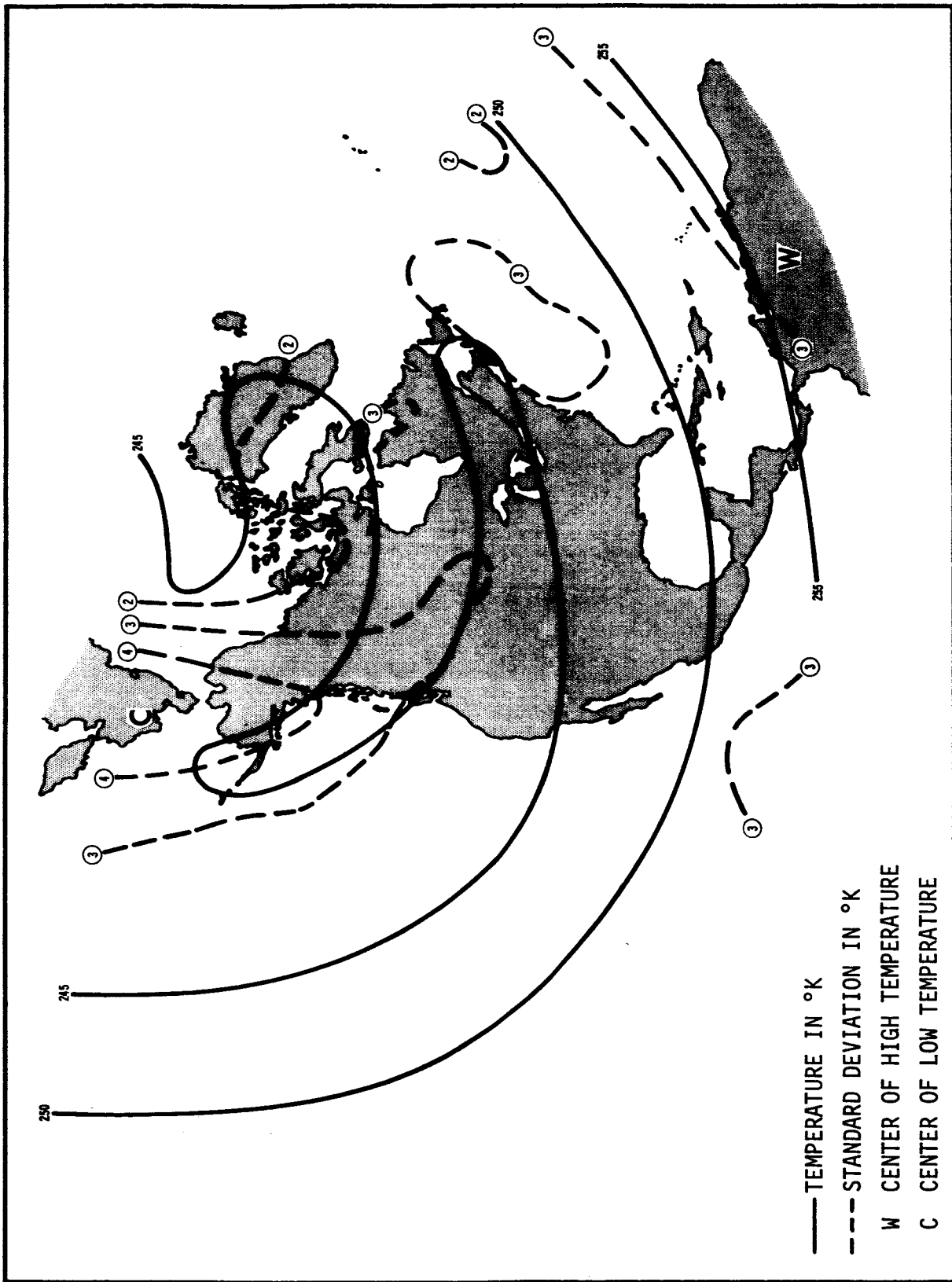
Figure 51. MONTHLY MEAN TEMPERATURE AND STANDARD DEVIATION FOR JANUARY, 60 KM ALTITUDE

——— TEMPERATURE IN °K

– – – STANDARD DEVIATION IN °K

W CENTER OF HIGH TEMPERATURE

C CENTER OF LOW TEMPERATURE
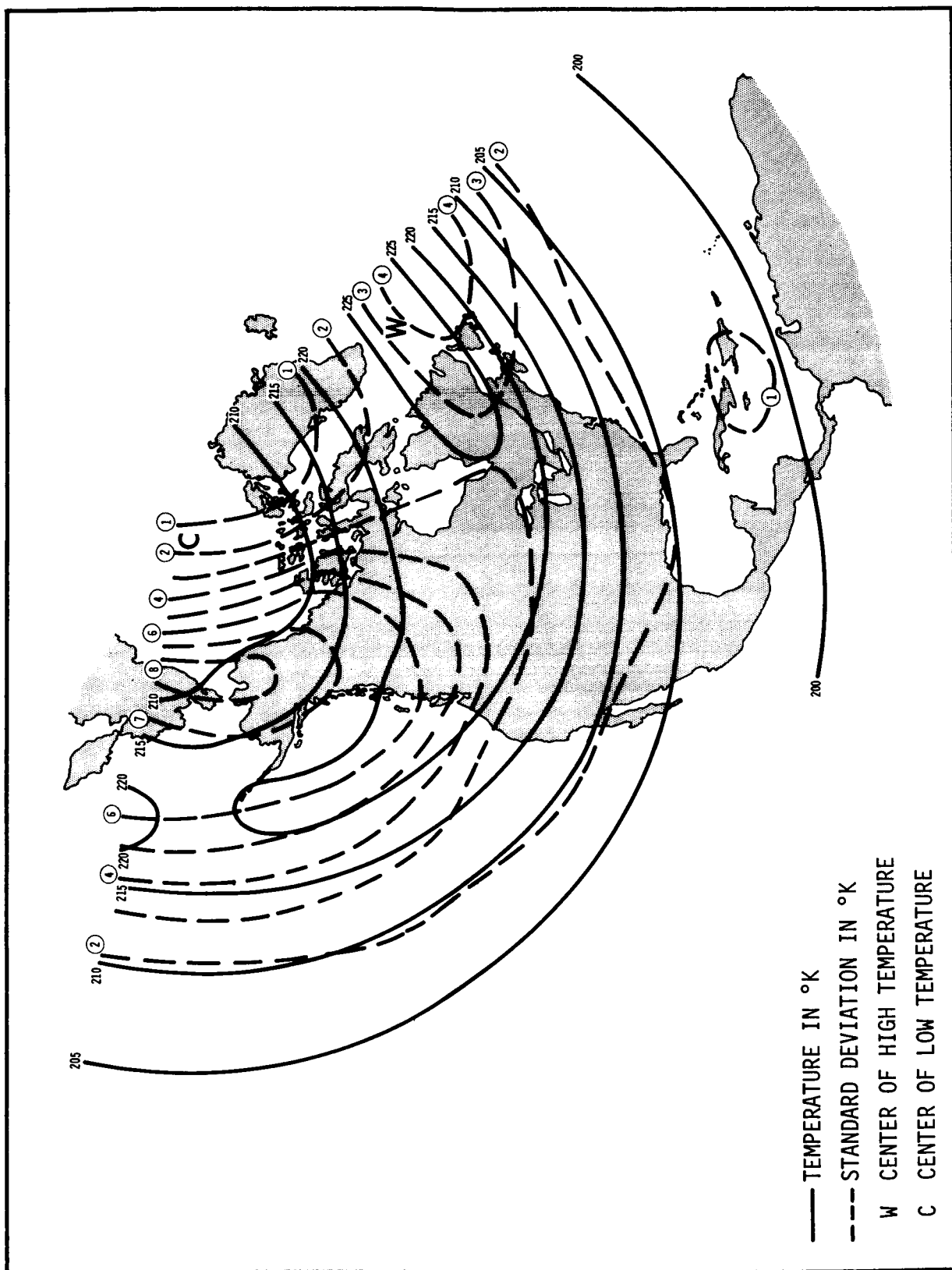
Figure 52. MONTHLY MEAN TEMPERATURE AND STANDARD DEVIATION FOR JANUARY, 76 KM ALTITUDE

— TEMPERATURE IN °K

--- STANDARD DEVIATION IN °K

W CENTER OF HIGH TEMPERATURE

C CENTER OF LOW TEMPERATURE
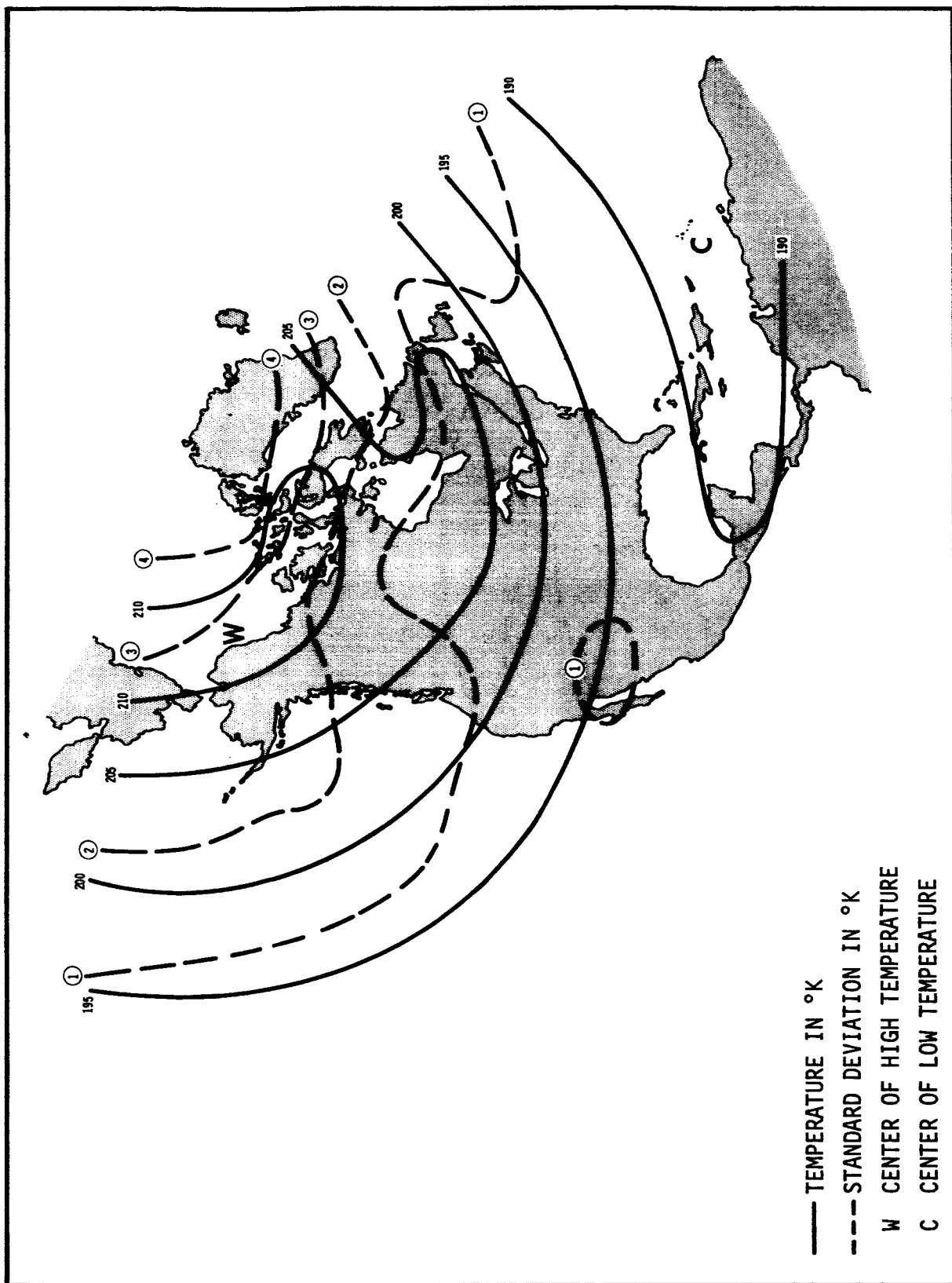
Figure 53. MONTHLY MEAN TEMPERATURE AND STANDARD DEVIATION FOR JANUARY, 90 KM ALTITUDE

—— TEMPERATURE IN °K

---- STANDARD DEVIATION IN °K

W CENTER OF HIGH TEMPERATURE

C CENTER OF LOW TEMPERATURE
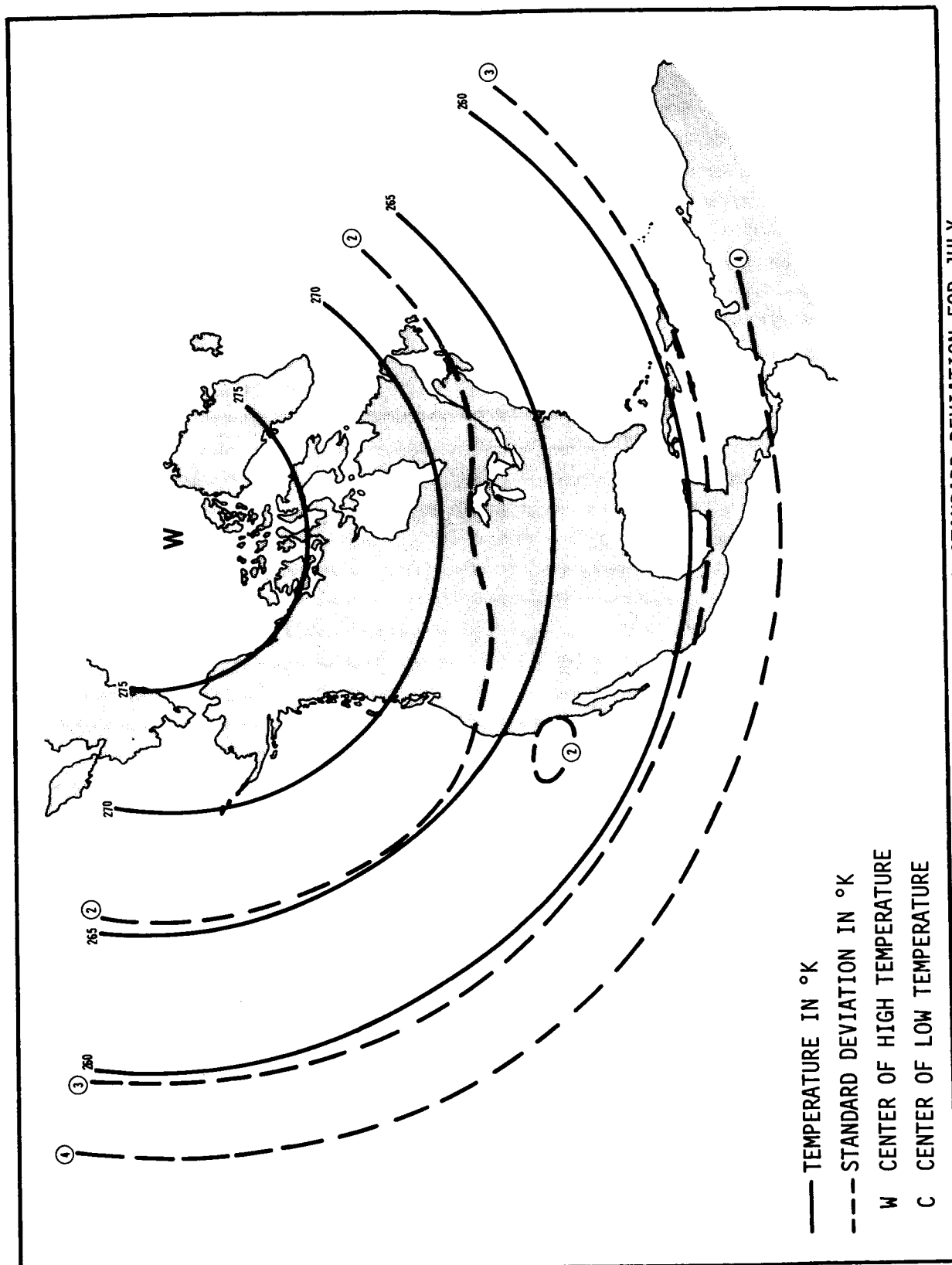
Figure 54. MONTHLY MEAN TEMPERATURE AND STANDARD DEVIATION FOR JULY, 44 KM ALTITUDE

——— TEMPERATURE IN °K
––– STANDARD DEVIATION IN °K
W CENTER OF HIGH TEMPERATURE
C CENTER OF LOW TEMPERATURE
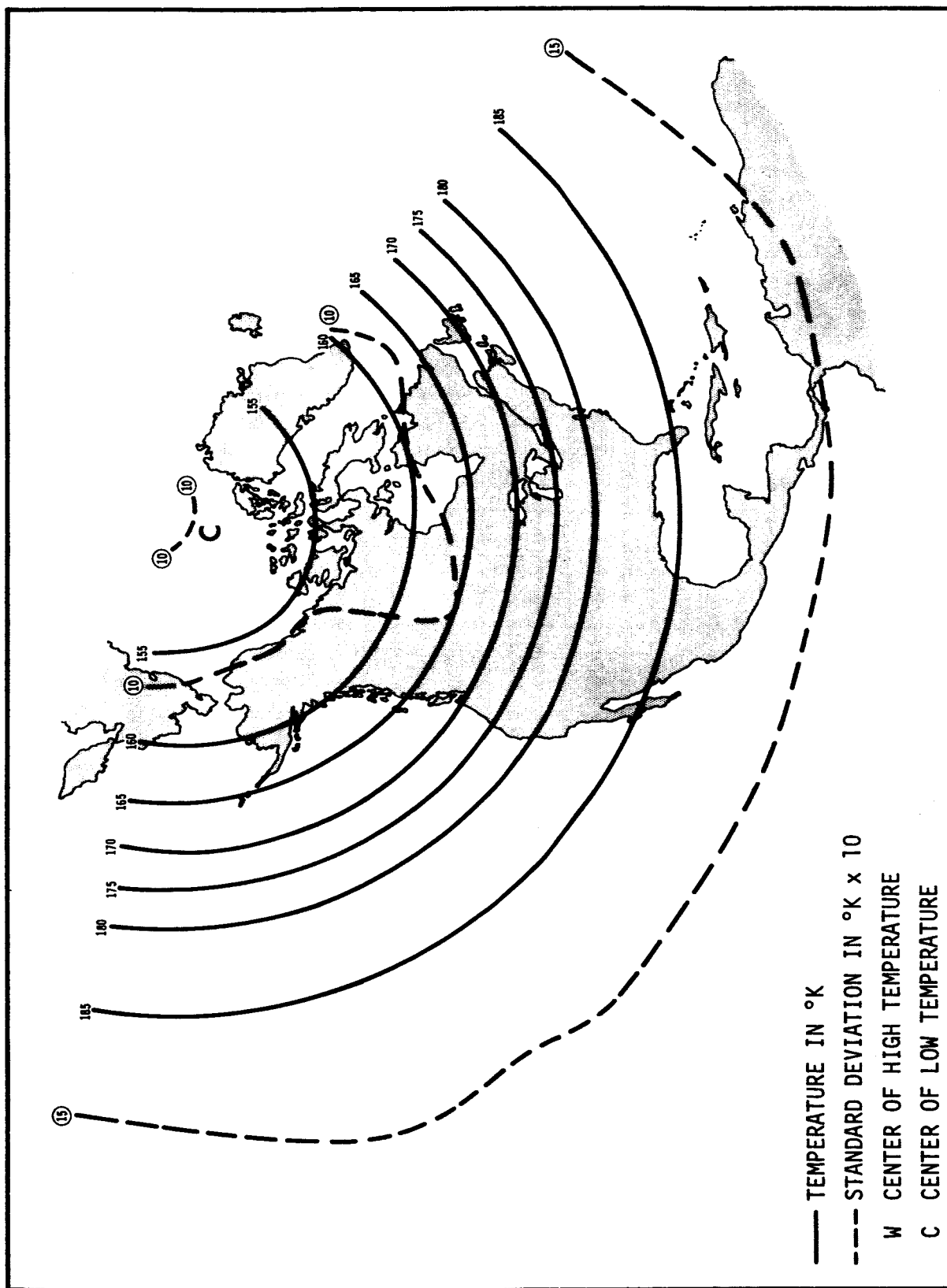
Figure 55. MONTHLY MEAN TEMPERATURE AND STANDARD DEVIATION FOR JULY,
90 KM ALTITUDE

—— TEMPERATURE IN °K

--- STANDARD DEVIATION IN °K x 10

W CENTER OF HIGH TEMPERATURE

C CENTER OF LOW TEMPERATURE
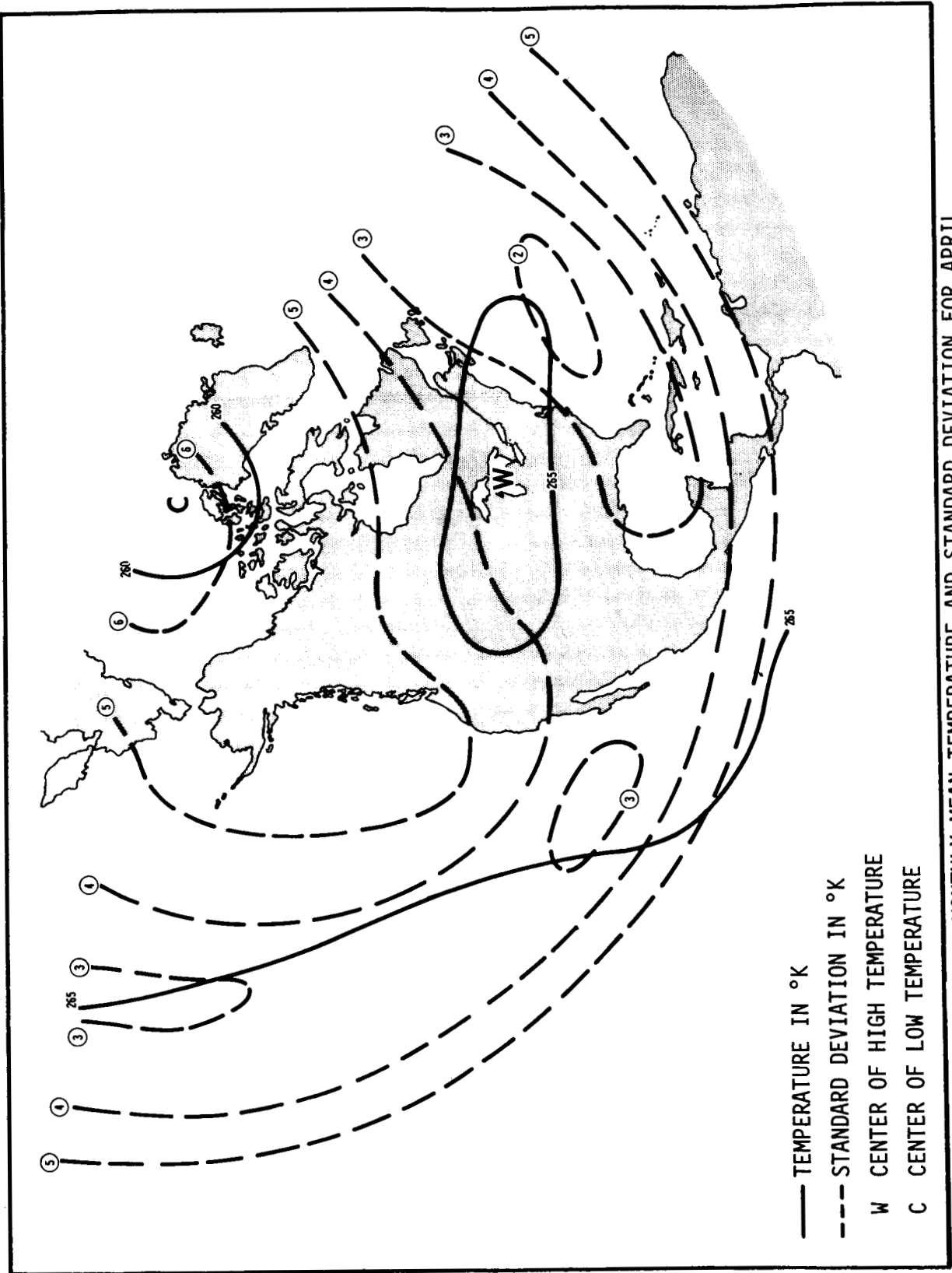
Figure 56. MONTHLY MEAN TEMPERATURE AND STANDARD DEVIATION FOR APRIL, 44 KM ALTITUDE

TEMPERATURE IN °K
STANDARD DEVIATION IN °K
W CENTER OF HIGH TEMPERATURE
C CENTER OF LOW TEMPERATURE
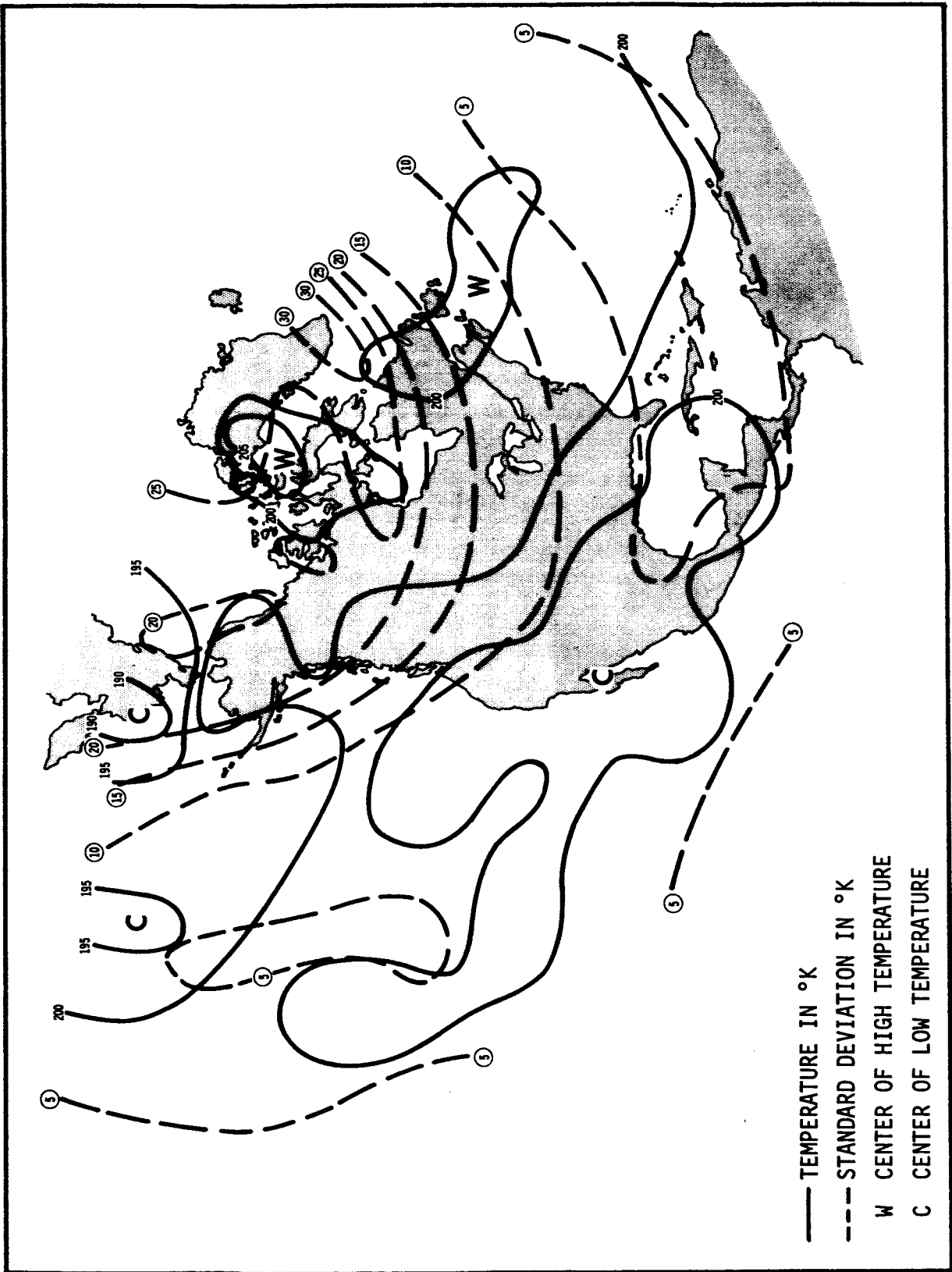
Figure 57. MONTHLY MEAN TEMPERATURE AND STANDARD DEVIATION FOR APRIL, 90 KM ALTITUDE

—— TEMPERATURE IN °K
--- STANDARD DEVIATION IN °K
W CENTER OF HIGH TEMPERATURE
C CENTER OF LOW TEMPERATURE
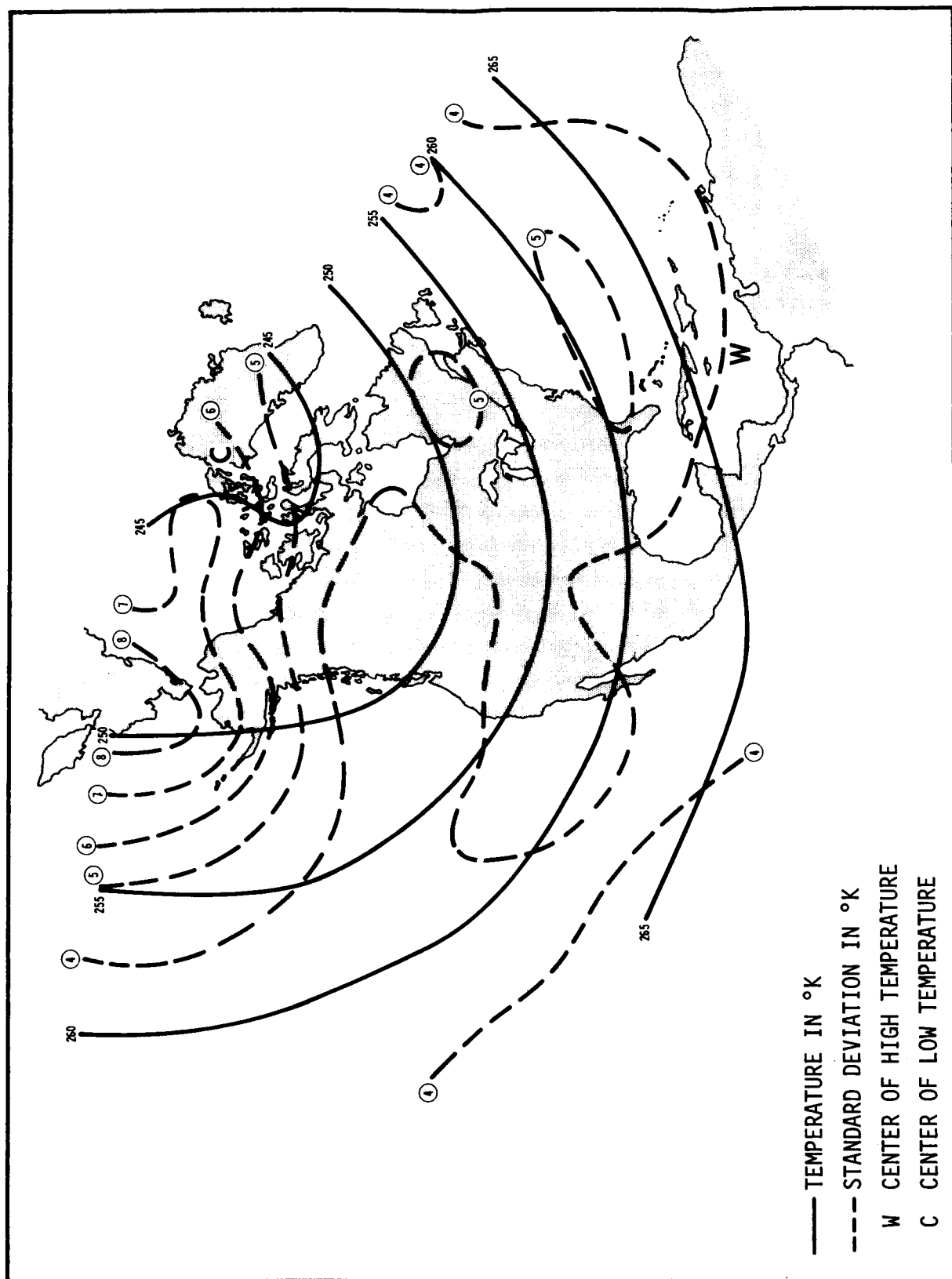
Figure 58. MONTHLY MEAN TEMPERATURE AND STANDARD DEVIATION FOR OCTOBER, 44 KM ALTITUDE

—— TEMPERATURE IN °K
--- STANDARD DEVIATION IN °K
W CENTER OF HIGH TEMPERATURE
C CENTER OF LOW TEMPERATURE

Figure 59. MONTHLY MEAN TEMPERATURE AND STANDARD DEVIATION FOR OCTOBER, 90 KM ALTITUDE

— TEMPERATURE IN °K

——— STANDARD DEVIATION IN °K x 10

W CENTER OF HIGH TEMPERATURE

C CENTER OF LOW TEMPERATURE

81
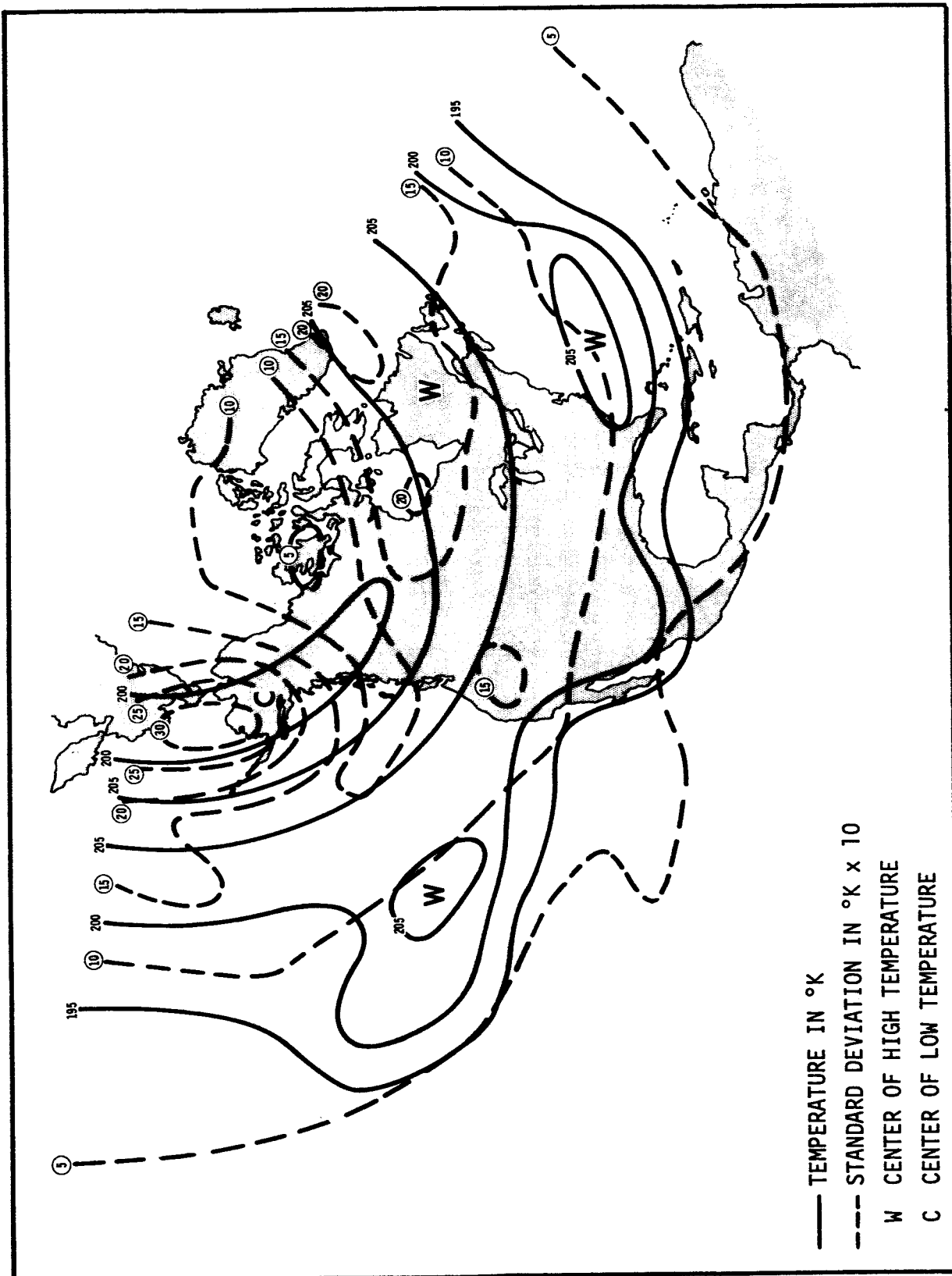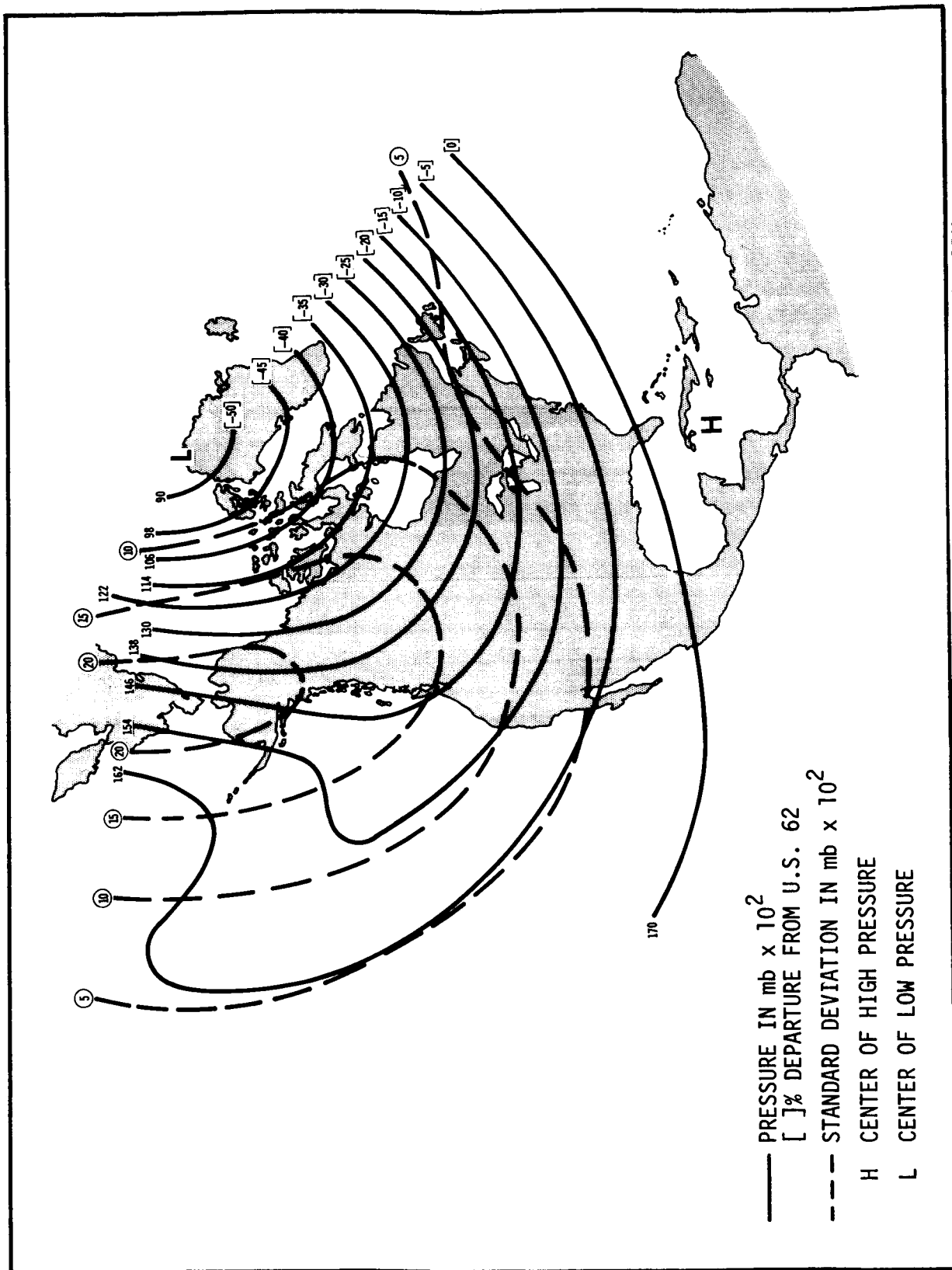
Figure 60. MONTHLY MEAN PRESSURE AND STANDARD DEVIATION FOR JANUARY, 44 KM ALTITUDE

PRESSURE IN mb x 10^2
[ ]% DEPARTURE FROM U.S. 62
STANDARD DEVIATION IN mb x 10^2
H CENTER OF HIGH PRESSURE
L CENTER OF LOW PRESSURE
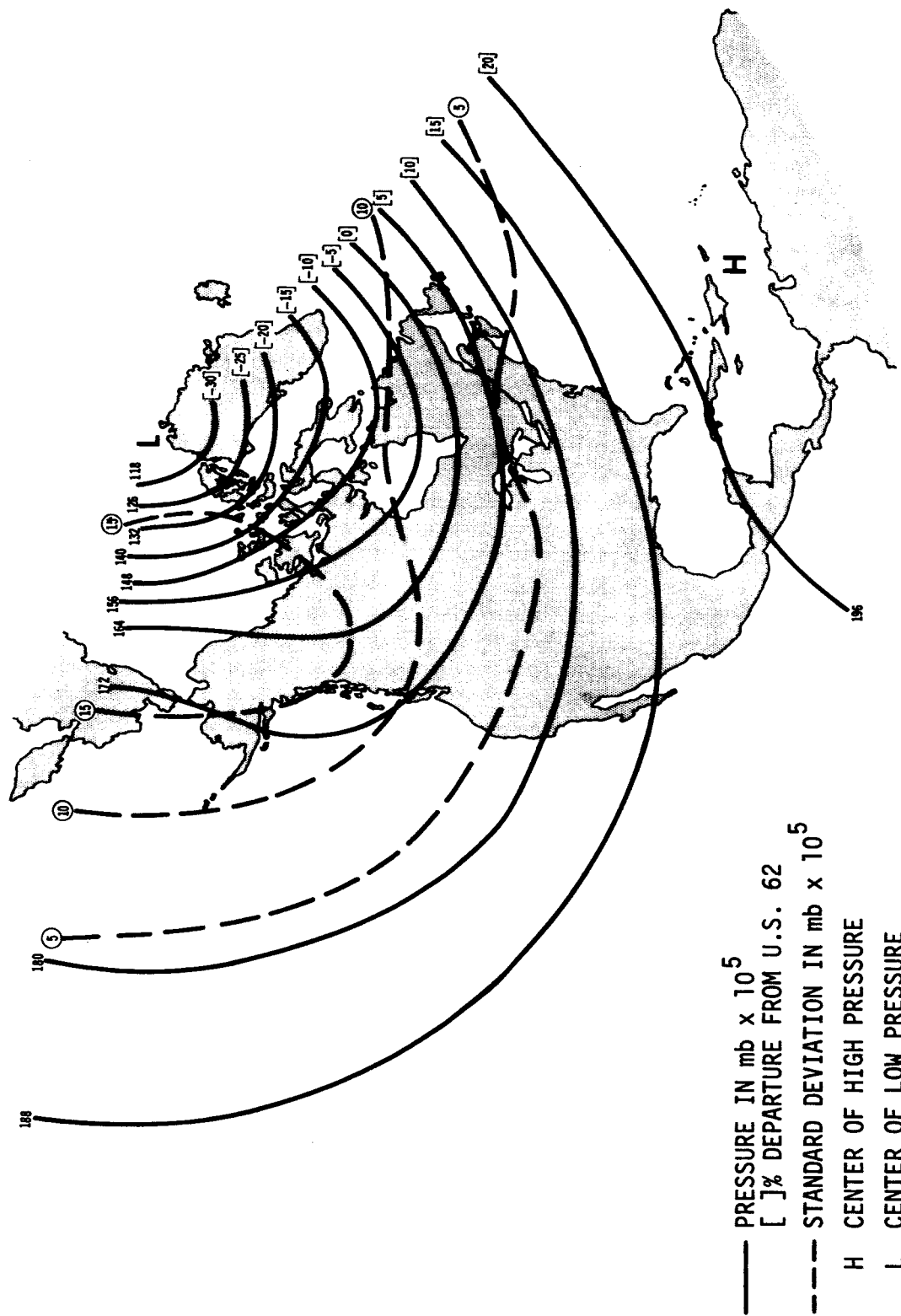
Figure 61. MONTHLY MEAN PRESSURE AND STANDARD DEVIATION FOR JANAURY, 90 KM ALTITUDE

PRESSURE IN mb x 10^5
[ ]% DEPARTURE FROM U.S. 62
STANDARD DEVIATION IN mb x 10^5
H CENTER OF HIGH PRESSURE
L CENTER OF LOW PRESSURE

temperature (Figures 54, 55) show simple mean fields with warm conditions over the North Polar zone at 44 km and cold conditions there at 90 km. The standard deviation of temperature in July is relatively small at both levels, decreasing with latitude. The transitional seasons of April and October (Figures 56-59) have more complex fields. The variability of temperature in high latitudes is considerable in these months.

Pressure charts for 44 km and 90 km (Figures 60, 61) are added for the month of January. They are quite similar to the density charts at these levels, and the 44 km chart is found to be typical of 2-mb analyses for January (ref. 14).

In retrospect, it may be noted that longitudinal variations of the atmospheric variables often exceed their latitudinal variations. The most probable regions and seasons for this to occur are indicated to some extent in the charts displayed in this report.

The representation of standard deviation on the charts may be challenged on two counts: smallness of the sample sizes and smoothing effect of the extrapolation technique, which involves regression. Both tend to minimize the variance. However, the observational error in the data broadens the range of 52 km data and thereby adds a fictitious increment to the variance of all the variables at levels above 52 km.

Section VI

COMPARISON CHECK AND CONSISTENCY TESTS

Comparison with Groves' Model. In Figures 34 through 41 of Section V, the latitudinal variation of the structure variables generated for the extrapolation procedure was given for a field which matches that of Groves' model, and for half of the eight data levels. Also entered on these diagrams are the values for Groves' model interpolated to the midpoint of the appropriate month. The 52 km level is included because it is the base level for the regression.

The principal predictor, which is pressure, shows good agreement with Groves' model at this level (Figures 39a, 39b). At higher levels such as 76 km and 90 km, the pressure curves have greater slope in mid-latitudes, implying that a stronger south-north pressure gradient exists with stronger zonal winds than in Groves' model.

At 52 km, the secondary predictor, which is temperature, departs from Groves' model values as much as 10°K in January and July (Figures 40a, 40b). Other differences appear, with the most prominent being at 90 km in April. Our temperatures at this level are considerably greater and more uniform along this latitude than Groves' model for April, which has very little supporting data at high latitudes.

The mean densities are in close agreement with Groves' model at 52 km and 60 km (Figures 41a, 41b). They tend to be lower than the model in April and January in the upper stratosphere and mesosphere, but higher in July and October. In most cases, the density curves are quite similar to the corresponding pressure curves, even in their minor fluctuations.

Triangle Relations. If the departures of density, temperature, and pressure from their average values are assumed to be very small, then certain algebraic relationships among the statistics for these quantities are valid. Such relationships are given by Buell (ref. 21), and they include the "triangle relations" among the variables, for example, let

$$a = \sigma(\rho)/\bar{\rho}, \ b = \sigma(T)/\bar{T}, \ c = \sigma(P)/\bar{P}$$

where a, b, c are coefficients of variation,

ρ, T, P are structure variables density, temperature, and pressure
σ is the standard deviation.

One of the "triangle relations" states that

$$a \leq b + c, \ b \leq c + a, \ c \leq a + b \quad . \tag{7}$$

When this relationship is not fulfilled at a particular level and grid point, the equation of state is not satisfied, e.g., there is an internal inconsistency in the data.

The value of a, b, and c at all eight levels and selected latitudes are listed in Table 4 for each midseasonal month along the 80 degree west meridian. There are seven violations of expression (7) in the table, with a majority occurring at the 76 km level. When similar calculations are made at 100 degrees West, only one violation is found, also at 76 km. The preponderance of violations at 76 km are not directly attributable to the adjustments to pressure and density made in the extrapolation, because the largest and the most variable adjustments are not applied at this level (cf. Figures 4 through 7).

As may be noted in Table 4, a violation of expression (7) always results in an illegitimate correlation coefficient, r_{PT}, between pressure and temperature, when r_{PT} is calculated from a, b, and c. This point is covered by Buell (ref. 22), who also obtains a criterion for hydrostatic consistency by use of a perturbation form of the hydrostatic equation. One outcome is that r_{PT} must agree in sign with the slope of $\sigma(P)/\bar{P}$. This test of signs is reported in Table 4, where six violations are found at 80 degrees West with no favored altitude, latitude, or season.

Table 4. COEFFICIENTS OF VARIATION AND CORRELATION COEFFICIENT FOR A SELECTED SAMPLE ALONG 80°W LONGITUDE

JANUARY

ALTITUDE (km)	LATITUDE = 10°N				LATITUDE = 30°N				LATITUDE = 50°N				LATITUDE = 70°N			
	$\sigma_p/\bar{P}$	$\sigma_T/\bar{T}$	$\sigma_\rho/\bar{\rho}$	r_{PT}	$\sigma_p/\bar{P}$	$\sigma_T/\bar{T}$	$\sigma_\rho/\bar{\rho}$	r_{PT}	$\sigma_p/\bar{P}$	$\sigma_T/\bar{T}$	$\sigma_\rho/\bar{\rho}$	r_{PT}	$\sigma_p/\bar{P}$	$\sigma_T/\bar{T}$	$\sigma_\rho/\bar{\rho}$	r_{PT}
36	.0109	.0090	.0133	.117	.0098	.0158	.0119	.659	.0498	.0194	.0500	.184	.0710	.0448	.0827	.033
44	.0207	.0133	.0178	.524	.0143	.0224	.0254	.095	.0526	.0332	.0633	-.040	.0859	.0298	.0847	.214
52	.0242	.0180	.0242	.372	.0224	.0187	.0185	.599	.0568	.0221	.0580	.140	.0908	.0353	.0927	.140
60	.0328	.0101	.0258	.773	.0345	.0116	.0252	.862	.0620	.0108	.0588	.377	.0970	.0099	.0955	.201 *
68	.0392	.0048	.0369	.526	.0420	.0056	.0384	.682	.0627	.0063	.0676	-.792	.0924	.0124	.1050	-1.018
76	.0385	.0059	.0443	-.980	.0403	.0082	.0483	-.971	.0530	.0135	.0667	-1.019 **	.0798	.0094	.0892	-1.000
84	.0294	.0072	.0361	-.914	.0291	.0091	.0380	-.971	.0387	.0097	.0483	-.987 **	.0742	.0036	.0728	.410
90	.0236	.0048	.0277	-.827	.0229	.0038	.0263	-.878	.0324	.0034	.0339	-.399 *	.0797	.0118	.0681	.986

APRIL

ALTITUDE (km)	LATITUDE = 10°N				LATITUDE = 30°N				LATITUDE = 50°N				LATITUDE = 70°N			
	$\sigma_p/\bar{P}$	$\sigma_T/\bar{T}$	$\sigma_\rho/\bar{\rho}$	r_{PT}	$\sigma_p/\bar{P}$	$\sigma_T/\bar{T}$	$\sigma_\rho/\bar{\rho}$	r_{PT}	$\sigma_p/\bar{P}$	$\sigma_T/\bar{T}$	$\sigma_\rho/\bar{\rho}$	r_{PT}	$\sigma_p/\bar{P}$	$\sigma_T/\bar{T}$	$\sigma_\rho/\bar{\rho}$	r_{PT}
36	.0110	.0129	.0157	.144	.0130	.0090	.0162	.396	.0290	.0153	.0255	.216	.0550	.0353	.0667	-.046 **
44	.0130	.0191	.0222	.082	.0160	.0098	.0145	.452	.0400	.0148	.0308	.735	.0630	.0213	.0544	.545
52	.0200	.0152	.0138	.725	.0180	.0136	.0196	.125	.0470	.0155	.0437	.370	.0710	.0206	.0668	.343
60	.0300	.0092	.0225	.867	.0230	.0080	.0188	.651	.0530	.0089	.0479	.629	.0800	.0119	.0727	.660
68	.0360	.0046	.0343	.628	.0280	.0045	.0259	.530	.0570	.0049	.0571	.002	.0840	.0062	.0837	.085
76	.0340	.0051	.0413	-1.045	.0280	.0042	.0322	-1.000	.0520	.0125	.0637	-.921	.0760	.0181	.0929	-.918
84	.0290	.0074	.0358	-.899 *	.0230	.0062	.0285	-.858	.0360	.0134	.0489	-.949	.0510	.0207	.0714	-.980
90	.0250	.0027	.0272	-.140	.0190	.0029	.0206	-.499	.0260	.0071	.0324	-.876	.0340	.0124	.0459	-.945

JULY

ALTITUDE (km)	LATITUDE = 10°N				LATITUDE = 30°N				LATITUDE = 50°N				LATITUDE = 70°N			
	$\sigma_p/\bar{P}$	$\sigma_T/\bar{T}$	$\sigma_\rho/\bar{\rho}$	r_{PT}	$\sigma_p/\bar{P}$	$\sigma_T/\bar{T}$	$\sigma_\rho/\bar{\rho}$	r_{PT}	$\sigma_p/\bar{P}$	$\sigma_T/\bar{T}$	$\sigma_\rho/\bar{\rho}$	r_{PT}	$\sigma_p/\bar{P}$	$\sigma_T/\bar{T}$	$\sigma_\rho/\bar{\rho}$	r_{PT}
36	.0080	.0066	.0124	.438	.0070	.0053	.0098	-.255 **	.0090	.0100	.0122	.179	.0100	.0124	.0096	.052
44	.0160	.0153	.0150	.541	.0130	.0094	.0079	.798	.0120	.0072	.0121	.286	.0150	.0060	.0159	.046
52	.0300	.0173	.0174	.864	.0220	.0105	.0163	.711	.0200	.0143	.0114	.415	.0250	.0194	.0068	.985 *
60	.0440	.0113	.0336	.940	.0290	.0064	.0240	.824	.0310	.0092	.0229	.914 *	.0410	.0123	.0286	1.006
68	.0520	.0045	.0491	.670	.0340	.0031	.0329	.395	.0390	.0045	.0351	.881	.0510	.0084	.0433	.930
76	.0490	.0106	.0593	-.966	.0320	.0073	.0389	-.933	.0390	.0054	.0446	-1.042	.0550	.0036	.0581	-.853 **
84	.0340	.0124	.0463	-.990	.0210	.0088	.0297	-.984	.0300	.0078	.0377	-.984	.0490	.0056	.0542	-.921
90	.0230	.0075	.0304	-.982	.0130	.0061	.0184	-.834	.0220	.0072	.0285	-.873	.0440	.0052	.0480	-.745

OCTOBER

ALTITUDE (km)	LATITUDE = 10°N				LATITUDE = 30°N				LATITUDE = 50°N				LATITUDE = 70°N			
	$\sigma_p/\bar{P}$	$\sigma_T/\bar{T}$	$\sigma_\rho/\bar{\rho}$	r_{PT}	$\sigma_p/\bar{P}$	$\sigma_T/\bar{T}$	$\sigma_\rho/\bar{\rho}$	r_{PT}	$\sigma_p/\bar{P}$	$\sigma_T/\bar{T}$	$\sigma_\rho/\bar{\rho}$	r_{PT}	$\sigma_p/\bar{P}$	$\sigma_T/\bar{T}$	$\sigma_\rho/\bar{\rho}$	r_{PT}
36	.0090	.0104	.0086	.062	.0370	.0150	.0249	.877	.0190	.0066	.0149	.728	.0520	.0121	.0464	.554
44	.0130	.0136	.0160	.028	.0450	.0199	.0369	.592	.0230	.0195	.0210	.522	.0590	.0174	.0568	.272
52	.0170	.0109	.0163	.038	.0590	.0199	.0475	.690	.0300	.0138	.0277	.390	.0660	.0184	.0636	.267
60	.0220	.0067	.0170	.081	.0710	.0103	.0638	.736	.0360	.0084	.0305	.721	.0720	.0096	.0697	.302
68	.0250	.0032	.0236	.049	.0760	.0044	.0784	-.525	.0410	.0051	.0382	.208	.0710	.0084	.0785	-.881
76	.0250	.0035	.0286	-1.033 *	.0650	.0186	.0827	-.938	.0380	.0065	.0452	-1.127 **	.0590	.0147	.0736	-.992
84	.0210	.0040	.0238	-.651	.0430	.0180	.0604	-.953	.0300	.0068	.0363	-.910	.0430	.0109	.0539	-1.000
90	.0180	.0025	.0187	-.216	.0300	.0080	.0377	-.953	.0230	.0040	.0270	-1.000	.0360	.0032	.0377	-.499

*The coefficient of variation violates the triangle relationships given in Reference 18.

**The slope of the coefficient of variation $\sigma_\rho/\bar{P}$ is opposite in sign to the correlation coefficient r_{pr}.

Figure 62 illustrates three examples of the consistency tests in which the coefficient of variation $\sigma_p/\bar{P}$ and the correlation coefficient r_{PT} are plotted against altitude. Figure 62a represents a case in which both the triangle relations and the criteria for hydrostatic consistency are satisfied, while these requirements are not fulfilled in the cases of Figures 62b and 62c.

The tests for internal consistency have thus yielded violations of hydrostatic conditions in about 5 percent of a moderate-sized output sample. This is not believed to indicate a serious deficiency of the model, as it may well reflect the considerable observational error in the data used in all phases of the investigation. The results of these tests are useful in providing adjustment factors to be applied to the coefficients of variation (cf. Buell, ref. 22).

Figure 62a.   COEFFICIENT OF VARIATION $\sigma_p/\bar{P}$ AND CORRELATION COEFFICIENT r_{PT} FOR
THE MONTH OF JULY AT LATITUDE 10°N AND LONGITUDE 80°W

Figure 62b. COEFFICIENT OF VARIATION $\sigma_p/\bar{P}$ AND CORRELATION COEFFICIENT r_{PT} FOR THE MONTH OF JANUARY AT LATITUDE 50°N AND LONGITUDE 80°W
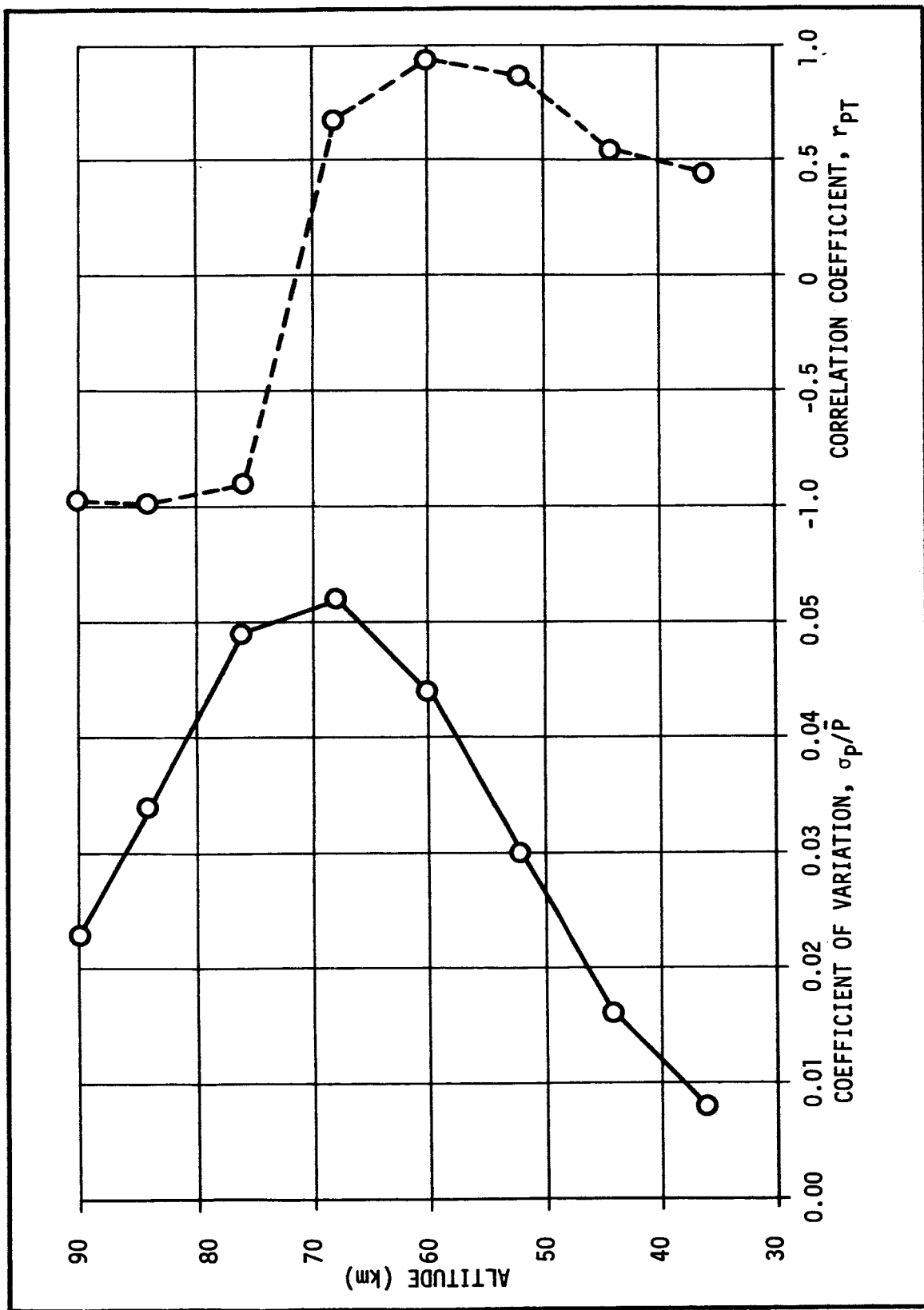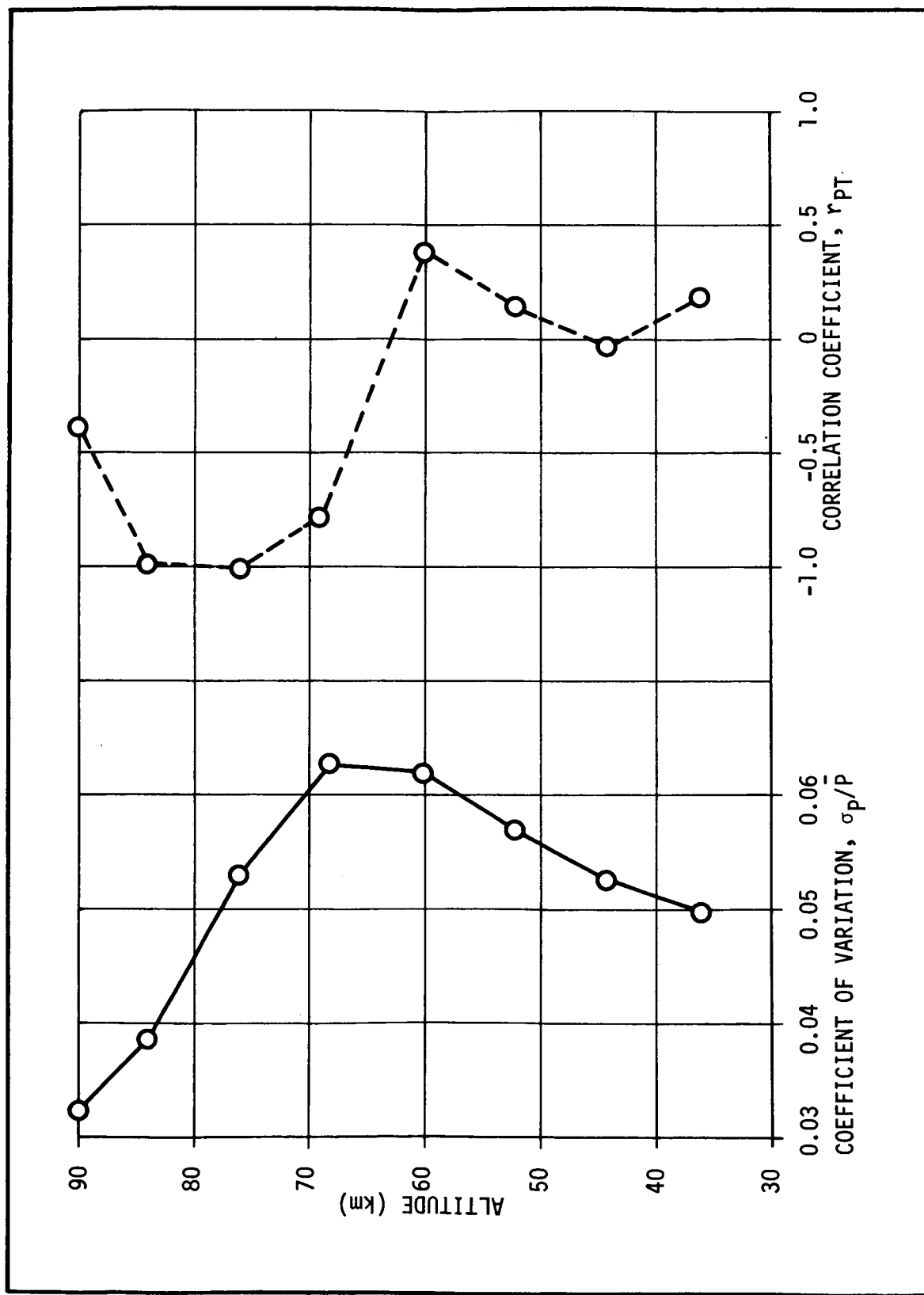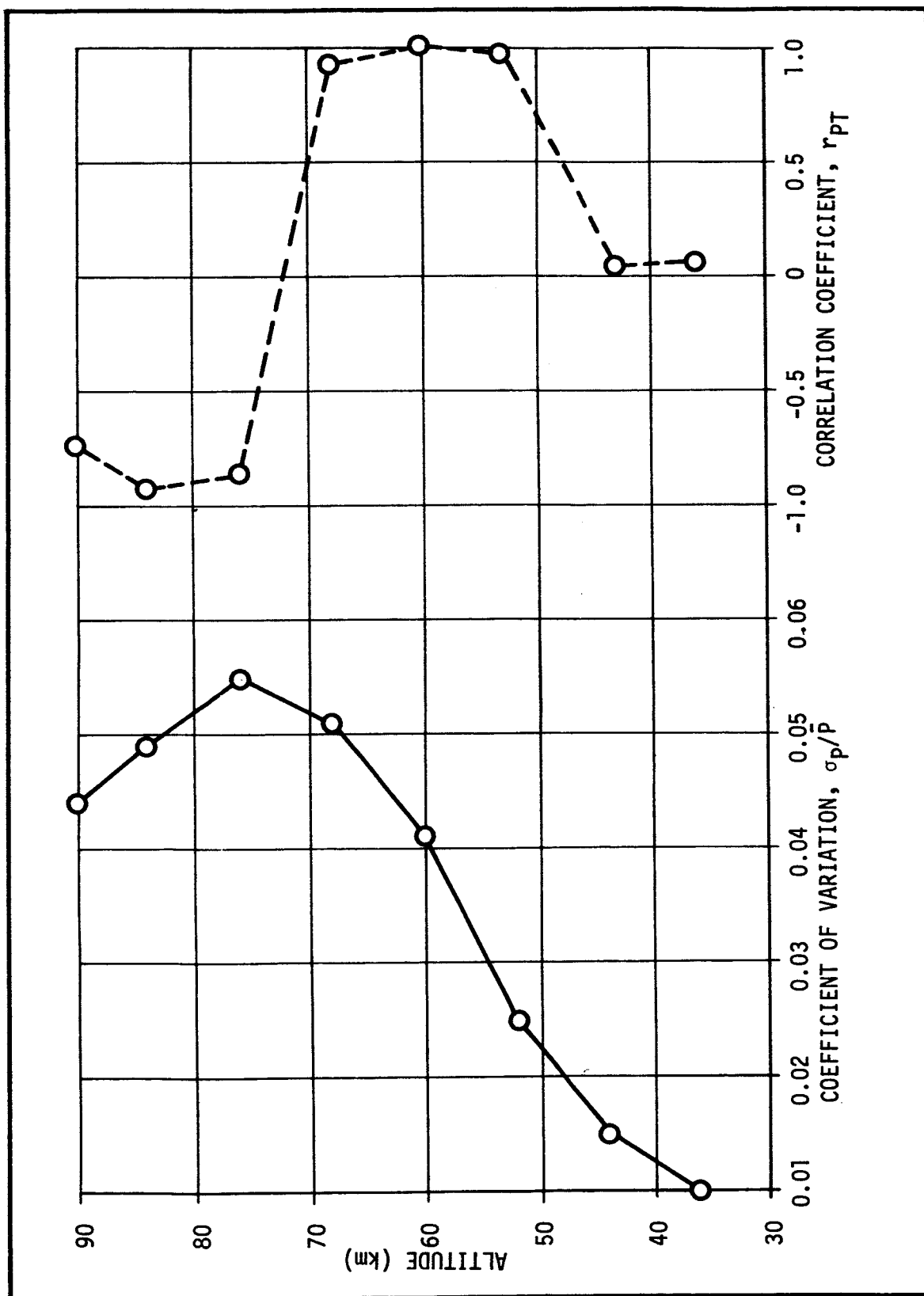
Figure 62c. COEFFICIENT OF VARIATION $\sigma_p/\bar{P}$ AND CORRELATION COEFFICIENT r_{PT} FOR
THE MONTH OF JULY AT LATITUDE 70°N AND LONGITUDE 80°W

Section VII

CONCLUSIONS AND RECOMMENDATIONS FOR FURTHER STUDY

An extrapolation procedure for specifying density, temperature, and pressure from 36 km to 90 km has been developed. Tests of the procedure have given reasonably accurate results, with root-mean-square errors in the derived quantities being less than 6 percent up to 68 km. These errors increase with height to 16 percent at 90 km; however, these comparisons with the observed quantities include the random and systematic errors of measurement. The measurement errors are estimated to account for about half of the difference between observed and derived quantities.

The technique has been applied to the grid values of geopotential height and temperature at 5, 2, and 0.4 mb over North America and its environs. Fifty cases for the midseasonal months of January, April, July, and October have been evaluated, and the means and standard deviations have been recorded at each grid point. The stratospheric warming event of 3 January 1968 has also been processed.

Verification of the consistency of the resulting statistical model of atmospheric structure has been carried out successfully through a comparison with Groves' model of mean latitudinal values and the use of certain relationships introduced by Buell.

There are a number of ways to apply the results of this study, in particular, the new estimates of variability of the structure variables in four dimensions. However, the statistics presented here apply to the quiet solar period which occurred between 1964 and 1966. At the mesospheric levels investigated, one would expect a significant atmospheric response to an active solar period. Therefore, data from such a period should be processed, based upon the procedures of Sections II, IV, and V.

The development of the procedure to obtain map data up to 90 km is an extension of atmospheric modeling at lower levels. For example, the four-dimensional model created by Spiegler and Greaves (ref. 23) can generate

92

profiles for an atmospheric variable at any location of the world between
the ground and 25 km. Since the National Meteorological Center (NMC) grid
is more compatible with current models than the longitude-latitude grid, an
interpolation program has been adapted to the 496-point grid area used in this
study to produce interpolated data on the NMC grid. Although not on magnetic
tape, such data can be procured readily.

A program is also available which computes density gradients at a
particular level over the field area being used to compile the statistics of
the structure variables. With this density gradient program, one can deal
with individual charts to produce a map of the density gradient field, or one
may set up a perturbation field which allows the density to vary by perhaps
± 3 standard deviations. This should provide a basis for analysis of reentry
heating problems and trajectory control problems.

Reference atmospheres must be updated when new information permits
revision. The extrapolation technique has yielded much new data up to 90 km,
especially with regard to longitudinal variation of the atmospheric parameters
in the upper stratosphere and mesosphere.

A present, the computer program is configured to produce pressure,
temperature, and density at an 8-km interval. However, it can easily be
modified to derive the three structure variables at a 1-km interval, and it can
be used to provide detailed vertical cross-sections for case studies of
extreme atmospheric departures in the stratosphere and mesosphere. A density
perturbation study by King (ref. 24) has recently used the mesospheric
spatial distributions predicted by the extrapolation procedure.

Section VIII

REFERENCES

1. Webb, Willis L., et al., "Meteorological Rocket Network Probing of the Stratosphere and Lower Mesosphere", Bulletin of the American Meteorological Society, Vol. 47, No. 10, October 1966, 788-799.

2. Gelman, Melvyn E., Miller, Alvin J., and Woolf, Harold M., "Regression Technique for Determining Temperature Profiles in the Upper Stratosphere from Satellite-Measured Radiances", Monthly Weather Review, Vol. 100, No. 7, July 1972, 542-547.

3. Nordberg, W., Katchen, L., Theon, J., and Smith, W. S., "Rocket Observations of the Structure of the Mesosphere", Journal of the Atmospheric Sciences, Vol. 22, November 1965, 611-622.

4. Smith, W. S., Theon, J., Katchen, L., and Swartz, P., "Temperature, Pressure Density and Wind Measurements in the Upper Stratosphere and Mesosphere, 1964", NASA Technical Report, NASA TR-R-245, 1966, 84 pages.

5. Faire, Andrew C., Champion, K. S. W., and Murphy, E. A., "ABRES Density Variations", AFCRL-72-0042, 7 January 1972, 16 pages.

6. Verniani, Franco and Viani, Elena Reggiani, "Diurnal and Seasonal Variations of the Atmospheric Temperature at the 90-Kilometer Altitude", Journal of Geophysical Research, Vol. 77, No. 24, August 20, 1972, 4581-4585.

7. Kochanski, Adam, "Semiannual Variation at the Base of the Thermosphere", Monthly Weather Review, Vol. 100, No. 3, March 1972, 222-234.

8. Quiroz, Roderick S. and Thompson, 1st Lt. Gary L., "Regression Equations for Specifying Atmospheric Density above 30 km from Observational Data at Radiosonde Altitudes", Air Weather Service Technical Report 187, August 1966, 1-27.

9. Bowman, Alan W., Palmer, B. L., and Schuknecht, L. A., "Structure Models of the Stratosphere and Lower Mesosphere", TM 54/50-150, Lockheed Missiles and Space Company, Huntsville Research and Engineering Center, June 1971.

10. Quiroz, Roderick S. and Miller, Alvin J., "Height-Lag Correlations of Density With Pressure and Temperature at Rocket Altitudes of the Stratosphere", Journal of the Atmospheric Sciences, Vol. 25, January 1968, pp. 104-112.

11. "U. S. Standard Atmosphere, 1962", COESA, Government Printing Office, Washington, D. C., 1962.

12. "U. S. Standard Atmosphere Supplements, 1966", COESA, Government Printing Office, Washington, D. C., 1966.

13. Groves, G. V., "Atmospheric Structure and Its Variations in the Region from 25 to 120 km", AFCRL-71-0410, 27 July 1971, 200 pages.

14. Finger, Frederick G., Woolf, Harold M., and Anderson, Calvin E., "Synoptic Analyses of the 5-, 2-, and 0.4-Millibar Surfaces for the IQSY Period", Monthly Weather Review, Vol. 94, No. 11, November 1966, 651-661.

15. Johnson, Keith W., "Accuracy of Objective Analysis at Stratospheric Levels", Monthly Weather Review, Vol. 100, No. 3, March 1972, pp. 218-221.

16. Miller, A. H., "Errors in Temperature, Pressure, and Density Due to Interpolation Through the Stratopause", TN-241-1085, Northrop Services, Inc., Huntsville, Alabama, April 1972.

17. Quiroz, Roderick S., "Synoptic Density Maps of the Upper Atmosphere", Journal of Applied Meteorology, Vol. 7, No. 6, December 1968, pp. 969-976.

18. Staff, Upper Air Branch, National Meteorological Center, "Weekly Synoptic Analyses, 5-, 2-, and 0.4-Millibar Surfaces for 1968", NOAA Technical Report NWS 14, May 1971, 169 pages.

19. Williams, Ben H. and Miers, Bruce T., "The Synoptic Events of the Stratospheric Warming of December 1967 - January 1968", Atmospheric Sciences Research Office, White Sands Missile Range, N. M., September 1968, 35 pp.

20. Quiroz, Roderick S., "Modification of the Atmospheric Density Field in Response to Stratospheric Warmings", Fourth National Conference on Aerospace Meteorology, AMS-AIAA, May 4-7, 1970, Las Vegas, Nevada.

21. Buell, C. Eugene, "Statistical Relations in a Perfect Gas", Journal of Applied Meteorology, Vol. 9, No. 5, October 1970, 729-731.

22. Buell, C. Eugene, "Adjustment of Some Atmospheric Statistics to Satisfy Physical Conditions", Journal of Applied Meteorology, to be published.

23. Spiegler, David B. and Greaves, James R., "Development of Four-Dimensional Atmospheric Models (Worldwide)", NASA CR-61362, August 1971, 90 pages.

24. King, R. L., "On Density Perturbations in the Upper Stratosphere and Mesosphere", TR-241-1146, Northrop Services, Inc., Huntsville, Alabama, 1972, 51 pages.